UNIVERSIDADE FEDERAL DO CEARÁ
CENTRO DE TECNOLOGIA
DEPARTAMENTO DE ENGENHARIA DE TELEINFORMÁTICA
PROGRAMA DE PÓS-GRADUAÇÃO EM ENGENHARIA DE TELEINFORMÁTICA

VICTOR FARIAS MONTEIRO

ADDRESSING 5G ENHANCED MOBILE BROADBAND AND LEAN SIGNALING BASED ON DUAL-CONNECTIVITY AND CHANNEL HARDENING OCCURRENCE

FORTALEZA
2018

VICTOR FARIAS MONTEIRO

ADDRESSING 5G ENHANCED MOBILE BROADBAND AND LEAN SIGNALING BASED ON DUAL-CONNECTIVITY AND CHANNEL HARDENING OCCURRENCE

Tese apresentada ao Curso de Doutorado em Engenharia de Teleinformática da Universidade Federal do Ceará, como parte dos requisitos para obtenção do Título de Doutor em Engenharia de Teleinformática. Área de concentração: Sinais e Sistemas

Orientador: Prof. Dr. Francisco Rodrigo Porto Cavalcanti

Coorientador: Dr. Igor Moaco Guerreiro

FORTALEZA
2018

Dados Internacionais de Catalogação na Publicação
Universidade Federal do Ceará
Biblioteca Universitária
Gerada automaticamente pelo módulo Catalog, mediante os dados fornecidos pelo(a) autor(a)

M78a Monteiro, Victor Farias.
Addressing 5G Enhanced Mobile Broadband and Lean Signaling Based on Dual-Connectivity and Channel Hardening Occurence / Victor Farias Monteiro. – 2018.
100 f. : il. color.

Tese (doutorado) – Universidade Federal do Ceará, Centro de Tecnologia, Programa de Pós-Graduação em Engenharia de Teleinformática, Fortaleza, 2018.
Orientação: Prof. Dr. Francisco Rodrigo Porto Cavalcanti.
Coorientação: Prof. Dr. Igor Moaco Guerreiro.

1. Dual connectivity. 2. Channel hardening. 3. CQI measurement and reporting. 4. Radio resource allocation. I. Título.

CDD 621.38

VICTOR FARIAS MONTEIRO

ADDRESSING 5G ENHANCED MOBILE BROADBAND AND LEAN SIGNALING BASED ON DUAL-CONNECTIVITY AND CHANNEL HARDENING OCCURRENCE

Tese apresentada ao Curso de Doutorado em Engenharia de Teleinformática da Universidade Federal do Ceará, como parte dos requisitos para obtenção do Título de Doutor em Engenharia de Teleinformática. Área de concentração: Sinais e Sistemas

Aprovado em: 11/12/2018.

BANCA EXAMINADORA

Prof. Dr. Francisco Rodrigo Porto Cavalcanti (Orientador)
Universidade Federal do Ceará

Dr. Igor Moaco Guerreiro (Coorientador)
Universidade Federal do Ceará

Prof. Dr. Taufik Abrão
Universidade Estadual de Londrina

Prof. Dr. Vicente Angelo de Sousa Junior
Universidade Federal do Rio Grande do Norte

Prof. Dr. Emanuel Bezerra Rodrigues
Universidade Federal do Ceará

Prof. Dr. Tarcisio Ferreira Maciel
Universidade Federal do Ceará

ACKNOWLEDGEMENTS

Though only my name appears on the cover of this work as author, many people have contributed to its production. I would like to offer my sincere thanks to all of them.

First and above all, I thank God for providing me this opportunity and granting me the capability to successfully proceed.

Special thanks go to my supervisor Prof. Dr. Fco. Rodrigo P. Cavalcanti. I greatly appreciate the freedom you have given me to find my own path and the guidance and support you offered when needed. Your advice on both research as well as on my career have been invaluable.

I would also like to thank my co-supervisor Dr. Igor Moaco Guerreiro who guided me step by step into the MIMO research area and advised me with insights.

I am also very grateful to my supervisors at Ericsson in Sweden - Mårten Ericson, Magnus Stattin and Icaro Leonardo da Silva. Important discussions arose at our meetings.

Most important, none of this would have been possible without the love and patience of my family. I am extremely grateful to my parents, my sister and my girlfriend, for their love, prayers and caring. Although they hardly understand what I research on, they are willing to support every decision I take.

Finally, I acknowledge the technical and financial support from FUNCAP, CAPES under grant 88881.132080/2016-01 and Ericsson Research, Sweden, and Ericsson Innovation Center, Brazil, under UFC.40 and UFC.43 Technical Cooperation Contracts Ericsson/UFC.

RESUMO

Sistemas 5G serão baseados na implantação de largos conjuntos de antenas operando no espectro de ondas milimétricas para suportar o aumento significativo no tráfego de dados. Com mais antenas e maior largura de banda, a estimação da qualidade do canal e o envio dessas medidas do usuário para a estação rádio base serão processos computacionalmente mais complexos que os atuais e envolverão maior sinalização. Neste contexto, a presente tese analisa duas estratégias para tratar ambos os problemas: aumento de tráfego de dados e de sinalização. A primeira estratégia consiste em explorar a redução das flutuações do canal devido ao uso de feixes estreitos com largos conjuntos de antenas (o canal "endurece"). Quando este fenômeno ocorre, funções de camadas superiores baseadas em medições podem ser otimizadas. A segunda estratégia é relacionada à integração entre sistemas 5G e LTE. Mais precisamente, os usuários têm a capacidade de se conectarem simultaneamente a sistemas de ambas as tecnologias. Isto é chamado conexão dual. Antes de abordar essas duas estratégias, apresentamos uma visão geral das principais características do 5G usadas nessa tese e padronizadas pelas especificações do 3GPP versão 15. Depois disso, apresentamos análises gerais relacionadas à conexão dual e ao endurecimento do canal. Finalmente, investigamos esses dois conceitos da perspectiva da alocação de recursos de rádio. Mais especificamente, propomos soluções baseadas no endurecimento do canal e relacionadas à medição da qualidade do canal e ao envio destes dados. Além disso, também apresentamos soluções para seleção de estação rádio base e alocação de recursos em sistemas com múltiplas tecnologias e múltiplas conexões. Análises numéricas considerando parâmetros 5G são apresentadas para validar os métodos propostos.

Palavras-chave: conexão dual, endurecimento do canal, medição e envio da qualidade do canal, alocação de recursos.

ABSTRACT

Fifth Generation (5G) systems are expected to deploy massive Multiple Input Multiple Output (MIMO) antennas and operate with millimeter waves in order to support a significantly increasing data traffic. With more antennas and wider bandwidth, Channel Quality Indicator (CQI) estimation and reporting will be computationally demanding, increasing signaling between Base Stations (BSs) and User Equipments (UEs). In this context, the present thesis analyzes two strategies to address both problems: increasing data traffic and signaling. The first strategy is to exploit the reduction of channel fluctuations due to the use of narrow beams with large antenna arrays, i.e., the channel "hardens". When this phenomenon happens, upper layer functions related to measurements can be optimized and signaling reduced. The second strategy concerns the adoption of a tight integration between 5G NR and LTE. More precisely, the UEs would be allowed to be simultaneously connected to both Radio Access Technologies (RATs), the so-called Dual Connectivity (DC). Before addressing these two strategies, we present an overview of the main 5G features used in this thesis and standardized in 3rd Generation Partnership Project (3GPP) specification release 15. After that, we present general analyses related to DC and Channel Hardening (CH) occurrence. Finally, we investigate these concepts from the perspective of Radio Resource Allocation (RRA). More specifically, frameworks related to CQI measurement and reporting based on CH occurrence are proposed. Besides, we also propose procedures for base station selection and resource assignment in a multi-RAT multi-connectivity system. Numerical analyses considering 5G system parameters are presented validating the proposed methods and showing that they improve system performance.

Keywords: dual connectivity, channel hardening, CQI measurement and reporting, radio resource allocation.

LIST OF FIGURES

LIST OF TABLES

LIST OF ABBREVIATIONS AND ACRONYMS

3GPP	3rd Generation Partnership Project
4G	Fourth Generation
5G	Fifth Generation
5GC	5G Core Network
AP	Access Point
BB	Branch and Bound
BLER	BLock Error Rate
BS	Base Station
CDF	Cumulative Distribution Function
CH	Channel Hardening
CN	Core Network
CQI	Channel Quality Indicator
CRI	CSI-RS resource indicator
CRS	Cell specific Reference Signal
CSI	Channel State Information
CSI-RS	Channel State Information Reference Signal
DC	Dual Connectivity
eMBB	Enhanced Mobile Broadband
EPA	Equal Power Allocation
EPC	Evolved Packet Core
FS	Fast-RAT Scheduling
HetNet	Heterogeneous Network
HPBW	Half Power Beamwidth
IID	Independent and Identically Distributed
ITU	International Telecommunication Union
KPI	Key Performance Indicator
LI	Layer Indication
LOS	Line of Sight
LTE	Long Term Evolution
MCS	Modulation and Coding Scheme
METIS	Mobile and Wireless Communications Enablers for the Twenty-twenty Information Society 5G
MF	Matched Filter
MIB	Master Information Block
MILP	Mixed Integer Linear Programming
MIMO	Multiple Input Multiple Output

mmMAGIC	Millimetre-Wave Based Mobile Radio Access Network for Fifth Generation Integrated Communications
MMSE	Minimum Mean Square Error
mMTC	Massive Machine-Type Communications
mmWave	Millimeter Wave
MN	Master Node
MSE	Mean Squared Error
NLOS	Non-Line of Sight
NR	New Radio
OFDM	Orthogonal Frequency Division Multiplexing
PBCH	Physical Broadcast Channel
PDCP	Packet Data Convergence Protocol
PDU	Protocol Data Unit
PF	Proportional Fairness
PMI	Precoding Matrix Indicator
PSS	Primary Synchronization Signal
QoS	Quality of Service
QuaDRiGa	QUAsi Deterministic RadIo channel GenerAtor
RAT	Radio Access Technology
RB	Resource Block
RI	Rank Indicator
RMSI	Remaining Minimum System Information
RRA	Radio Resource Allocation
RRC	Radio Resource Control
RRM	Radio Resource Management
RSRP	Reference Signal Received Power
RSRQ	Reference Signal Received Quality
RSSI	Received Signal Strength Indicator
SINR	Signal to Interference-plus-Noise Ratio
SN	Secondary Node
SNR	Signal to Noise Ratio
SSB	Synchronization Signal Block
SSS	Secondary Synchronization Signal
TDD	Time Division Duplex
TR	Technical Report
TS	Technical Specification
TTI	Transmission Time Interval
TTT	Time-To-Trigger
UDP	User Datagram Protocol

UE	User Equipment
URLLC	Ultra-Reliable and Low-Latency Communications
V2X	Vehicle-to-Everything
Wi-Fi	Wireless Fidelity
WiMAX	Worldwide Interoperability for Microwave Access
WLAN	Wireless Local Area Network
WMAN	Wireless Metropolitan Area Networks
WPAN	Wireless Personal Area Networks
WWAN	Wireless Wide Area Networks
ZF	Zero-Forcing

LIST OF SYMBOLS

$(\cdot)^{\mathrm{T}}$	Vector/Matrix transposition operator
$\odot$	Hadamard product operator
$\otimes$	Kronecker product operator
$\mathbf{0}_{a\times b}$	Matrix with dimension $a \times b$ composed by 0's
$\mathbf{0}_a$	Column vector with length a with all elements equal to 0
$\mathbf{1}_a$	Column vector with length a with all elements equal to 1
B_n	Number of BSs of RAT n
$\mathcal{B}$	Set of BSs
B	Number of BSs
$\mathbf{I}_a$	Identity matrix with order a
K_n	Number of RBs used by BSs of RAT n
$\mathcal{K}$	Set of RBs
K	Number of RBs
$\mathcal{N}$	Set of RATs
N	Number of RATs
$\mathcal{O}(\cdot)$	Complexity order
P_n	Total available power at each BS of RAT n
$\mathcal{U}$	Set of UEs
U	Number of UEs
Y	Number of beams considered in the beam consolidation
Ω	Matrix with element (k,n) equal to $\omega_{k,n}$
$\mathrm{vec}\{\cdot\}$	Vectorization operator
$\gamma_{u,k,b}$	SNR between BS b and UE u in RB k
$\lambda_{b,n}$	Binary variable which indicates if BS b belongs to RAT n
N_{slot}^{frame}	Number of slots in one frame
N_{symbol}^{slot}	Number of symbols in one slot
$N_{slot}^{subframe}$	Number of slots in one subframe
Λ	Matrix with element (b,n) equal to $\lambda_{b,n}$
$\mathbf{R}^{(2)}$	Mode-2 unfolding of $\overline{\mathbf{R}}$, with element $(k,u+(b-1)U)$ equal to $r_{u,k,b}$
$\mathbf{X}^{(2)}$	Mode-2 unfolding of $\overline{\mathbf{X}}$, with element $(k,u+(b-1)U)$ equal to $x_{u,k,b}$
Ξ	Binary assignment matrix with element (u,b) equal to $\xi_{u,k}$
$\omega_{k,n}$	Binary variable which indicates if RB k can be used by the BSs of RAT n
$\overline{\mathbf{R}}$	Tensor composed by the elements $r_{u,k,b}$
$\overline{\mathbf{X}}$	Binary assignment tensor composed by the elements $x_{u,k,b}$
ψ_u	Minimum rate requirement of the UE u
$\mathcal{B}_n$	Set of BSs of RAT n

$\mathcal{K}_n$	Set of RBs used by BSs of RAT n
$\mathcal{U}_b$	Set of UEs of BS b
σ^2	Thermal noise power
θ_u	Mean throughput of UE u
$\mathbf{g}$	Binary assignment vector with element (u) equal to g_u
$\boldsymbol{\psi}$	Column vector with element u equal to ψ_u
$\xi_{u,b}$	Slack binary variable which indicates if BS b has allocated any RB to UE u
$\arg\max_{x \in \mathcal{A}} \{f(x)\}$	Maximum argument $x \in \mathcal{A}$ of a function $f(x)$
$\arg\min_{x \in \mathcal{A}} \{f(x)\}$	Minimum argument $x \in \mathcal{A}$ of a function $f(x)$
b	BS index
g_u	Number of received bits by UE u
$h_{u,k,b}$	Channel coefficient between BS b and UE u in RB k
k	RB index
$l_{u,n}$	Maximum number of BSs of RAT n that UE u can connect to at the same time
$\mathbf{L}$	Matrix with element (u, n) equal to $l_{u,n}$
n	RAT index
$p_{u,k,b}$	Power allocated by BS b to UE u through RB k
$r_{u,k,b}$	Number of transmitted bits to UE u by BS b in RB k, if this RB is allocated to UE u
t	TTI index
u	UE index
$x_{u,k,b}$	Binary variable which indicates if the RB k is assigned to the UE u by BS b

SUMMARY

1 INTRODUCTION

In the last few years, academia and industry were together in international consortia, e.g. the Mobile and Wireless Communications Enablers for the Twenty-twenty Information Society 5G (METIS) project, discussing scenarios and requirements related to the next generation of wireless cellular networks, the Fifth Generation (5G). Based on the agreements of these discussions, the International Telecommunication Union (ITU) categorized the envisioned use cases into 3 groups [1]:

- **Enhanced Mobile Broadband (eMBB)** — This is an evolution of today's human-centric cases for access to multimedia content, but with significantly increased data traffic and transmission rates;
- **Ultra-Reliable and Low-Latency Communications (URLLC)** — This category includes services with strict requirements of latency, reliability and availability, such as self-driving cars and remote medical surgery;
- **Massive Machine-Type Communications (mMTC)** — This scenario addresses a very large number of connected devices, each transmitting a low volume of data and with constraints on their prices and battery life. Sensors and actuators in a smart city are examples of these devices.

For each of these use cases, ITU set the key requirements that must be achieved in 5G networks. They are listed in [2]. For example: the network must provide for eMBB User Equipments (UEs) a downlink data rate of at least 100 Mbps when accessing multimedia content in dense urban areas; URLLC UEs must experience a maximum latency of 1 ms; and mMTC scenarios must support a minimum of one million connected devices per square kilometer.

Aiming at supporting this wide range of services, the 3rd Generation Partnership Project (3GPP) has already released the first sets of 5G standards, known as 3GPP specification 38 series release 15 [3]. They were delivered in December 2017 and June 2018 [4], and they are called as non-standalone and standalone 5G radio specifications, respectively. On one hand, in the non-standalone, the control plane connection to the core network is done through Long Term Evolution (LTE), while data capacity is boosted through 5G New Radio (NR). On the other hand, in the standalone, 5G NR has full control plane support and does not need to rely on LTE for control plane communications.

To achieve the performance requirements set by ITU in [2], the 5G specifications not only improve features already present in LTE, but also consider new ones. Some of the key NR features are [5, 6]: adoption of a flexible and scalable physical layer numerology, support to low and high frequency bands, deployment of massive Multiple Input Multiple Output (MIMO) antenna arrays and multi-beam operation. Regarding the scalable numerology, a frequency dependent frame structure will enable service-specific adaptations, improving energy and spectral efficiency. Concerning the wide spectrum, low frequency bands, e.g., below 6 GHz, will be useful for mMTC cases where coverage is important, while high frequency bands, e.g., 60 GHz, will be useful for eMBB cases where higher throughput can be achieved.

In Millimeter Wave (mmWave) frequencies, there is still a huge amount of underutilized spectrum resources [7]. However, in this part of the spectrum, the propagation conditions are challenging [7]: lower diffraction, higher path loss, and so on. This means that signals have less ability to propagate around corners and penetrate walls. In addition, atmospheric/rain attenuation and higher blockage attenuation could also contribute to making the coverage of the new 5G air interface spotty.

In order to overcome these issues, beamforming with the use of large antenna arrays is one of the considered solutions [8]. Beamforming is an array signal processing technique where multiple antenna elements are adaptively phased to form a concentrated and directed beam pattern. The narrower the beam, the higher the directivity gain is, which helps mitigate propagation losses. In order to deploy narrow beams, one needs large antenna arrays, which is not a problem in mmWaves, since their small wavelengths enable placing a large number of antenna elements into a small area.

At least two major problems arise with this solution. The system's reliability might decrease [9] while its complexity might increase [10].

Concerning the system's reliability, although beamforming overcomes the problem of high propagation losses in mmWave frequencies, a UE can be out-of-coverage if it is not well aligned with a beam. Thus, there will be a tight interworking between the 5G Radio Access Technology (RAT), called NR, and legacy standards, such as LTE. 3GPP has even standardized a Dual Connectivity (DC), where UEs are simultaneously served by LTE and NR. This tight interworking is expected to enable an early deployment of 5G NR, besides improving the throughput and ensuring connectivity when 5G NR link fails. In this thesis, we exploit solutions related to DC in order to improve Quality of Service (QoS) metrics of the system.

Regarding the system's complexity, the amount of UE measurements and reports will drastically increase [10]. This is due to the fact that 5G BS deployed in mmWaves are expected to support dozens of beams and 5G measurement model is based on beam measurements [11], instead of cell measurements as in LTE [12]. Besides, upper layer functions as Radio Resource Allocation (RRA) and UE mobility management rely on accurate channel quality estimation, thus the complexity of these functions will also increase. In order to overcome this issue, we investigate solutions that take advantage of the Channel Hardening (CH) effect [13]. As it will be explained in more details later, narrow beams may spatially filter out angular-separated taps of the channel response. This reduces the effective channel delay spread, and, as a consequence, channel variations due to fast fading also decrease (the channel "hardens"). If the channel fluctuations might decrease, one can take advantage of it and optimize functions based on measurements.

Next section presents the state-of-the-art of both concepts: DC and CH.

1.1 State-of-the-Art

1.1.1 Dual-Connectivity

From the earliest days of wireless communications, networks based on different RATs have co-existed, each of them with its own characteristics. According to their coverage range, the networks are usually classified as: Wireless Personal Area Networks (WPAN), Wireless Local Area Network (WLAN), Wireless Metropolitan Area Networks (WMAN) and Wireless Wide Area Networks (WWAN). Examples of these networks are: Bluetooth, Wireless Fidelity (Wi-Fi), Worldwide Interoperability for Microwave Access (WiMAX) and LTE, respectively. Despite their different coverage ranges, they are usually deployed in overlapping areas, hence forming a Heterogeneous Network (HetNet).

Currently, an unprecedented escalation of network densification and heterogeneity is taking placing due to the growing consumer demand for higher throughput. Besides, UEs, e.g., smartphones, are being equipped with multiple RAT interfaces, e.g., Wi-Fi and LTE interfaces, in order to be able to access the most suitable network in a giving instant of time. In [14], the author highlights seven aspects that should be taken into account in this process:

- traditional methods of *interference management* like frequency reuse or Base Station (BS) coordination may not be adequate for HetNets;
- different networks might have different *backhaul constraints* and they should be taken into account;
- one must consider *metrics* that are valid for all the networks being compared;
- since the distance to desired and interfering BSs is important in determining performance, a reasonable *topology model* is required;
- HetNets might introduce asymmetries between *uplink and downlink*, so they should be considered as two different systems;
- another topic of high importance is related to *network selection* policies as the system load fluctuates;
- moreover, it is interesting to support *mobility* between the different networks, mainly focused on how and when the users are handed off.

Regarding the aspect of RAT selection, [15] presents an overview of the most important mathematical theories for modeling the network selection in HetNets. Some of these theories are: combinatorial optimization, utility theory, Fuzzy logic, game theory and Markov chain.

An example of inter-RAT handover decision mechanism can be found in [16]. It considers the co-existence of Wi-Fi Access Points (APs), representing small cells, and LTE

BSs, representing macro cells. In order to avoid the ping-pong effect, the authors prioritize UEs with high mobility to be connected to a LTE BS, which has a broader coverage, while UEs with low mobility tend to be connected to a Wi-Fi AP. The main reason for this is that UEs with low mobility are expected to keep a more stable connection to a Wi-Fi AP than a UE with high mobility.

Unfortunately, in the method presented in [16], moving UEs do not benefit from the advantages of both RATs. In order to address this problem, 3GPP specification 36 series release 12 [17] standardized the concept of DC for LTE. This mechanism allows the UEs to consume radio resources provided by two different network points at the same time. For this, it was proposed the split of user and control planes, where the control plane manages system information and the user plane transmits user data.

Many works have already investigated the concept of DC proposed in [17]. Usually, a centralized entity, called *cloud*, is considered in order to centralize system information and take better decisions regarding resource management [18]. For example, [19] considered a Time Division Duplex (TDD) based system and proposed a framework based on the channel quality of uplink rather than downlink signal quality, as in traditional LTE systems. The use of uplink signals eliminates the need for the UE to send measurement reports back to the network and thereby removes a point of failure in the control signaling path. The framework proposed in [19] is split into 3 stages. In the first one, the UEs broadcast uplink reference signals, which are measured by the BSs. After that, these measurements are sent to a centralized controller, which will finally make handover and scheduling decisions based on these measurements.

Centralized processing has practical issues related to backhaul constraints, e.g., limited capacity and delay on the interfaces, which can reduce the spectrum efficiency gain achieved by the cloud [20]. Besides, a centralized solution is computationally intensive and also incurs in signaling overhead due to the need of global information.

One possible solution for overcoming the centralized processing drawbacks is presented in [21]. The authors studied the problem of traffic offloading via dual connectivity in the uplink. Since data flows from the UEs to the BSs, each UE independently selects its percentage of data to transmit to each BS.

As one can see, different approaches can be adopted when implementing DC. Thus, 3GPP specification release 15 standardized in [22] the options that will be accepted for DC between 5G NR and LTE. The technical details will be presented in Chapter 2.

Before being standardized, DC between 5G NR and LTE was discussed by academia and industry in international consortia, e.g., the METIS project. Report [23] was one of the first works to propose a tight interwork between 5G air interface and legacy standards such as LTE. Until then, the majority of works covering heterogeneous systems either considered Wi-Fi associated with LTE, as in [16], or considered only LTE BSs with different coverage ranges, as in [24].

The authors of [25] performed initial analyses related to mobility robustness and reliability in a dense urban scenario using DC between LTE macro BSs and 5G small BSs. They concluded that the reliability is still below the target expected for 5G. To achieve the desired target, other features should also be considered as make-before-break, packet duplication and handover prediction.

A make-before-break scheme based on DC is proposed in [26]. The main objective is to get 0 ms interruption during a handover procedure. In this approach, DC allows a target BS to be added as a secondary BS while the UE is still connected to the serving one. Thus, the UE will keep its connection with the source BS until it is able to receive packets from the target BS. At this time, target and source BSs can switch the roles of primary and secondary, and, finally, the old BS can be released.

In the previous strategy, it is quite challenging to know the right timing when a UE should stop receiving from the source BS and start receiving from target one without interruption or loss of packets. Thus, packet duplication on both links could be used in URLLC, as done in [27]. The authors of [27] adopted this strategy to improve the connection robustness for Vehicle-to-Everything (V2X) use cases while ensuring that packets are reliably transmitted with low interruption time. They admit that this approach increases resource usage. Thus, to achieve a balanced trade-off between reliability and resource usage they suggest to dynamically control the activation of packet duplication to certain scenarios when channel conditions are typically unfavorable.

Regarding handover prediction, an example can be found in [28]. The authors propose a scheme operated at the UE that predicts the expected handover time in addition to the target BS. The UE speed and direction are utilized to narrow down the candidate BSs and minimize processing. DC is used together with this scheme to allow the UEs to perform advanced handover signaling via a second link.

A final remark concerning DC is that it is not always better than a single connection. One can think that a UE will always benefit from a larger transmission bandwidth. However, from the network's perspective, when the load is high and the UEs are trying to connect to more than one BS at the same time, the network becomes interference-limited and the system's performance decreases very fast. In this case, a single connection might be preferable. This conclusion is analytically demonstrated in [29].

1.1.2 Channel Hardening

The idea that the channel fluctuations might decrease due to the deployment of large antenna arrays and the use of narrow beams is not new. In 1966, W. C. Y. Lee confirmed this experimentally and reported his results in [30]. He noticed that the number of times the fading signal crossed an arbitrarily chosen level below the average signal strength increased significantly with the beamwidth. Furthermore, in 1968, R. H. Clarke concluded in [31] that narrow beams reduces not only the rate of fading but also the fading depth.

Although this is not a new concept, the term CH is quite new. One of the first works to use it was [32]. The authors analyzed this effect from the perspective of information theory. They considered a MIMO channel matrix with independent zero-mean complex-Gaussian entries to demonstrate that, as the number of antennas increases, the variance of channel mutual information decreases rapidly relative to its mean. Hence, the distribution of the mutual information approaches a Gaussian [32]. In other words, the channel fluctuations relative to its mean decreases (the channel "hardens") and the channel gains become nearly deterministic. This definition can be formulated as [33]:

$$\frac{||\mathbf{h}_k||^2}{\mathrm{E}\left\{||\mathbf{h}_k||^2\right\}} \longrightarrow 1, \text{ as } M \longrightarrow \infty, \; k = 1, \ldots, K, \tag{1.1}$$

where $\mathbf{h}_k$ is the $M \times 1$ channel vector between UE k and a BS with M antennas, $||\cdot||$ is the Euclidian norm and $\mathrm{E}\{\cdot\}$ is the expectation operator.

In the following, a simple example is presented to illustrate this concept. The left hand side of Fig. 1.1 presents a transmitter with M antennas, while the right hand side presents the evolution in time of the h_i links. Suppose that all the h_i links are independent and that the probability of one of them is facing a deep fading is P, then the probability of all of them is fluctuating is P^M. Thus, when the number of antennas grows (i.e., $M \longrightarrow \infty$), this probability becomes too small. The red dashed line in the right hand side of Fig. 1.1 presents the envelope link. Notice that in this example there is always at least one link in good conditions, so the envelope fluctuates much less than the links themselves.

Figure 1.1 – CH due to the deployment of large antenna array.

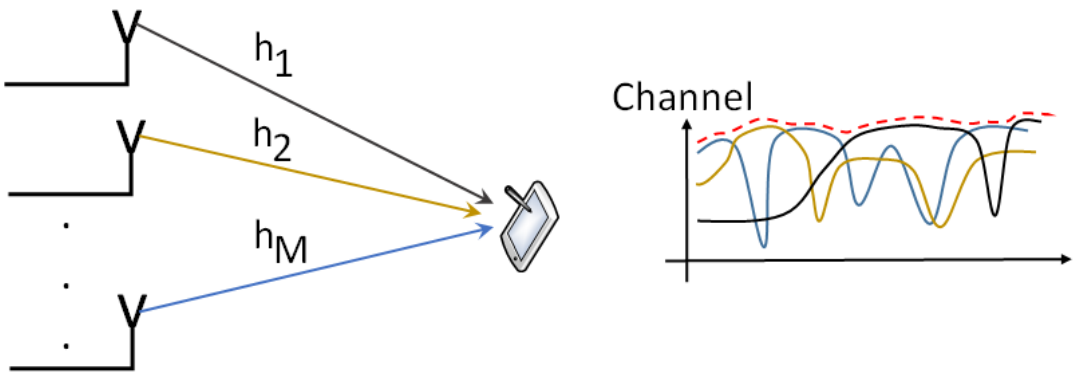

Source: Created by the author.

CH depends on the characteristics of the channel. Some works, as [33] and [34], assume the uncorrelated Rayleigh channel model to demonstrate that (1.1) can be achieved. For this model, the channel becomes flat in both time and frequency domains when $M \longrightarrow \infty$. This is due to the law of large numbers. Many random channel realizations are combined, which reduces the total channel variation. However, this assumption may not be verified in real 5G systems. Firstly, the number of antennas cannot tend to infinity. Secondly, spatially correlated fading has been observed in practical measurements [35].

Figure 1.2 – CH due to the use of narrow beams.

(a) Wide beam. (b) Narrow beam.

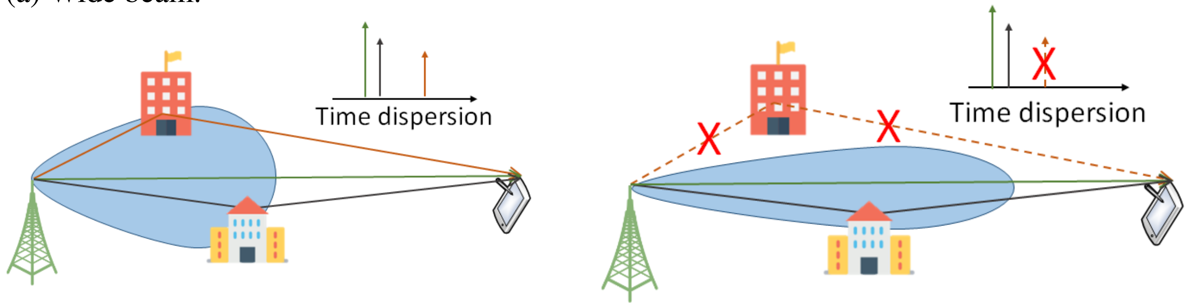

Source: Created by the author.

The authors of [36] analyzed how close to the asymptotic CH one can be with a practical number of antennas. They concluded that, under uncorrelated fading, $M = 100$ is typically sufficient to benefit from almost perfect CH. They also concluded that under spatially correlated fading, it is still possible to achieve CH, however the number of required antennas increases compared to the previous case. Moreover, they demonstrated that in the extreme case when the spatial correlation matrix has rank one, CH does not occur. Complementary to this work, the authors of [37] also analyzed the CH in a scenario not limited to classically assumed Rayleigh fading. They used a physically motivated ray-based channel model to derive an expression of CH measure.

From another perspective, one can also obtain the CH as a consequence of the use of narrow beams, allowed by the deployment of large antenna arrays. As illustrated in Fig. 1.2, transmitter and receiver are surrounded by objects which reflect and scatter the transmitter energy, causing several waves to arrive at the receiver via different routes [38]. These multipath components usually have different phase and amplitude leading to frequency selective fading and time dispersion [39]. In the frequency domain, the coherence bandwidth of a channel is a metric used to measure the range of frequencies over which all spectral components have approximately equal gain and linear phase, i.e., the range of frequencies over which the channel can be considered "flat". In the time domain, the RMS delay spread is used as an indicator of dispersion. It takes into account the relative power of the different taps as well as their delays. Important to highlight that the coherence bandwidth and the RMS delay spread are inversely proportional. When deploying narrow beams, as in Fig. 1.2b, they might act as a spatial filter (with narrow spatial bandwidth) on different delay taps of the channel response. Since part of the scatters are no longer illuminated, the channel delay spread might be reduced and the overall channel response might look flat. In general, the narrower the beam the flatter the channel response is. This effect was predicted in [40].

Based on measurement campaigns, the authors of [41] used massive MIMO antennas with beamforming and verified the existence of CH in a real environment. The results were compared with an Independent and Identically Distributed (IID) Gaussian random channel with the same average power. Even if the measured hardening was not as strong as in the Gaussian

Figure 1.3 – CH in an indoor environment.

(a) Scenario.

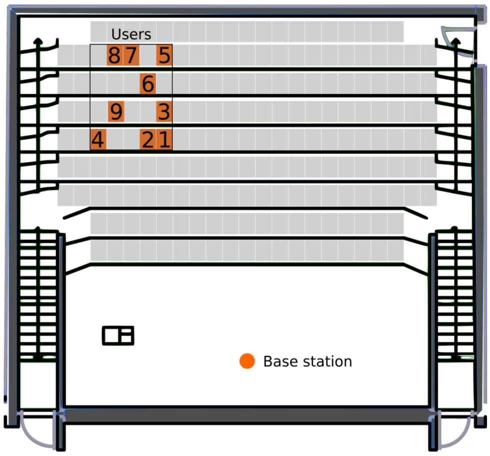

(b) Result.

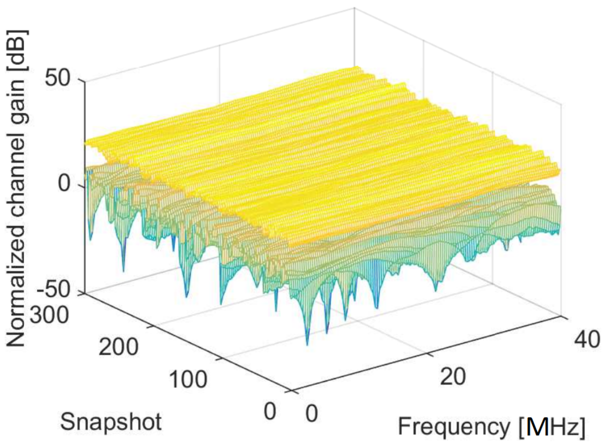

Source: [43].

channel, it was observed.

Works [42, 43, 44] also identified the existence of CH in real environments based on measurements. On one hand [42, 43] conducted measurements in indoor environments, more specifically, a subway station and an auditorium, respectively. On the other hand, [44] considered moving UEs in an outdoor environment.

Regarding [43], the authors considered an indoor crowded auditorium at Lund University with one BS and nine closely-spaced UEs placed as depicted in Fig. 1.3a. Line of Sight (LOS) propagation conditions predominated, with occasional blocking due to other UEs or room furniture. The BS acted as a receive unit and it was equipped with 64 dual-polarized patch antennas, i.e., 128 antenna elements. UEs and BS were communicating at center frequency of 2.60 GHz and bandwidth of 40 MHz, resulting in 129 measured points in frequency and 300 snapshots taken over 17 s. Fig. 1.3b presents the normalized channel gains of UE 1 when using one antenna (green lower layer) versus the case of combining the channel of all 128 antenna elements (yellow upper layer). Notice that the channel of just one antenna element presents many severe dips and varies much more than the case with 128 antenna elements. In other words, the channel hardened when considering more antenna elements.

Concerning [44], the authors considered the uplink communication between single antenna UEs and a BS with 100 antenna elements deployed at 3.70 GHz and bandwidth of 20 MHz. Fig. 1.4a presents one of the analyzed scenarios as viewed from the BS. The considered UE was moving at a speed of 29 km/h. Its trajectory is indicated by the yellow arrow in Fig. 1.4a. Fig. 1.4b presents the relative channel magnitude measured by a single antenna and the composite channel of the 100 antenna elements. The authors concluded that the composite channel tends to follow the average of the single antenna case, smoothing out the fast fading. In the analyzed scenario, larger variations started to occur over the course of seconds rather than milliseconds. They also noticed improvements in robustness and latency due to the mitigation of fast-fading error bursts. Another verified benefit of CH was the possibility to relax the update rate of power

Figure 1.4 – CH in an outdoor environment.

(a) Scenario.

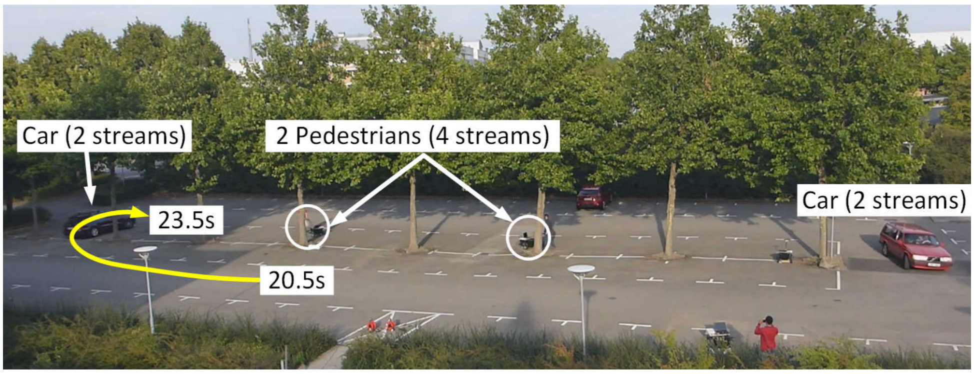

(b) Result.

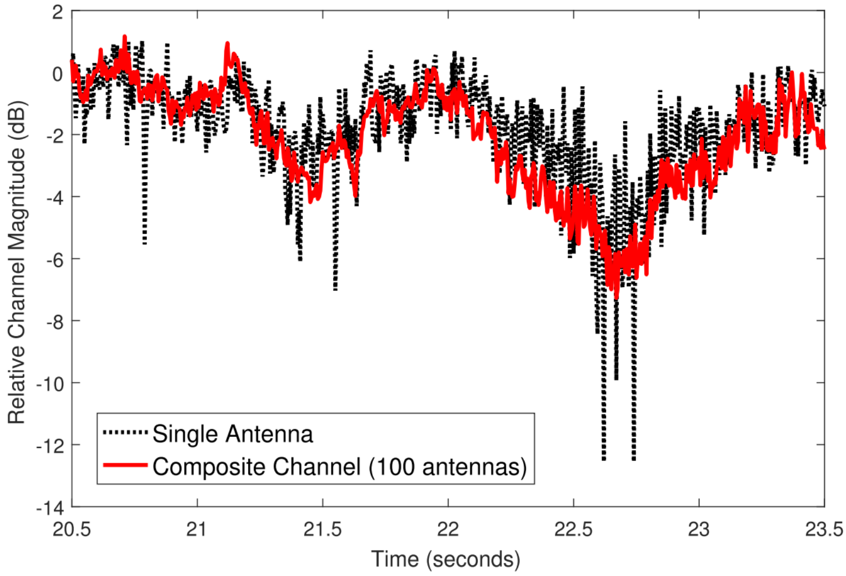

Source: [44].

control when increasing the number of antennas. In [45], some of the authors of [44] investigated the practicality of relying on the CH in their design and proposed a power control algorithm exploiting CH properties.

In the literature, it is possible to find works assuming the existence of CH to simplify the adopted models. In [46], the power allocation matrix is based only on the large-scale fading characteristics and the same power control is applied over the whole spectrum. In [47], the authors assumed that the UEs detect downlink data coherently by assuming that the channel gain is equal to its expected value due to CH. In [48], a receiver is presented based on message passing. This receiver exploits the CH for the purposes of detection and channel estimation. In [49], CH and spatial resolution properties of massive MIMO are used to derive a new protocol enabling distributed collision detection and resolution at the UEs.

As already mentioned, CH is not always sufficiently pronounced, so one needs to be careful when making these assumptions. Works [50] and [51] considered a different deployment of massive MIMO called cell free or distributed. In this scenario, multiple antennas of a BS are clustered in geographically separated APs which jointly serve the UEs. These works showed that more antennas are needed in this kind of system to achieve the same level of CH as in co-located massive MIMO antennas, since it is very likely that each UE is most effectively served by only part of the APs.

It is also important to remark that, although the majority of the works exploits the CH in the time domain, CH is also present in the frequency domain, as demonstrated in [52]. That work showed that the asymptotic Mean Squared Error (MSE) of the estimated transmitted symbols may converge to a deterministic quantity not depending on the subcarrier index, i.e., the channel becomes flat across the frequency band. They presented this result for three types of linear receivers, namely, Zero-Forcing (ZF), Matched Filter (MF) and Minimum Mean Square Error (MMSE).

Furthermore, the authors of [53] introduced a general definition for the hardening phenomena that includes, but is not limited to, CH. They verified that other metrics in MIMO systems, after being normalized by their mean, as the channel is in Equation (1.1), converge to 1 as the number of antennas increases. They provide a simple example considering the distance between arbitrary received code words.

1.2 Objectives and Thesis Structure

Considering what has been presented in the previous section, the main objective of this thesis is to address, in the downlink, the eMBB requirements and the expected lean signaling in 5G based on DC and CH occurrence.

The thesis structure is presented in Fig. 1.5 and is described in the following. On one hand, general analyses related to DC and CH occurrence are presented in Chapter 3 and Chapter 4, respectively. On the other hand, these concepts are addressed from the perspective of Radio Resource Management (RRM) in Chapter 5 and Chapter 6.

More specifically, Chapter 3 aims at exploiting multi-connectivity solutions to improve QoS metrics of the system by means of efficient RAT scheduling. This chapter presents analyses concerning the metrics that should be used as RAT scheduling criterion and how frequently switching evaluations should be done. Besides, the performance of DC and Fast-RAT Scheduling (FS) solutions are compared, highlighting the scenarios in which each one of them performs better than the other.

Chapter 4 proposes a framework for CH detection and L1 measurement optimization, where the CH is detected based on the standard deviation of Reference Signal Received Power (RSRP) measurements in a sliding window and the measurement periodicity is dynamically adjusted according to the level of CH.

Chapter 5 formulates an optimization problem in order to manage resources in a multi-RAT scenario. Its objective is to maximize the minimum user throughput in the system subject to the constraint that, for each UE, its throughput must be higher than its requirement. The referred problem is non-linear and hard to solve. However, we get to transform it into a simpler form, a Mixed Integer Linear Programming (MILP), that can be optimally solved using standard optimization methods. This solution is categorized as a centralized solution. Thus, a distributed framework is also proposed to overcome the drawbacks of centralized processing. This framework is divided into two parts: a BS selection procedure (performed by the UEs) and a resource assignment algorithm (performed by the BSs). Besides, a performance evaluation is conducted, considering LTE and 5G NR parameters.

Finally, Chapter 6 focuses on RRA in order to illustrate how the proposed solutions can improve the reliability and decrease the complexity of a 5G system. Three different schedulers are considered and three different Key Performance Indicators (KPIs) are used to analyze the impact of using either FS or DC strategies and reducing Channel Quality Indicator (CQI) reporting due to CH occurrence.

Besides the already described chapters, Chapter 2 presents an overview of the main 5G features used in this thesis and specified in 3GPP specification release 15. Moreover, Chapter 7 summarizes the main conclusions of this thesis.

Figure 1.5 – Thesis structure.

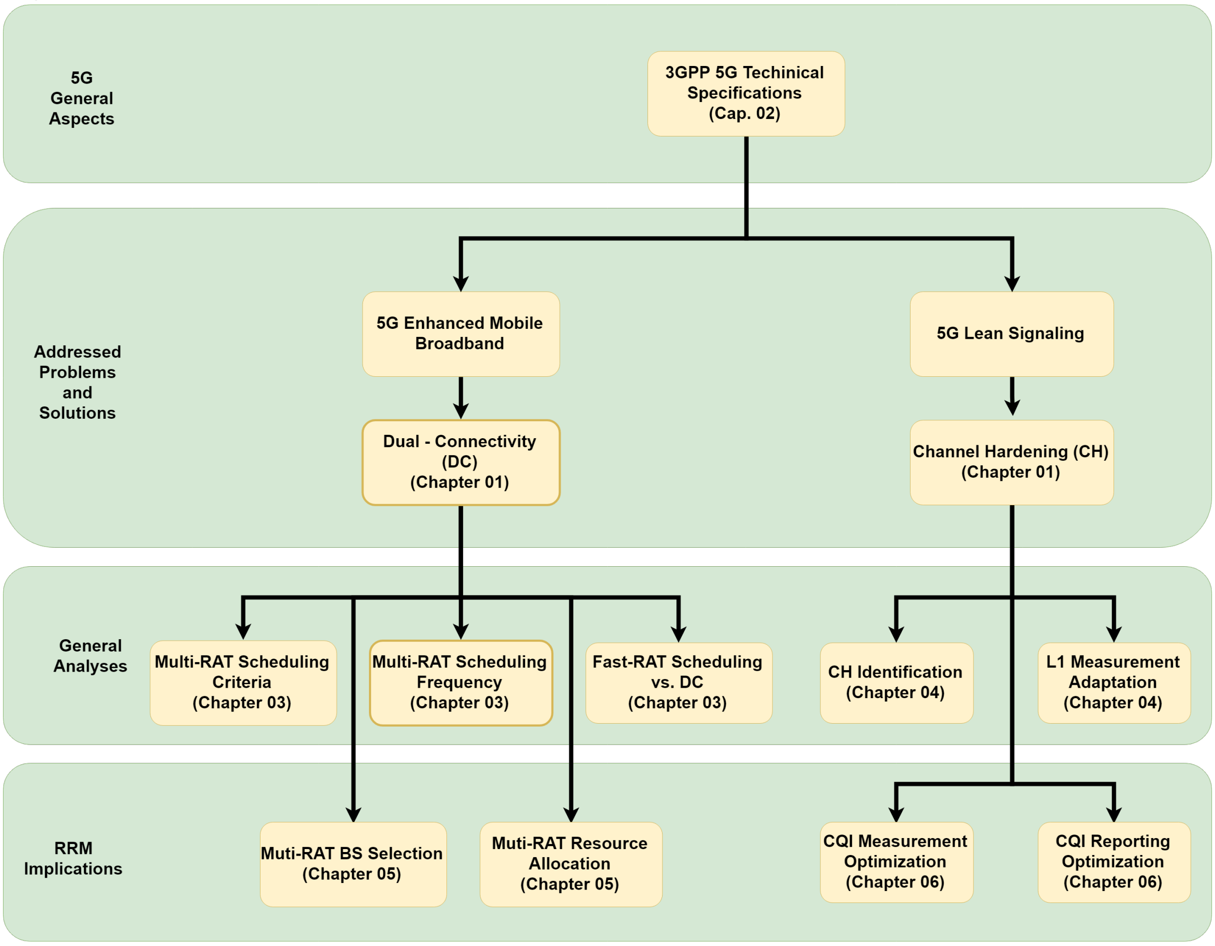

Source: Created by the author.

1.3 Scientific Contributions

Currently, the content of this thesis has been partially published with the following bibliographic information:

Journal Papers

- **MONTEIRO, V. F.**; ERICSON, M.; CAVALCANTI, F. R. P. Fast-RAT Scheduling in a 5G Multi-RAT Scenario. **IEEE Communications Magazine**, v. 55, n. 6, p. 79–85, June 2017. DOI: `10.1109/MCOM.2017.1601094`

  - This paper is listed as a publication of METIS II project in `https://metis-ii.5g-ppp.eu/documents/publications/`

- **MONTEIRO, V. F.**; SOUSA, D. A.; MACIEL, T. F.; CAVALCANTI, F. R. P.; SILVA, C. F. M.; RODRIGUES, E. B. Distributed RRM for 5G Multi-RAT Multi-Connectivity Networks. **IEEE Systems Journal**, p. 1–13, 2018. ISSN 1932-8184. DOI: `10.1109/JSYST.2018.2838335`

Patents

- **MONTEIRO, V. F.**; GUERREIRO, I. M.; FRESIA, M. **A Method, a Base Station and a User Equipment for Selecting a Set of Beams to be Monitored by Said UE**. Aug. 2017. PCT/EP2017/069410. Patent Application

- **MONTEIRO, V. F.**; ERICSON, M.; CHRISTOFFERSSON, J.; WANG, M. **Methods and Apparatus for Measurement Reporting in a Wireless Network**. Apr. 2018. WO/2018/063073. Patent Application. Available from: <`https://patentscope.wipo.int/search/en/detail.jsf?docId=WO2018063073`>. Visited on: 24 Sept. 2018

- **MONTEIRO, V. F.**; GUERREIRO, I. M.; DA SILVA, I. L. J. **Methods and Apparatus Relating to a Wireless Communication Network that Utilises Beamforming**. July 2018. PCT/EP2018/068453. Patent Application

- **MONTEIRO, V. F.**; RAMACHANDRA, P.; DA SILVA, I. L. **Measurement Adaptation Based on Channel Hardening Detection**. Nov. 2018. Provisional Patent Application

It is worth mentioning that this thesis was developed under the context of Ericsson/UFC technical cooperation projects:

- UFC.40 - *Quality of Service Provision and Control for 5th Generation Wireless Systems*, October/2014 - September/2016;

- UFC.43 - *5G Radio Access Network (5GRAN)*, November/2016 - October/2018, in which a number of eight technical reports, four in each project, have been delivered. Besides, due to this partnership, two Ph.D. internships took place during this Ph.D.:

- Feb/2016-Jun/2016: Ph.D. internship at Ericsson Research in Luleå-Sweden;
- Sep/2017-Aug/2018: Ph.D. internship at Ericsson Research in Stockholm/Kista - Sweden.

Also in the context of these projects, the author collaborated in the following scientific publication:

Journal Papers

- SOUSA, D. A.; **MONTEIRO, V. F.**; MACIEL, T. F.; LIMA, F. R. M.; CAVALCANTI, F. R. P. Resource Management for Rate Maximization with QoE Provisioning in Wireless Networks. **Journal of Communication and Information Systems (JCIS)**, v. 31, n. 1, p. 290–303, 2016. DOI: `10.14209/jcis.2016.25`

2 IMPORTANT ASPECTS OF 3GPP 5G TECHNICAL SPECIFICATIONS

The system architecture adopted in this thesis is based on 3GPP specification release 15. Thus, for the sake of completeness, this chapter provides technical insights into some 5G NR features relevant to the remaining of this thesis. However, before addressing them, next section presents a brief overview of how the 3GPP standards are conceived.

2.1 3GPP Working Process

Nowadays, 3GPP is the largest standards body in charge of the development of 5G standards. It is a collaborative effort among hundreds of different entities, such as manufacturers, mobile service providers and research institutions.

5G standards must achieve the main requirements set by ITU, an agency under the United Nations. Fig. 2.1 presents a high-level view of 3GPP working process [54] in order to deliver new technical specifications. In step 1, 3GPP members submit technical documents, called *Contributions*, to propose new solutions. These *Contributions* are discussed in regular *3GPP Meetings* and, if approved by the other 3GPP members, it becomes a *Study Item*. The *Study Items* are responsible for conducting feasibility studies on multiple solutions based on the proposed *Contributions*. Besides, the *Study Items* must deliver *Technical Reports (TRs)* detailing the agreed concepts. Based on these *TRs*, *Working Items* investigate implementation details related to the proposed concepts. Their conclusions are released in the form of *Technical Specifications (TSs)*. The *TSs* are used by industry and academia to produce standard compliant products.

Figure 2.1 – 3GPP working process.

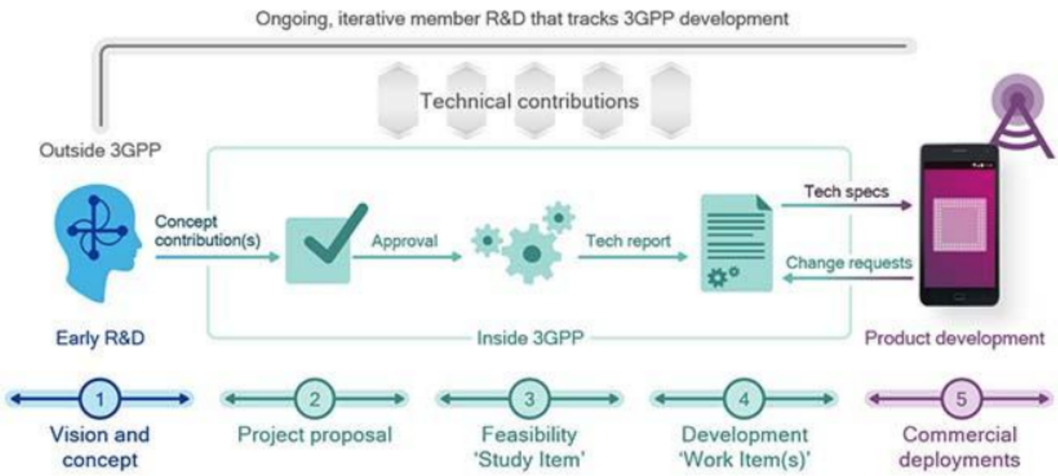

Source: [54].

Figure 2.2 – Simplistic overview of the DC architecture specified in 3GPP specification release 15, where eNB and ng-eNB provide E-UTRA protocol terminations towards the UE via EPC and 5GC, respectively, while en-gNB and gNB provide NR protocol terminations towards the UE via EPC and 5GC, respectively. The colored lines (black, brown and blue) represent the possible ways for control plane flow.

(a) DC with EPC. (b) DC with 5GC.

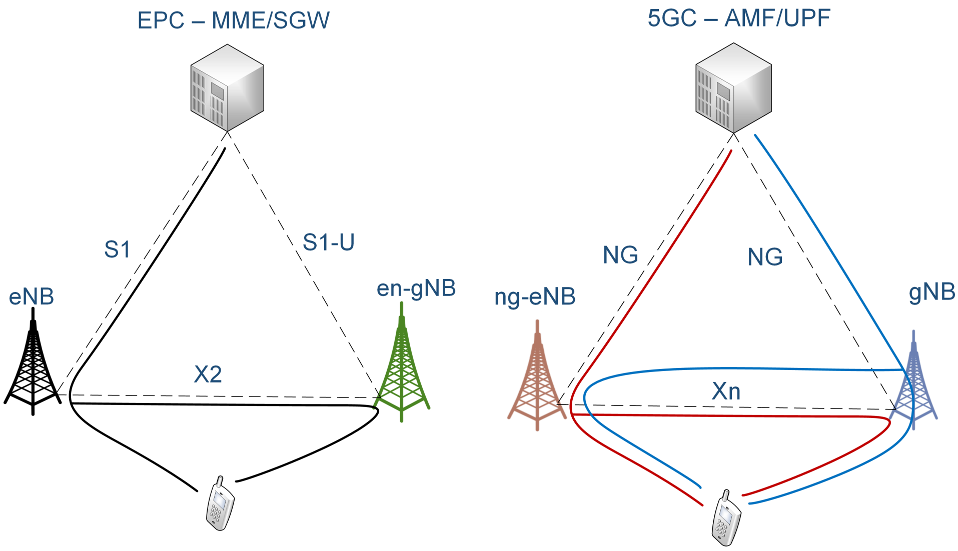

Source: Created by the author.

2.2 LTE/NR Dual Connectivity

One of the most important TS for this thesis is [22]. This TS provides the details regarding LTE and NR DC operation. It specifies that, when operating in DC mode, a UE is connected to a Master Node (MN) and a Secondary Node (SN) belonging to different RATs. These nodes are connected via non-ideal backhaul, in terms of capacity and latency, which can restrict the ability to perform inter-node coordination. The standardized architectures are presented in Fig. 2.2 according to the Core Network (CN) being used.

In Fig. 2.2a, the UE is connected to the LTE CN, i.e., the Evolved Packet Core (EPC). In this case, a LTE BS, i.e., a eNB, always acts as MN, while a 5G BS, i.e., a en-gNB, always acts as SN. This will allow an early introduction of 5G NR, since eNB and EPC are already deployed. The LTE network will handle control functionalities like connection set-up and paging, while 5G NR will be responsible for primarily providing data-rate and capacity boostering.

In Fig. 2.2b, the UE is connected to 5G Core Network (5GC). In this option, either the ng-eNB or the gNB can act as MN, while the other acts as the SN. As the eNB, the ng-eNB provides E-UTRA (the LTE air interface) protocol terminations towards the UE. The difference between them is the CN to which each one is connected to, i.e., ng-eNB connects to 5GC, while eNB is only able to connect to EPC. In a similar way, en-gNB and gNB provide NR protocol terminations towards the UE, but through different CNs.

Concerning the user plane, three bearer types exist: master, secondary and split. As

Figure 2.3 – Protocol stack for bearer flow.

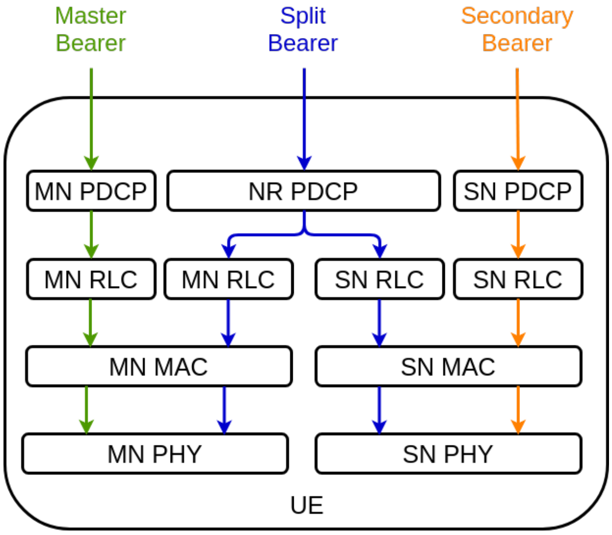

Source: Created by the author.

illustrated in Fig. 2.3, on one hand, the master and the secondary bearers are sent through the protocol stack (PDCP, RLC, MAC and PHY) related to the MN and SN, respectively. On the other hand, the split bearer is sent through the lower layers (RLC, MAC and PHY) of both nodes. In order to support this interworking, a common Packet Data Convergence Protocol (PDCP) layer is expected to be deployed across both master and secondary nodes. This common layer must be able to process Protocol Data Units (PDUs) coming from both air interfaces, i.e., NR and LTE. Thus, enhancements were made in LTE release 14 to support NR PDCP at LTE nodes and, in [22], it was standardized that the NR PDCP will be used as aggregation layer for the split bearer.

Besides the DC, this thesis also considered a FS architecture, proposed in [55] and illustrated in Fig. 2.4. The main difference between DC and FS is that, while, in DC, the UE user plane is allowed to stay simultaneously connected to both LTE and NR BSs, in FS, it is allowed to be connected to only one of them at a time. Concerning the UE control plane, it might stay always connected to the RRC layer of both master and secondary nodes. These RRC connections would be responsible for allowing the UE user plane in the FS mode to switch very fast between the RATs, since no signaling exchanging between the core and the master would be required.

2.3 Flexible Physical Layer

Besides the co-existence of NR and LTE, 3GPP also standardized a scalable physical layer design for NR. As in LTE, Orthogonal Frequency Division Multiplexing (OFDM) was adopted as waveform of 5G NR. However, different of LTE, 5G NR is expected to support more than one value of subcarrier spacing as specified in [56] and presented in Table 2.1.

A larger subcarrier spacing is beneficial from a frequency-error perspective as it reduces the impact of frequency errors and phase noise. However, for a certain cyclic prefix length, the relative overhead increases the larger the subcarrier spacing and from this perspective

Figure 2.4 – Comparison of DC and FS architectures. In DC, control and user planes from master and secondary can be simultaneously connected to the UE, while in FS, the user plane must switch between master and secondary.

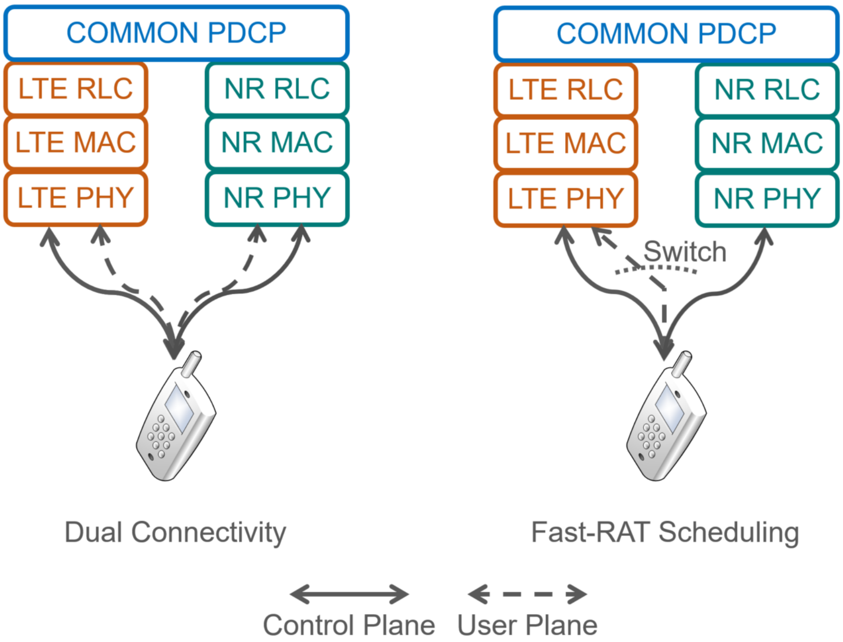

Source: Created by the author.

Table 2.1 – Supported transmission numerologies.

μ	**Subcarrier Spacing** $2^{\mu} \cdot 15$ **[kHz]**	**Cyclic Prefix** [μs]	**Slot Duration [ms]**	N^{slot}_{symbol}	$N^{subframe}_{slot}$	N^{frame}_{slot}
0	15	4.7	1	14	1	10
1	30	2.3	0.5	14	2	20
2	60	1.2	0.25	14	4	40
3	120	0.59	0.125	14	8	80
4	240	0.29	0.0625	14	16	160

Source: Created by the author.

a smaller cyclic prefix would be preferable [57]. The selection of the subcarrier spacing therefore needs to carefully balance overhead from the cyclic prefix against sensitivity to Doppler spread and phase noise.

In NR, having a single subcarrier spacing would not be possible, since it is designed to support a wide range of deployment scenarios, from large cells deployed in sub-6 GHz carrier frequency up to small cells deployed in mmWave band with very wide spectrum allocations.

For sub-6 GHz deployments, the cell size can be relatively large and a cyclic prefix capable of handling the delay spread (in the order of a couple of microsseconds) is necessary. Consequently, a subcarrier spacing equal to the one of LTE (15 kHz) or somewhat higher is needed.

In mmWave bands, phase noise becomes more critical, calling for higher subcarrier spacing. At the same time, due to the challeging propagation conditions in these frequencies, the expected cell size is smaller, which helps to reduce the delay spread. Thus, for these frequencies, a higher subcarrier spacing and a shorter cyclic prefix is suitable.

Regarding the time domain structure, illustrated in Fig. 2.5, regardless of the adopted numerology, NR transmissions are divided into *frames* of length equal to 10 ms, each of which is divided into 10 equally sized *subframes* of length equal to 1 ms. A *subframe* is in turn divided into *slots* consisting of 14 OFDM symbols each. Since, when doubling the subcarrier spacing the OFDM symbol duration halves due to the nature of OFDM, there is a different number of *slots* within one *subframe* for each numerology, as presented in Table 2.1 and in Fig. 2.5. Remark that the number of OFDM symbols in one *subframe* changes according to the value of subcarrier spacing.

It is important to highlight that some definitions in LTE and NR are the same, as the duration of a *frame* and of a *subframe*. However, other definitions changed. In LTE, a *slot* consists of 7 OFDM symbols, instead of 14 as in NR, and a LTE *subframe* always consists of 2 *slots* [58]. Due to these different definitions, in LTE, a *subframe* is the minimum scheduling unit, while in NR a *slot* is the typical scheduling unit.

Another difference between LTE and NR definitions is seen in the frequency domain structure. While the term *resource element* is used by both technologies to refer to one subcarrier during one OFDM symbol, the term *resource block* is used in different ways. On one hand, in NR, a *resource block* is an one-dimensional measure spanning only the frequency domain, more specifically, it corresponds to 12 consecutive subcarriers. On the other hand, in LTE, a *resource block* is a two-dimensional set consisting of 12 subcarriers in the frequency domain and one *slot* in the time domain. One reason for defining, in NR, a *resource block* only in the frequency domain is the flexibility in time duration for different transmissions.

2.4 CSI-RS and SSB

As presented in Chapter 1, procedures as RRA and UE mobility management rely on accurate channel quality estimation. For this, BSs and UEs are periodically transmitting and receiving synchronization and reference signals. Thus, in this section, we address two of them: Channel State Information Reference Signal (CSI-RS) and Synchronization Signal Block (SSB).

CSI-RS

As in LTE, in NR, the CSI-RSs are used for Channel State Information (CSI) acquisition, which is important for scheduling and link adaptation. Besides, in NR, their use has been broadened and they are also used for RSRP measurements, which are taken into account for example for mobility management.

Regarding the RSRP measurement procedure, the SSBs are also used to this purpose. In this case, the main difference between SSBs and CSI-RSs is the way how the UE can measure

Figure 2.5 – Frame, subframe and slots in NR.

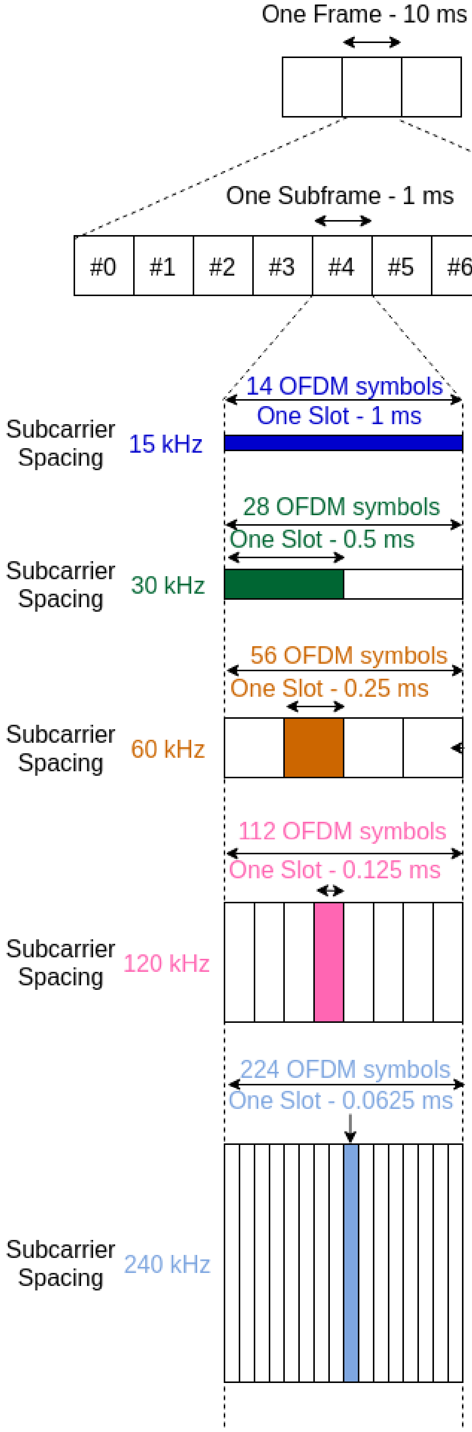

Source: Created by the author.

Figure 2.6 – SSB and CSI-RS beams.

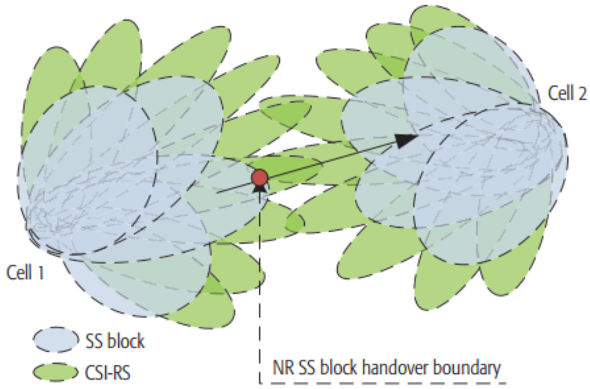

Source: [60].

them. The SSBs are blindly decoded, which means that even in idle mode the UEs can detect and decode them. However, in order to decode the CSI-RSs, the UEs must be already connected, since they need to be configured in advance by the BSs. Among other configurations, the BSs need to inform the UEs in which bandwidth part they should perform the measurements and which CSI-RSs they should monitor [59].

Another difference between SSB and CSI-RS is that the second one can be UE specifically configured. This way, one possible deployment is to associate SSBs with wider beams and CSI-RS with narrower beams [60], as illustrated in Fig. 2.6. On one hand, wider SSBs make the system more robust to blockage, since wider beams can propagate signals in more directions [61]. On the other hand, narrower CSI-RSs provide better Signal to Noise Ratio (SNR) due to the directivity gain. The negative side of using different beamwidth for SSB and CSI-RS is that the range at which a UE could send and receive data, which is based on CSI-RS measurements, will be longer than the range where a cell can be detected [62], which is based on SSB measurements.

Concerning the CSI reporting, it may consist of CQI, Precoding Matrix Indicator (PMI), CSI-RS resource indicator (CRI), Layer Indication (LI), Rank Indicator (RI) and L1-RSRP [63]. The CQI informs the BS how good/bad the channel quality is. This information can be used by the BS as an input in order to select the Modulation and Coding Scheme (MCS) that will be used in future transmissions.

The UE estimates a CQI for each defined subband, in addition to a wideband CQI, where a subband is a contiguous set of Resource Blocks (RBs) [63]. A UE is configured via higher layer signaling with one out of two possible subband sizes depending on the total number of RBs in the considered carrier bandwidth part according to Table 2.2.

Furthermore, for each defined subband the UE calculates the difference between its estimated CQI and the wideband one. Then, it maps this difference into a 2-bit subband differential CQI defined in [63]. Finally, according to the selected reporting mode (periodic, semi-persistent or aperiodic), the UE reports the wideband CQI with or without some of the 2-bit subband differential CQIs.

Table 2.2 – Configurable subband size.

Bandwidth part size (# of RBs)	Subband size (# of RBs)
< 24	N/A
24 - 72	4, 8
72 - 144	8, 16
145 - 275	16, 32

Source: Created by the author.

Figure 2.7 – Time-frequency structure of a SSB.

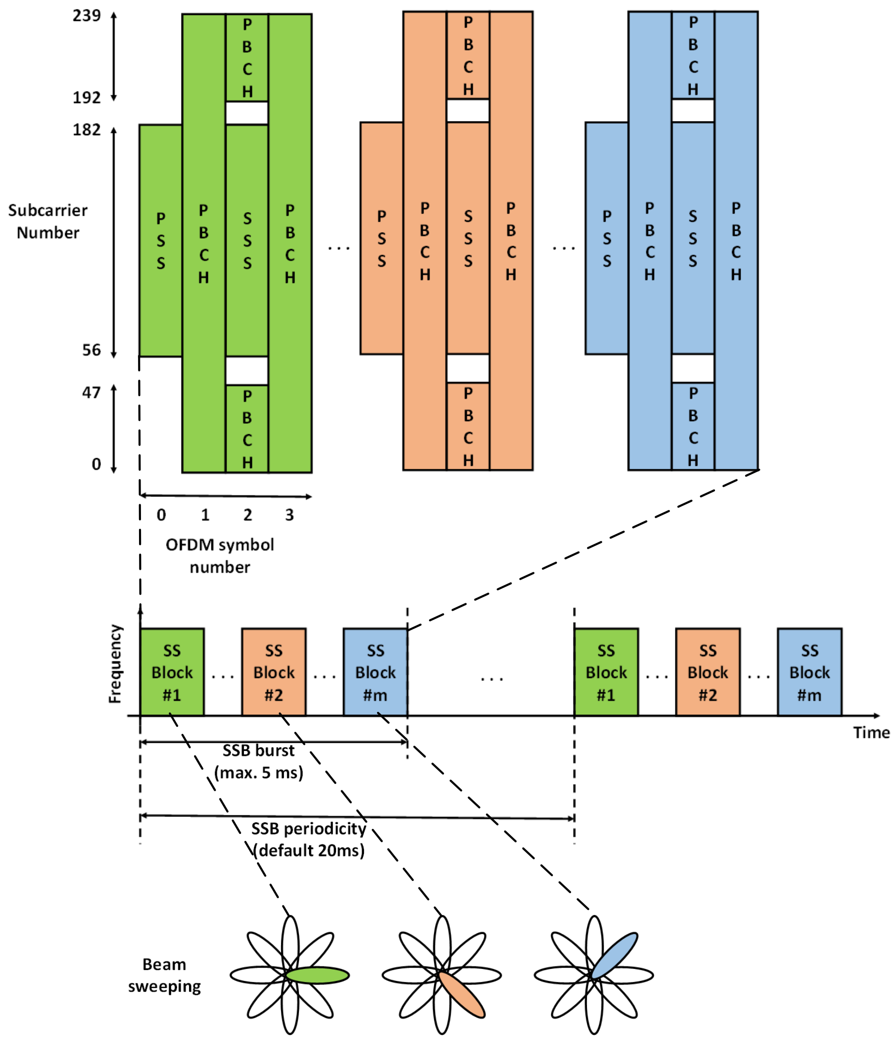

Source: Created by the author.

SSB

Regarding the SSB, as illustrated in the top part of Fig. 2.7, it is a group of 4 OFDM symbols along 240 subcarriers [56]. It consists of Primary Synchronization Signal (PSS), Secondary Synchronization Signal (SSS) and Physical Broadcast Channel (PBCH).

As in LTE, in NR there are 3 possible values for PSS. The UE applies a time domain matched filter to search for one of them. After finding it, the UE knows the timing of the SSB and can also find the SSS. The SSS can assume 336 different values, twice more options than in LTE. Together, PSS and SSS indicate the physical cell ID, which can then assume $3 \times 336 = 1008$ different values [56]. After decoding the PSS and SSS, the UE can also decode the PBCH and have access to the Master Information Block (MIB) [59]. Since the amount of information in the MIB is quite limited, one of the most important information that it carries is the searching spacing for the Remaining Minimum System Information (RMSI) scheduling, which contains the necessary information for getting initial access to the system.

When operating with beams, the BSs will transmit SSBs in bursts. Beams from the same cell have the same PSS and SSS. The main difference between them is the content of PBCH, which tells the beam index and is usually associated with a given transmission direction, as illustrated in the bottom part of Fig. 2.7. The number of SSBs that can be broadcast in a burst depends on the frequency range. Frequency ranges up to 3 GHz may have a maximum of 4 SSBs in a burst, while for 3 GHz-6 GHz the maximum is 8 and for mmWaves is 64 [64]. Furthermore, the time duration of the burst must be lower than or equal to 5 ms.

When accessing the network for the first time, the UEs should assume a SSB periodicity of 20 ms. Other values for the SSB burst periodicity are standardized in [59], which are: 5 ms, 10 ms, 40 ms, 80 ms and 160 ms. Compared to LTE Cell specific Reference Signal (CRS), the NR SSB design is leaner, since the NR SSBs are transmitted less frequent than the LTE CRSs, which are transmitted at every millisecond and over all the spectrum. This minimizes "always on" broadcasting of system information, allowing power saving and minimizing interference.

2.5 Physical Layer Measurements

As in LTE, the most important metrics on power measurements are RSRP, Reference Signal Received Quality (RSRQ), Received Signal Strength Indicator (RSSI) and Signal to Interference-plus-Noise Ratio (SINR). However, while in LTE these metrics are based on CRSs measurements, in NR they can be based on measurement of either SSBs or CSI-RSs, as standardized in [65]. Below, you can find a summarized description of them:

- **RSRP:** it is the linear average over the power contributions (in watts) of the resource elements carrying either SSBs or CSI-RSs within the considered measurement frequency bandwidth.

- **RSSI:** it is the total received power over the entire bandwidth, including signals from co-channel serving and non-serving cells.

- **RSRQ:** while RSRP is the absolute strength of the reference radio signals, the RSRQ is the ratio:

$$\frac{(\text{number of resource blocks in which the RSSI was measured}) \times \text{RSRP}}{\text{RSSI}} \tag{2.1}$$

- **SINR:** it is the linear average over the power contributions (in watts) of the resource elements carrying either SSBs or CSI-RSs divided by the linear average of the noise and interference power contribution (in watts) over the resources carrying either SSBs or CSI-RSs within the considered measurement frequency bandwidth.

In order to demonstrate these concepts, consider Fig. 2.8, which illustrates the structure of a two-port CSI-RS [57] consisting of two resource elements within an RB/slot block. The blue squares represent resource elements with reference signals and the other squares represent resources carrying other data channels. We assume that the power of all of them is the same, i.e., 0.021 watt. It is important to highlight that RSRP and RSSI are measured only in OFDM symbols containing reference signals. Thus, in Fig. 2.8, we have illustrated the power of resource elements in only one OFDM symbol.

As previously stated, RSRP is the linear average of downlink reference signals for a given channel bandwidth, therefore in the example of Fig. 2.8:

$$\text{RSRP} = \frac{0.021 + 0.021}{2} = 0.021\text{W} = 13.2\text{dBm}. \tag{2.2}$$

RSSI is the total received power, thus:

$$\text{RSSI} = 12 \times 0.021 = 0.252\text{W} = 24\text{dBm}. \tag{2.3}$$

Finally, RSRQ is the ratio between RSRP and RSSI:

$$\text{RSRQ} = 10 \times \log\left(\frac{0.021}{0.252}\right) = -10.79\text{dB}. \tag{2.4}$$

Comparing RSRP and RSRQ, it is possible to determine if coverage or interference problems occur in a specific location. If RSRP remains stable or becomes even better, while RSRQ is declining, this is a symptom of rising interference. If, on the other hand, both RSRP and RSRQ decline at the same time, this clearly indicates an area with weak coverage.

The most important difference between RSRQ and SINR, is that the first one considers self-interference, since if the UE is receiving data from the serving cell this power will be included in the value of RSSI. For example, in Fig.2.8, the data being received by a UE is accounted in a blue square, which is not considered by the SINR, but it is by the RSSI, and therefore, by the RSRQ.

2.6 Measurement Model

As already mentioned, SSBs and CSI-RSs are used for beam and cell measurements. The measurement model adopted in 5G is specified in [11] and presented in Fig. 2.9. According to this model, in connected mode, the UEs measure multiple beams of a cell and the measurement results are averaged to derive the cell quality. In order to derive beam and cell qualities, filtering takes place at two different levels: at the physical layer (L1) and at upper layers (L3).

Figure 2.8 – Structure of a two-port CSI-RS consisting of two resource elements within an RB/slot block.

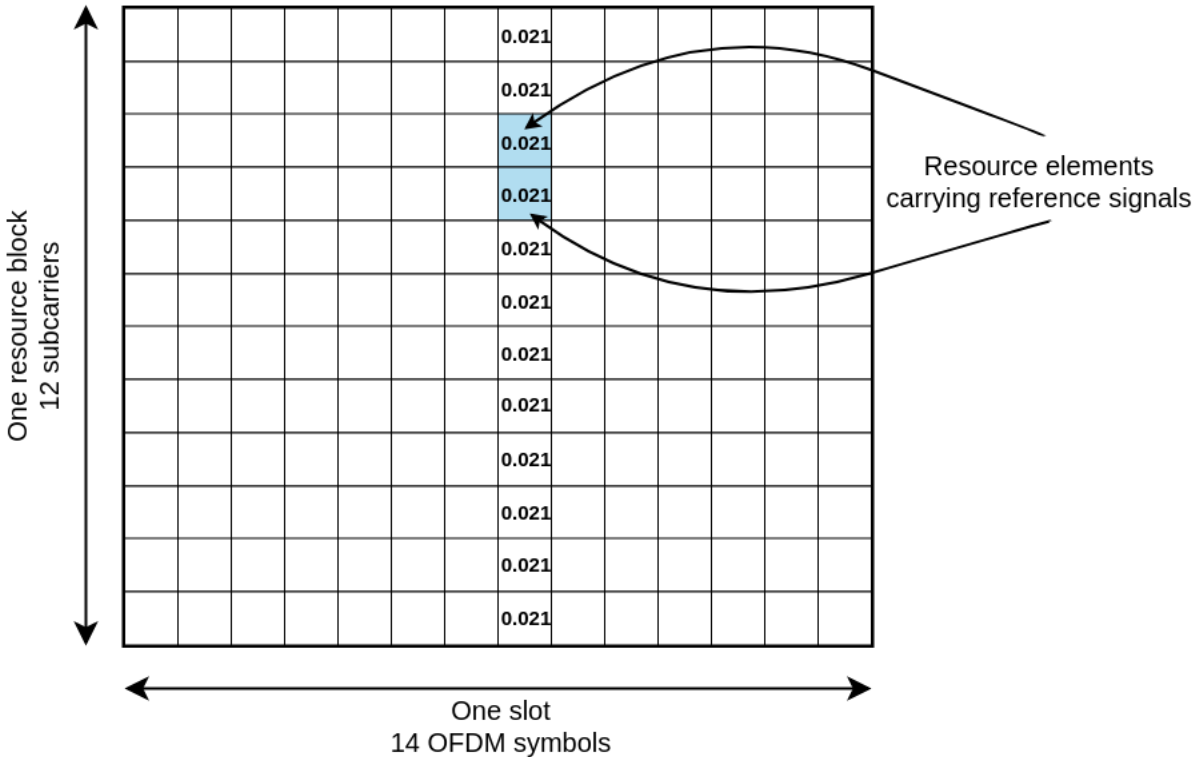

Source: Created by the author.

Figure 2.9 – Beam and cell quality measurement model.

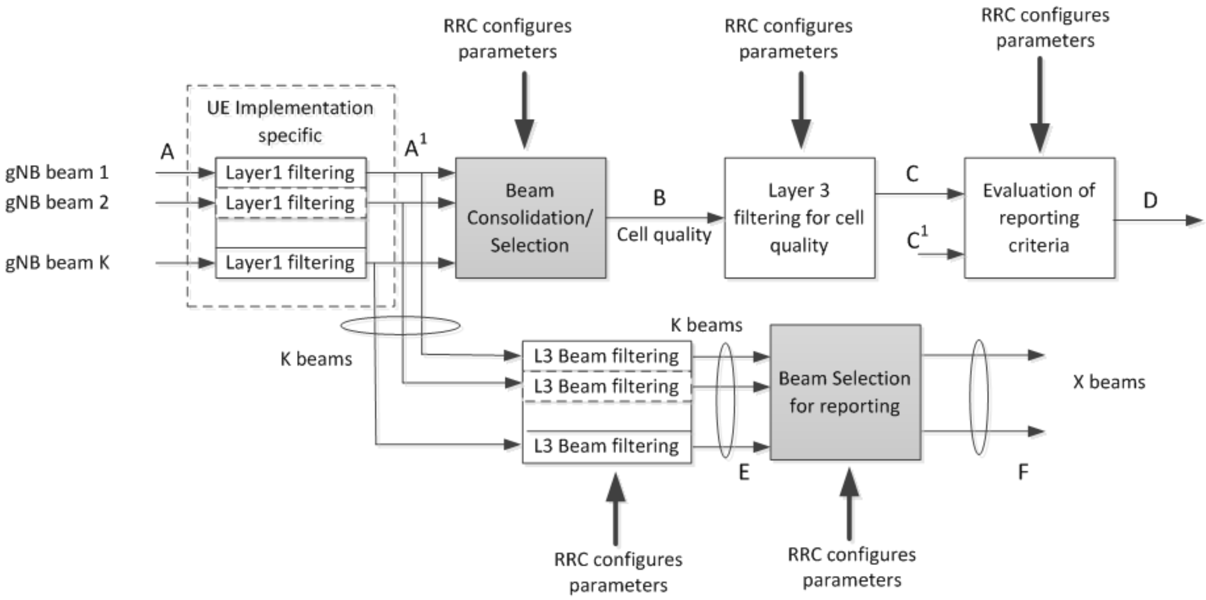

Source: [11].

On one hand, the L1 filtering is not constrained by the standard. Each vendor can implement its own filtering method. On the other hand, the beam consolidation and the L3 filtering are standardized.

Regarding the beam consolidation procedure, it averages the Y best beams above a given threshold. The values of Y and of the threshold are provided by Radio Resource Control

Figure 2.10 – Measurement report triggering events.

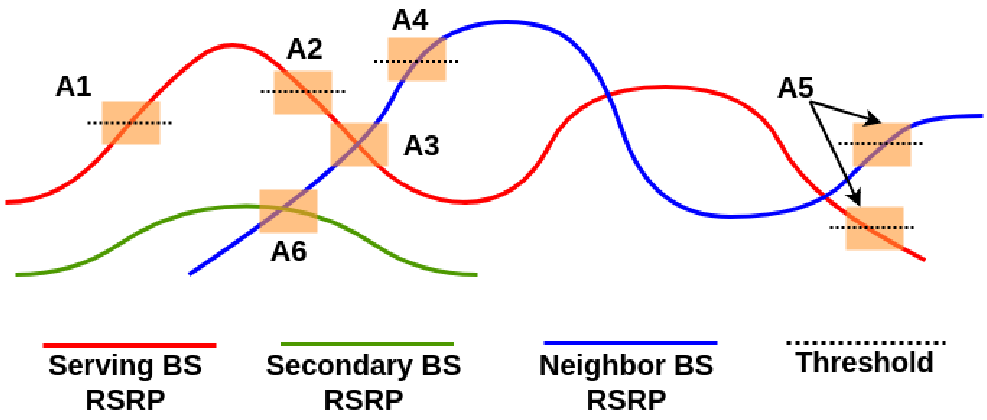

Source: Created by the author.

(RRC) signaling. Concerning the L3 filtering, the UEs should use the following formula [59]:

$$F_n = (1-a) \cdot F_{n-1} + a \cdot M_n, \tag{2.5}$$

where M_n is the latest received measurement from the physical layer; F_n is the updated filtered measurement result; F_{n-1} is the previous filtered measurement result; and $a = 1/2^{k/4}$, where k is the filter coefficient. F_0 is set to M_1 when the first measurement is received.

It is important to highlight that the measurement periodicities at points A^1, B, C and E are equal.

2.7 Measurement Report Triggering Events

Previous sections have already presented the 3GPP specifications related to 5G physical layer, the reference and synchronization signals used to derive power measurements, the power measurements themselves and the measurement model. Finally, regarding measurements related to mobility management, e.g., RSRP and RSRQ, this section addresses the events that trigger measurement reporting from the UEs to the BSs. Besides, regarding measurements related to RRA, e.g., CQI, next section addresses how the BSs must perform link adaptation based on the reported CQI.

In order to keep connected to the most suitable BS, the UEs are constantly "hearing" their surroundings. If the signal of either the serving or some neighboring cell reaches predefined conditions, the UEs report this to its serving BS, which will then evaluate the need of taking actions like initiating a handover procedure. These predefined conditions are known as measurement report triggering events and are standardized in 3GPP technical specification [59]. Some of these events are illustrated in Fig. 2.10 and listed in Table 2.3.

Event A3 is one of the most important events for this thesis. It is illustrated in Fig. 2.11. Its main idea is to report a measurement when a neighbor BS becomes better than the serving one. The red and blue solid lines represent the serving and neighbor BS RSRP after L3 filtering, respectively. In order to avoid unnecessarily frequent measurement reporting caused by small range of fluctuations, 3GPP defines the following parameters: hysteresis, offset and

Table 2.3 – Measurement report triggering events.

Event	Entering condition
A1	Serving BS becomes better than predefined threshold
A2	Serving BS becomes worse than predefined threshold
A3	Neighbor BS becomes offset better than serving BS
A4	Neighbor BS becomes better than predefined threshold
A5	Serving BS becomes worse than threshold1 and neighbor BS becomes better than threshold2
A6	Neighbor BS becomes offset better than secondary BS

Source: Created by the author.

Figure 2.11 – Measurement report triggering event A3.

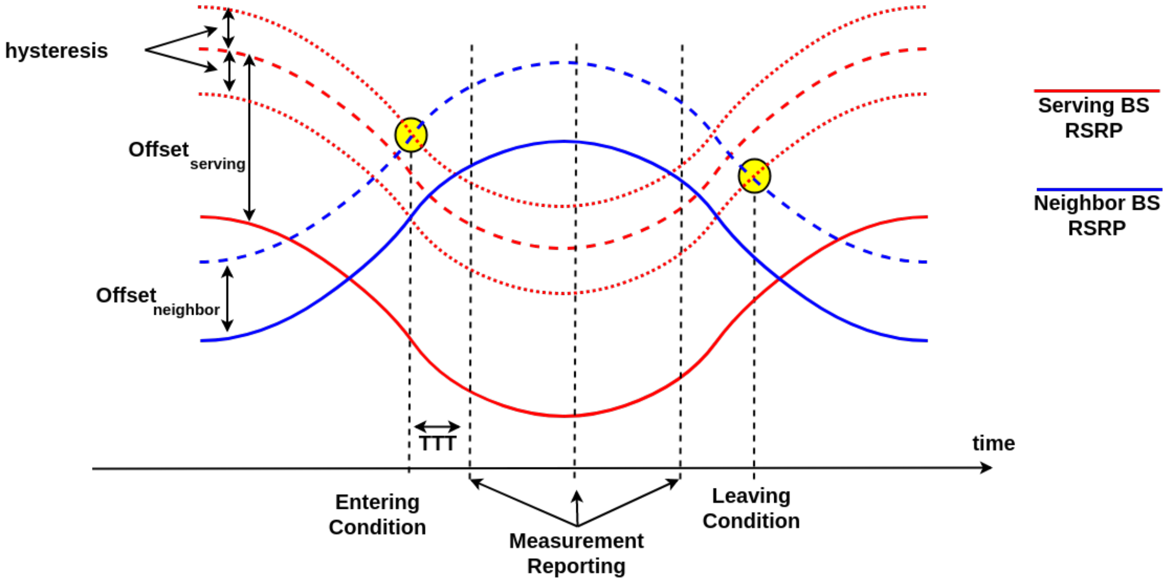

Source: Created by the author.

Time-To-Trigger (TTT). On one hand, the role of hysteresis and offset is to make the neighbor BS looks worse than serving BS to ensure it is really stronger before the UE decides to send a measurement report. On the other hand, the role of TTT is to ensure that entering condition was reached for real, instead of just for a few instants of time.

Notice in Fig. 2.11 that the entering conditions is only reached when:

$$\text{RSRP}_{\text{serving}} + \text{offset}_{\text{serving}} + \text{hysteresis} < \text{RSRP}_{\text{neighbor}} + \text{offset}_{\text{neighbor}}. \tag{2.6}$$

After this inequality is satisfied, it must be valid at least for time equal to TTT before the UE starts sending the measurement reports to its serving BS. Then, the UE will periodically send a new measurement to the BS until either it receives a RRC message from its BS or the leaving condition is reached, i.e.,

$$\text{RSRP}_{\text{serving}} + \text{offset}_{\text{serving}} - \text{hysteresis} > \text{RSRP}_{\text{neighbor}} + \text{offset}_{\text{neighbor}}. \tag{2.7}$$

2.8 Link Adaptation

Link adaptation consists of dynamically adjusting the transmission parameters, such as MCSs, to match the conditions of the UEs' radio links. During good propagation conditions, a high order modulation scheme with low coding redundancy is used in order to increase the transmission data rate, while during a signal fade, the system selects a more robust modulation scheme and a higher coding rate to maintain both connection quality and link stability without increasing the signal power [66].

Table 2.4 presents the mapping of CQI into MCS in NR standardized in [63]. Note that larger CQI indexes, i.e., better channel conditions, allow to transmit more bits on each OFDM symbol and to use the channel more efficiently.

Differences in MCS imply different BLock Error Rate (BLER) performances, which can be seen in Fig. 2.12. This data is available in [67] and it represents the relationship between SNR, BLER and MCS. Note that for the same SNR, higher MCS index represents higher BLER, which means that a given MCS requires a certain SNR to operate with an acceptably low BLER.

Table 2.4 – CQI and MCS mapping standardized in [63].

CQI index	**Modulation**	**Code rate (x 1024)**	**Rate (bits/symbol)**	**CQI index**	**Modulation**	**Code rate (x1024)**	**Rate (bits/symbol)**
0		Out of range		8	16QAM	490	1.9141
1	QPSK	78	0.152	9	16QAM	616	2.4063
2	QPSK	120	0.234	10	64QAM	466	2.7305
3	QPSK	193	0.377	11	64QAM	567	3.3223
4	QPSK	308	0.602	12	64QAM	666	3.9023
5	QPSK	449	0.877	13	64QAM	772	4.5234
6	QPSK	602	1.176	14	64QAM	873	5.1152
7	16QAM	378	1.477	15	64QAM	948	5.5547

Source: Created by the author.

Figure 2.12 – Relationship between SNR, BLER and MCS.

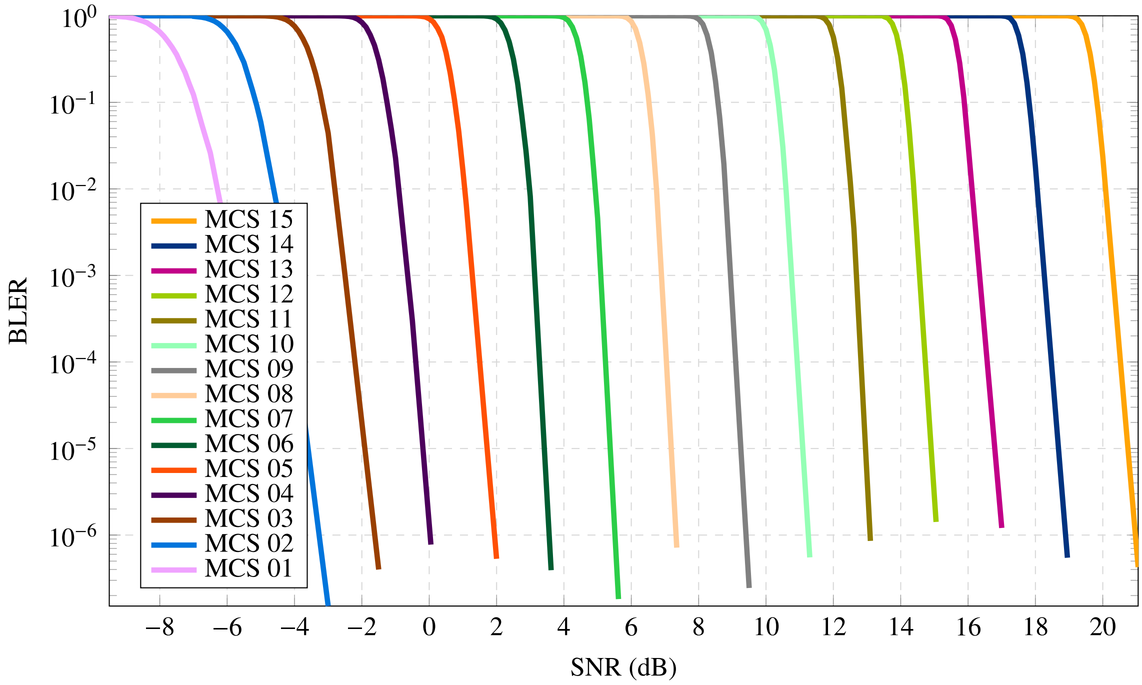

Source: Created by the author.

3 RAT SCHEDULING IN 5G MULTI-RAT SCENARIO

This chapter presents general insights related to 5G Multi-RAT networks that will support the studies presented in the next chapters related to multi-RAT. It aims at investigating which measurement configuration is more efficient in a multi-RAT scenario. More specifically, we present an analysis concerning the metrics that should be used as RAT scheduling criterion and how frequent these switching evaluations should be done. Finally, we also compare the performance of DC and FS solutions, highlighting the scenarios in which each one of them performs better than the other.

3.1 HetNet Challenges

Section 1.1.1 presented seven aspects that should be taken into account in HetNets. By optimizing the measurement configuration, we address 4 of these aspects as follows:

1. **Guarantee a reasonable system performance despite of the *user mobility***: It is addressed by means of adjusting the time between consecutive RAT scheduling evaluations, here called selection of multi-RAT scheduling frequency.

2. **Reduce the signaling overhead in the *CN* due to frequent handover**: It is ensured by the adoption of the FS solution proposed in [55].

3. **Use the *radio resources* across different technologies**: It is addressed by the comparison between FS and DC performances.

4. **Choose a *measurement configuration* to monitor the channel propagation conditions of multiple RATs**: It is addressed by selecting a metric defined by the 3GPP that gives better results when considered as a RAT scheduling criterion.

Before addressing these challenges, the considered LTE-NR scenario will be presented in the next section.

3.2 Simulation Assumptions

The deployment scenario considered in this chapter corresponds to 3 hexagonal cells, within which there are co-sited LTE and NR BSs, with inter-site distance equal to 500 m. The BSs are three-sectored. The system parameters are aligned with the 3GPP case 1 typical urban channel model. They are based on Table A-6 of [68]. We consider that LTE operates at 2 GHz with a subframe duration of 1 ms, while NR operates at 15 GHz with a slot duration of 0.20 ms. It is also assumed that both RATs have the same bandwidth of 20 MHz and the same transmit

Figure 3.1 – Average number of UEs in the system.

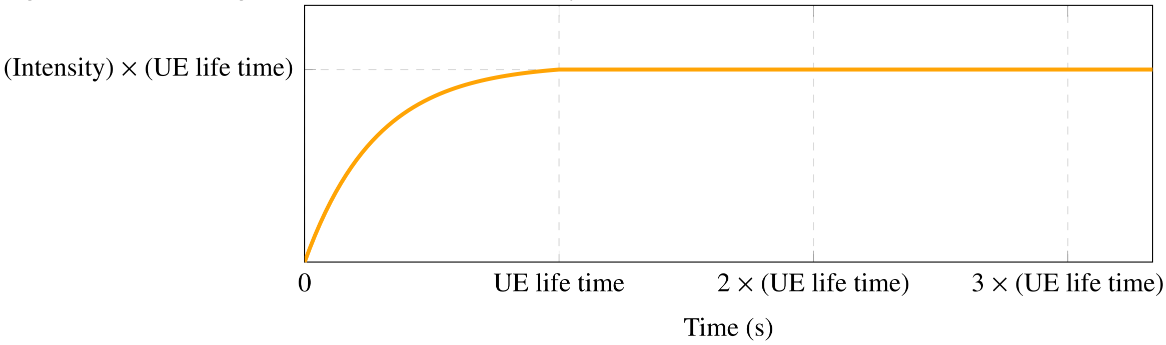

Source: Created by the author.

power of 40 W. Since LTE operates at a lower frequency than NR, we assume that the coverage of a NR cell is smaller than the coverage of a LTE cell. The main parameters are summarized in Table 3.1.

We consider that the BSs are connected to a central entity, which is aware of the value of the main reference signals measured by the UEs.

When not explicitly defined, the UEs were moving at 0.83 m/s (i.e., 3 km/h). For all of them, it is considered a video traffic using UDP with constant packet sizes. The UEs' inter-arrival time follows an exponential distribution, which average number of arrivals per second is a predefined value called intensity. The UE life time is also a predefined value. Fig. 3.1 illustrates the evolution of the average system load in time. For the analyses we only consider UEs which appear in the system after time equal to "UE life time". Before this, the system is not yet stable, since the number of UEs is still increasing. It is interesting to highlight that between time equal to "UE life time" and "2 × (UE life time)" there are still UEs which appeared in the system before time equal to "UE life time", i.e., before the stationary state, thus only the results after "2 × (UE life time)" are considered. In this chapter, we consider "UE life time" equal to 15 s and different values for intensity.

In the next sections, we consider the presented scenario to analyze the challenges concerning RAT scheduling, such as, the selection of the multi-RAT scheduling criterion and the

Table 3.1 – Simulation parameters.

Parameter	**LTE**	**NR**
Carrier frequency	2 GHz	15 GHz
System bandwidth	20 MHz	20 MHz
Subframe (LTE) \ Slot (NR) duration	1 ms	0.20 ms
Resource blocks per 20 MHz	100	20
Inter-site distance	500 m	–
BS transmit power	40 W	40 W
Fast fading	Typical urban	Typical urban
Log-normal shadowing std. dev.	8 dB	8 dB

Source: Created by the author.

Figure 3.2 – UE throughput for different multi-RAT scheduling criteria, and different average number of UE arrivals per second.

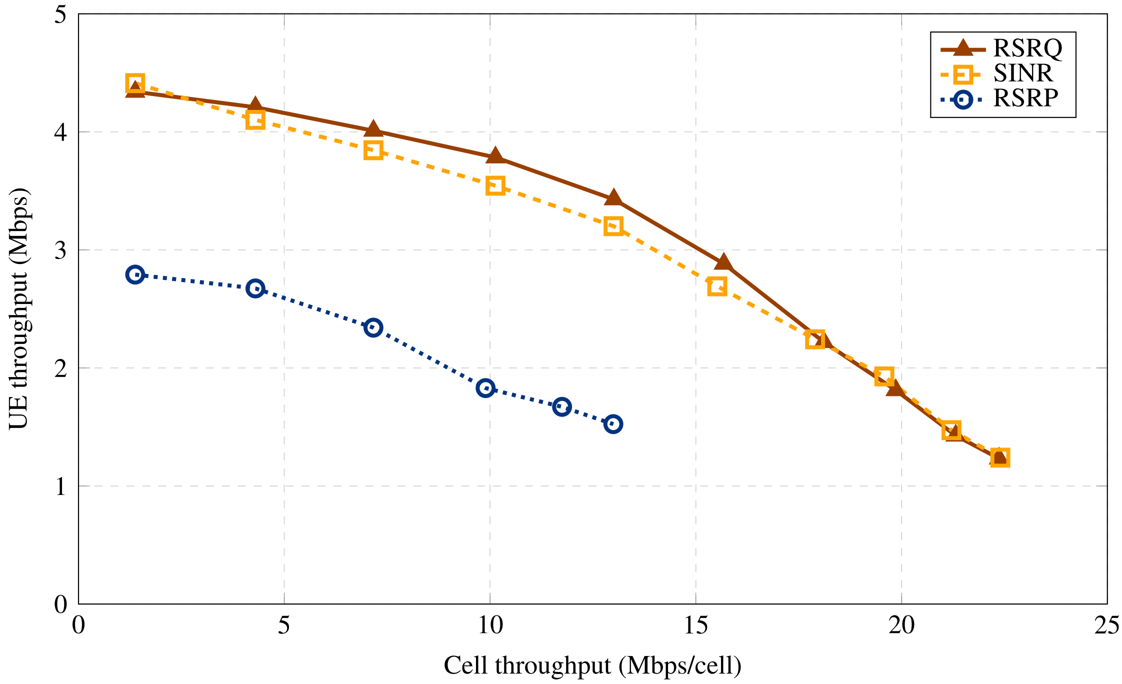

Source: Created by the author.

selection of the scheduling frequency. We compare the performance of FS and DC.

3.3 Selection of Multi-RAT Scheduling Criteria

NR is aiming to operate in a wide range of frequencies, and most of the available spectrum is in very high frequency bands. Thus, the NR signal may in many cases be weaker compared to the LTE signal. However, if a huge amount of data is being transmitted over a LTE BS, the interference will degrade the quality of the signal, even if the LTE coverage is good. Thus, when scheduling RATs, it could be interesting to consider not only the signal strength but also its quality. Hence, the first challenge considered here is the scheduling criterion. We investigate whether RSRQ and SINR are appropriated options to replace RSRP as RAT scheduling criterion in order to increase FS performance.

Fig. 3.2 presents the cell throughput versus the UE throughput for 3 different RAT scheduling criteria, i.e., RSRQ, SINR and RSRP. For each curve, each point with a marker is related to a different number of UEs arriving in the system, i.e., different values of intensity. From the left to right, the values of intensity are: 2, 6, 10, 14, 18, 22, 26, 30, 34 and 38. This figure shows the cases in which the packet loss is lower than 16%. This threshold was achieved by the RSRP curve for intensity equal to 22, i.e., the sixth point, while for the other curves, it was only achieved for intensity higher than 38. That's why there are only 6 points in the RSRP curve, but 10 in the others. We also highlight that the RSRP curve at its sixth point, i.e., for intensity equal to 22, achieves a cell throughput of 13 Mbps/cell and a UE throughput of 1.50 Mbps, while RSRQ and SINR achieve a cell throughput of approximately 15.60 Mbps/cell and a UE throughput of 2.70 Mbps.

We can see that RSRP presents the worst performance between the considered metrics. This is explained by the fact that RSRP only considers the signal strength. Thus, for high loads, UEs with strong signal for a given RAT, but suffering from high interference, will still connect to this RAT but their transmissions will probably fail. RSRQ is slightly better than SINR.

The presented results suggest that, for the considered scenario, RSRQ and SINR are better RAT scheduling criteria than RSRP in order to improve the UE throughput. Thus, in the next section, RSRQ will be considered as the RAT scheduling criterion. It will be analyzed the impact of reducing the time between consecutive RSRQ evaluations.

3.4 Selection of Multi-RAT Scheduling Frequency

In order to improve the system performance, FS should take advantage of different fading variations in different RATs, switching as fast as possible to the one that fits better. So, it is important to identify the factors that may produce such variations, e.g., the UE mobility. Thus, in this section, we will analyze the impact of reducing the interval between consecutive RAT scheduling evaluations for two different UE speeds: 0.10 m/s (a stationary UE) and 10 m/s.

Fig. 3.3 presents the LTE and NR SINR values in time for a specific UE moving at 2 different speeds, i.e., 0.10 m/s and 10 m/s. For each RAT we have two different curves, each one corresponding to a different time of consecutive RAT scheduling evaluations: 10 ms and 100 ms.

In Fig. 3.3a (UE speed equal to 0.10 m/s), we can see that LTE has slower SINR variations than NR. This was already expected, since LTE operates in a lower frequency. From

Figure 3.3 – SINR of a specific UE for two different UE speeds.

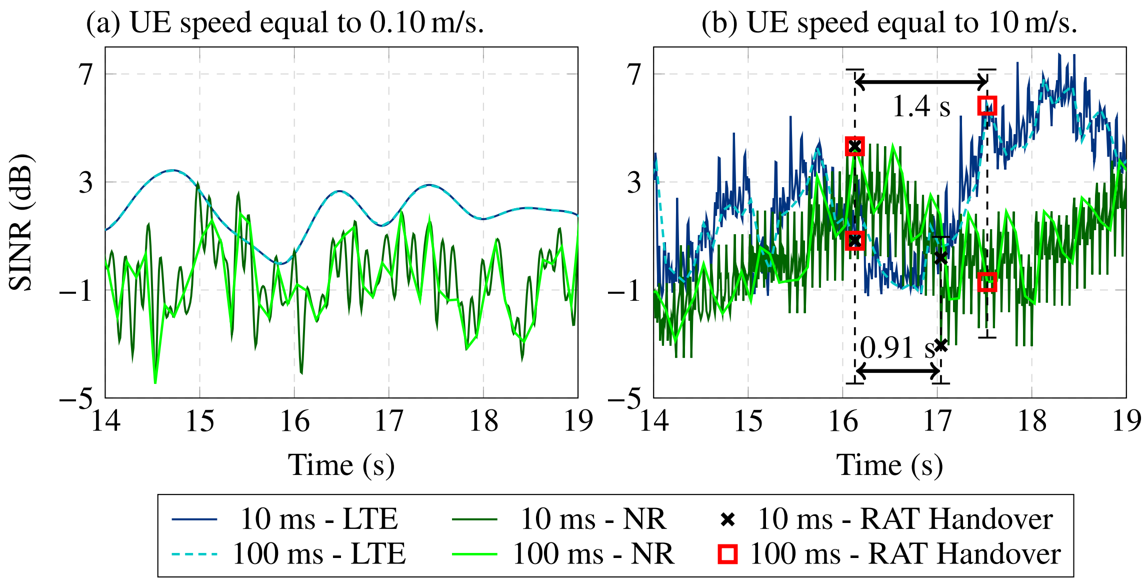

Source: Created by the author.

this figure, we can also conclude that, when the UE moves slowly, the SINR does not change too fast. Thus, to consider the time between consecutive RAT scheduling evaluations equal to 10 ms can be seen as unnecessary oversampling, since sampling the LTE link at 10 ms and 100 ms produces similar curves of SINR (in Fig. 3.3a, they are overlapped).

Fig. 3.3b presents the results related to UE speed equal to 10 m/s. The markers indicate the instant when there is a RAT switching. They are related to the 10 ms and 100 ms curves, respectively. From 15.44 s until 16.64 s, the LTE SINR decreases and the NR SINR increases. After that, they change their trend, the LTE SINR increases and the NR SINR decreases. Remark that both RAT switching procedures, i.e., 10 ms and 100 ms, identify at the same time the moment in which the NR SINR becomes 3 dB higher than LTE SINR. However, 100 ms takes 1.4 s - 0.910 s = 0.490 s more to switch back to LTE than 10 ms. It means that 100 ms stayed longer time using the bad link, which highlights the importance of reducing the time between consecutive evaluations.

Comparing Fig. 3.3a and Fig. 3.3b, we can see that the SINR varies faster when the UE speed increases. Thus, when the UE moves faster, the time between consecutive evaluations should be reduced in order to capture the channel variations. Different of Fig. 3.3a, in Fig. 3.3b, the curves concerning 10 ms and 100 ms present different shapes.

When analyzing the cell throughput versus the UE throughput for these 2 different UE speed values, 0.10 m/s and 10 m/s, similar results were obtained. For low speed, the different intervals between consecutive RAT evaluations presented similar results. However, when the UE speed increased, we could see that the system performance degraded more for higher intervals of time between consecutive evaluations. This is a consequence of what was explained in Fig. 3.3. For higher UE speeds, higher intervals between consecutive RAT evaluations implies longer time using the bad link.

It is important to highlight that, for instance, in LTE, the inter-frequency handover measurement period is 480 ms [69]. In that way, we conclude that, for 5G, it should be considered a faster measurement period which can vary according to the system conditions, e.g., the UE speed.

3.5 Fast-RAT Scheduling versus Dual Connectivity

The present study compares DC and FS performances considering the improvements suggested in the previous sections, such as the use of RSRQ as RAT scheduling criterion and the reduction of time between consecutive RAT scheduling evaluations to 50 ms.

Fig. 3.4 presents the UE throughput with DC and FS. This result proves that, for high loads and in the presence of tight integration between LTE and NR, FS can achieve higher UE throughput gains than DC.

DC increases the available bandwidth and the link diversity is improved for higher reliability. For low loads, this results in a throughput performance increase and DC performs better than FS. However, when the load increases in DC, there are more UEs competing for the

Figure 3.4 – UE throughput concerning FS versus DC.

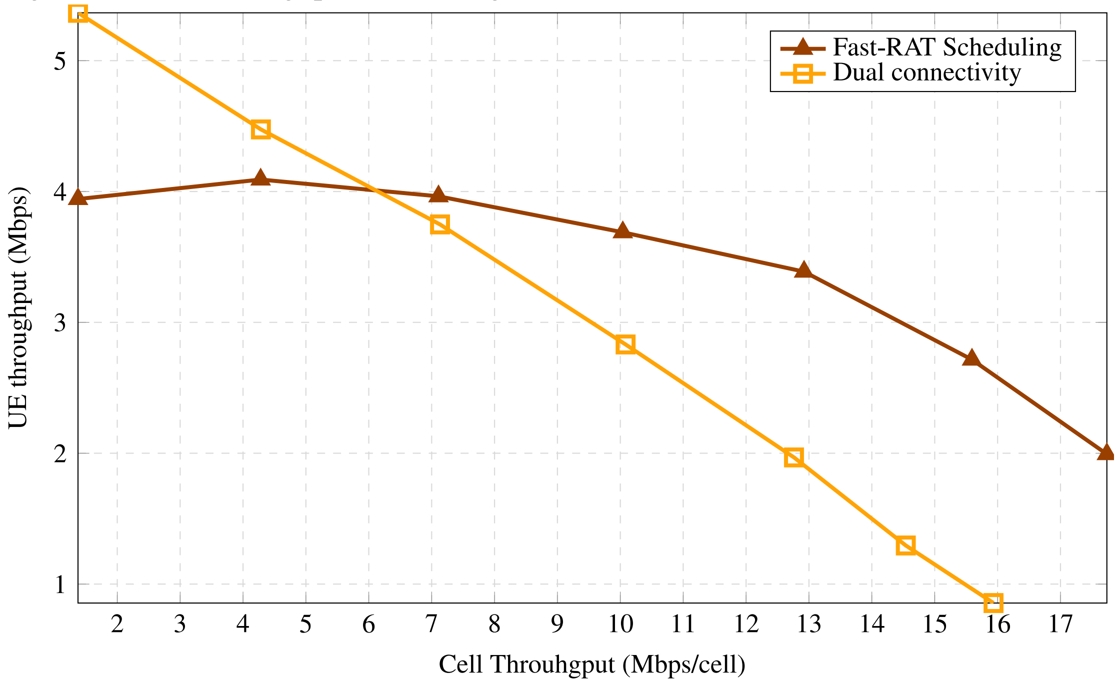

Source: Created by the author.

same resources, since the UEs can be connected to both RATs at the same time. Therefore, the system performance may decrease due to higher interference. On the other hand, in FS, the UEs are connected to either LTE or NR, thus they will not compete for the same resources, resulting in higher throughput than DC in high loads.

It is important to highlight that, for low loads, the double of bandwidth in DC does not mean the double of the throughput, since the instantaneous traffic load from a low number of UEs may not be enough to exploit all the system capacity.

Other interesting metric to consider when comparing DC and FS is the SINR per RAT, as presented in Fig. 3.5. Usually, FS UEs close to the BSs tend to be connected to NR, while the FS UEs far from NR BSs will connect to LTE BSs. On the other hand, the DC UEs transmitting in NR are not only the ones close to the NR BSs. That is why the SINR of DC UEs transmitting in NR (dashed line with square markers in Fig. 3.5) is worse than the SINR of FS UEs transmitting in NR (solid line with square markers in Fig. 3.5). Similarly, for low loads, the SINR of DC UEs transmitting in LTE (dashed line with triangle markers) is better than the SINR of FS UEs transmitting in LTE (solid line with triangle markers), since DC UEs transmitting in LTE are not only the ones far from the BSs. However, as already said, when the load increases the interference in LTE for DC becomes very important and its SINR decreases very fast.

Considering this, we can conclude that there is not a solution that fits better in all the cases. Thus, it could be interesting to merge DC and FS into a framework that could select the one that fits better in each case, for example, use DC in low loads and FS in high loads.

Figure 3.5 – SINR per RAT for DC and FS, considering UDP-based services and RSRQ as RAT scheduling criterion for FS and evaluating its value at every 50ms.

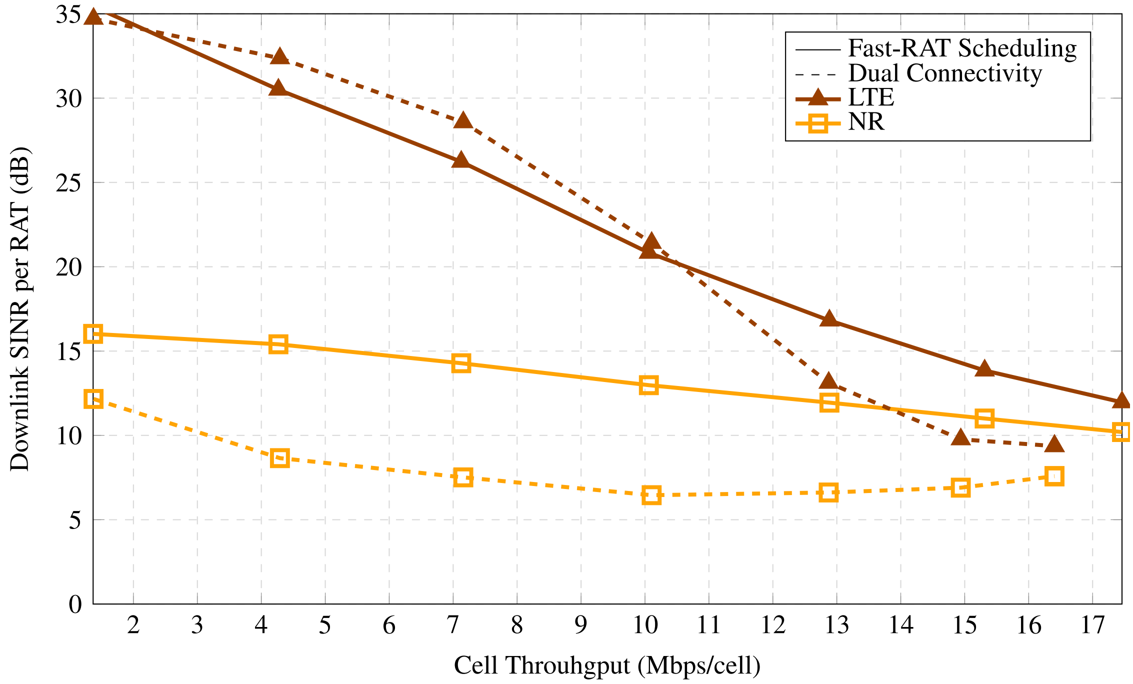

Source: Created by the author.

3.6 Chapter Summary

The analyses presented in this chapter helped in a better understanding of multi-RAT scheduling using either FS or DC. Concerning the measurement configuration, we figured out that metrics related to signal quality, e.g. RSRQ, should be prioritized instead of metrics only related to the signal strength, e.g., RSRP. In a multi-RAT scenario, decision criteria only related to the signal strength tend to overload the RAT with better propagation conditions.

In order to take advantage of channel variations, it was concluded that, in 5G, it should be considered shorter time between consecutive RAT scheduling evaluations, which can vary according to the system conditions, e.g., the UE speed.

Finally, the performance of DC and FS were compared, considering the improvements suggested in the previous sections. It was concluded that there is not a solution that fits better in all the cases. While DC performs better than FS for low loads, FS can present higher gains than DC for high loads. Thus, it could be interesting to merge DC and FS into a framework that could select the one that fits better in each case, for example, use DC in low loads and FS in high loads.

4 5G MEASUREMENT ADAPTATION BASED ON CHANNEL HARDENING OCCURRENCE

Now that we have already investigated general aspects related to multi-RAT scenario, we will focus on general aspects of CH. More precisely, this chapter proposes a framework for CH detection and L1 measurement optimization, where the CH is detected based on the standard deviation of RSRP measurements in a sliding window and the measurement periodicity is dynamically adjusted according to the level of CH, where the less the channel fluctuates the higher the level of CH is.

4.1 Introduction

As presented in Section 1.1.2, under specific conditions, the channel fluctuations of a link between a BS and a UE may decrease and, in the extreme case, the channel may become flat. Fig. 4.1 presents the RSRP measured by a random UE in the scenario presented in Table 4.1. The UE speed was 0.10 m/s, and the carrier frequency, 28 GHz. Two BS configurations were considered: one with 4 wide SSBs and 4 cross-polarized antennas; and other with 64 narrow SSBs and 64 cross-polarized antennas. Each cross-polarized antenna represents two antenna elements orthogonally deployed.

First, notice that, as expected, considering narrower SSBs (which, in this chapter, is equivalent to increasing the number of SSBs), the RSRP increases. This is due to the gain of directivity. Besides, remark that in the second case, i.e. 64 SSBs, the RSRP fluctuates less than in the first case, i.e., 4 SSBs. The narrow beams work as spatial filters, hardening the channel. Considering that between 12 s and 16 s the UE is in NLOS state and after 16 s it is in a LOS state, notice that the RSRP gap between these two states is higher in the second case, i.e., 64 SSBs.

Figure 4.1 – Simulation example of UE RSRP measurements.

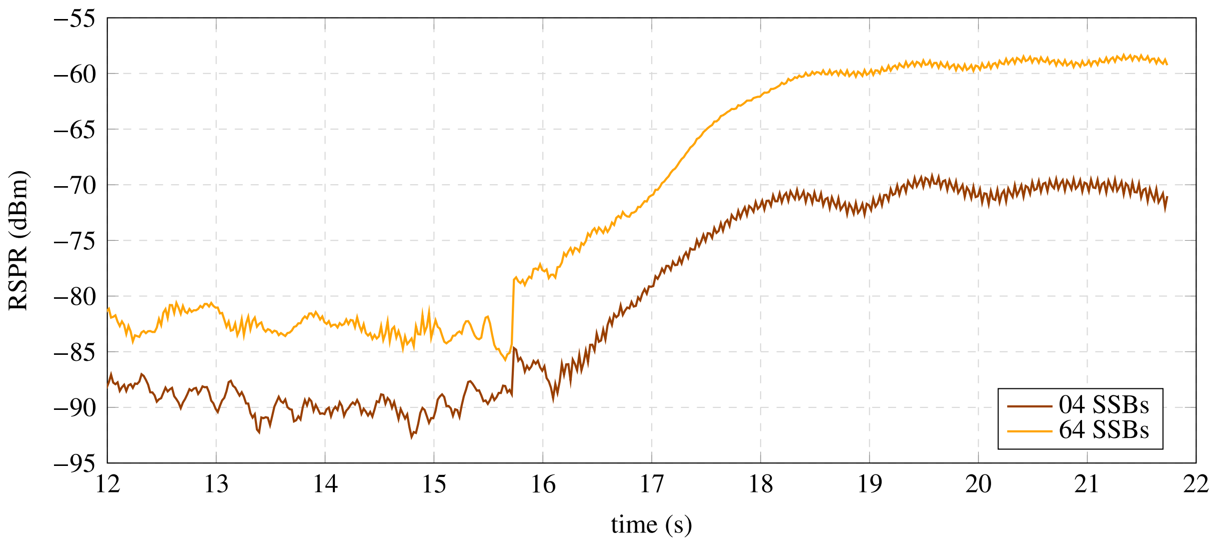

Source: Created by the author.

Table 4.1 – Simulation parameters.

Parameter	Value	Ref.'s
Layout	7 hexagonal sites with 3 sectors each	[70]
Scenario	3GPP 3D Urban Macro	[71]
Inter-site distance	200 m	
BS height	25 m	[71]
Carrier frequency	28 GHz	
System bandwidth	40 MHz	
Subcarrier spacing	120 kHz	[56]
Number of slots	25	
Slot duration	0.13 ms	[56]
BS Tx power (P_n)	49 dBm	

Source: Created by the author.

Also, in the Non-Line of Sight (NLOS) state, the flucuations are higher than in the LOS state.

In the presence of CH, a couple of actions can be done in order to reduce battery consumption, decrease signaling in the control plane, etc. Next section presents a method to identify when CH is happening.

4.2 Channel Hardening Identification

Since CH is characterized by the decrease in channel fluctuations, in order to detect whether it is happening or not in the time domain, we propose that the UEs use a sliding window to log the last X channel quality measurements and calculate their standard deviation. It is expected a low standard deviation when CH happens.

Based on the calculated value, the UE can estimate the "degree" of CH and execute a couple of actions. A simple example is shown in Table 4.2. In this case, the L1 measurement period value is being set according to the calculated standard deviation. Fig. 4.2 presents an illustrative drawing in order to clarify how our proposal would work in practice. The green curves are signal strengths in two situations: with and without CH. The red curves represent the standard deviation related to these signals. The blue lines show the time instants in which the UE would do a new measurement. In this example, if the standard deviation is lower than a given threshold (black dashed line) for at least a few instants of time (equivalent to the TTT in a handover procedure), thus the UE is allowed to change the measurement frequency from very often to seldom.

The standard deviation may depend on the value of X, i.e., the window size. If we have a larger window, a new sample may not have a huge impact on the standard deviation. In this case, a high measurement period could hinder reacting fast to sudden drops in the signal quality, since it would take longer time until we have enough measurements to produce an important change in the standard deviation. To overcome this possible problem, we could also decrease the window size, i.e., the number of samples X, when increasing the measurement period. A shorter

Table 4.2 – Example of actions based on the standard deviation.

Group	Standard deviation value	Action
01	< 0.30 dBm	Set L1 measurement period equal to 160 ms
02	0.30 dBm to 0.80 dBm	Set L1 measurement period equal to 80 ms
03	≥0.80 dBm	Set L1 measurement period equal to 20 ms

Source: Created by the author.

Figure 4.2 – In the presence of CH, the channel (green curves) presents less fluctuations, i.e., the standard deviation (red curves) decreases, thus it is not necessary to do so frequent measurements.

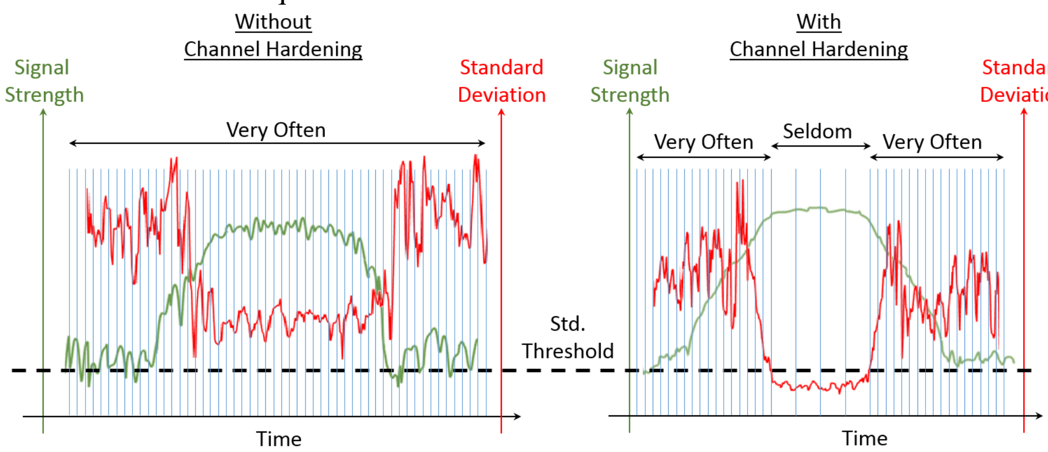

Source: Created by the author.

window size would counterbalance the higher measurement period and fewer samples would be necessary to detect when the signal fluctuations increase, allowing the UE to react faster to this change.

According to 3GPP standards, the network sends a measurement reporting configuration to each UE. This configuration typically indicates if the reporting shall be periodic and/or event triggered. It also contains the events and what the UE shall measure, e.g., RSRP, the number of cells, etc. One way to implement the proposed solution is to incorporate these settings in the measurement reporting configuration.

4.3 Channel Hardening in SSBs and CSI-RSs Measurements

Before evaluating the method proposed in the previous section, we analyze the fluctuations in both time and frequency domains. More specifically, this section evaluates the impact of the number of SSBs on the fluctuations of RSRP over the time. Besides, it is also evaluated the impact of the number of CSI-RSs on the fluctuations of CQI measurements along the subbands.

Regarding the RSRP measurements, it was considered a L1 measurement periodicity equal to 20 ms and it was analyzed the standard deviation of the samples inside of a sliding window of 640 ms. Fig. 4.3a presents the Cumulative Distribution Function (CDF) of the calculated standard deviation. Notice that the 64 SSBs case presents lower values of standard deviation. For example, the percentage of standard deviation samples with value lower than or equal to 0.30 dBm increases from 15% to 34% when increasing the number of SSBs from 4 to 64. This is due to the channel hardening.

Concerning the CQI measurements along the RBs, for each instant of time, it was estimated the power gain coefficient of variation of these measurements. Fig. 4.3b presents these statistics for 3 different numbers of CSI-RSs. The higher the number of CSI-RSs is (so, narrower beams) the higher the power gain is and the lower the coefficients of variation are.

CH occurrence in the frequency domain could be exploited to reduce the size of CQI reports. In this case, the UE could report to the BS the CQI of a small set of subbands and inform the BS that CH is happening. Thus, the report size would be reduced without loss of information related to subband quality on the BS side. Moreover, RRA algorithms could also be simplified due to the reduced frequency selectivity. This idea is exploited in Chapter 6.

Regarding the CH feasibility, it is important to highlight that CH is more accentuated after coherent precoding has been applied and the UE is aligned with a beam direction. Since CSI-RSs can be UE specific, it is possible to do this for each UE. However, SSBs are used for general broadcast. This is the reason why, in Fig. 4.3, we have lower levels of CH in the measurements based on SSB transmission, compared to the ones based on CSI-RS transmission.

4.4 L1 Measurement Periodicity

This section analyzes the framework proposed in Section 4.2. The analyses are focused on RSRP measurements based on SSBs.

It was considered a sliding window of 640 ms. Important to remark that although we realize the importance of optimizing the size of the sliding window, this was not studied in this work. We just tried to make sure that its value was neither too low nor too high, since with a large window, e.g., 6 s, we would not be able to quickly react to a change in the channel and with a small one, e.g. 6 ms, we would not have enough samples.

The cell RSRP was sampled using the measurement periodicities proposed in Table 4.2 and according to their respective standard deviation value. The RSRP samples generated

Figure 4.3 – Analyses of channel fluctuations in time and frequency domains.

(a) RSRP standard deviation (dBm).

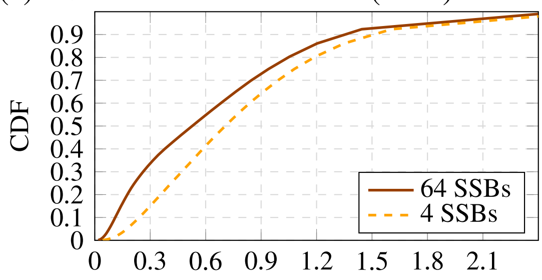

(b) Subbands power gain coefficient of variation.

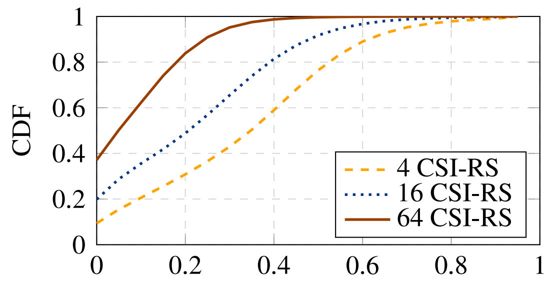

Source: Created by the author.

Figure 4.4 – Difference between RSRP measured with default periodicity, i.e., 20 ms, and higher periodicity.

(a) Group 01 - Std < 0.30 dBm.

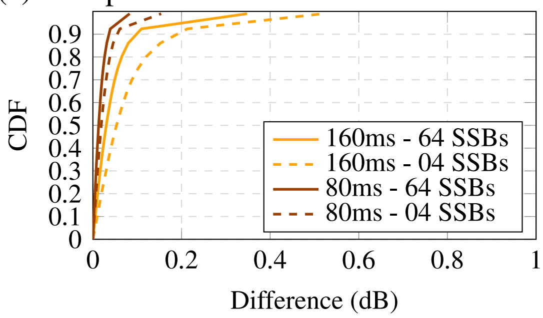

(b) Group 02 - 0.30 dBm ≤ std < 0.80 dBm.

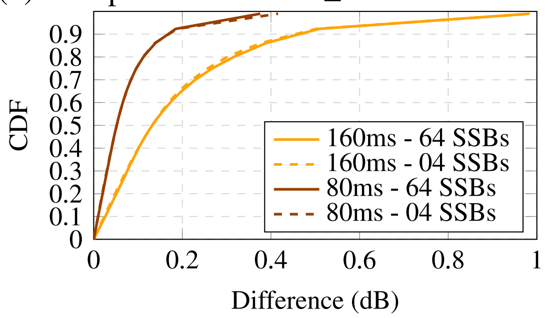

(c) Group 03 - Std ≥ 0.80 dBm.

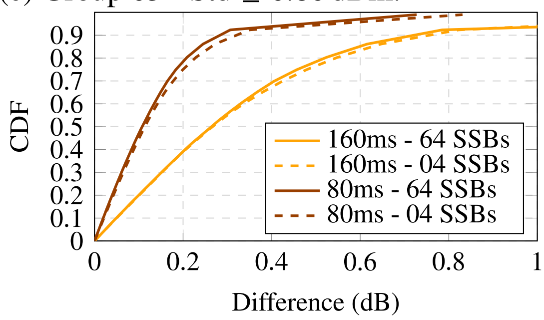

Source: Created by the author.

with a higher measurement periodicity, i.e., 160 ms and 80 ms, were interpolated and we analyzed the difference between them and the samples obtained with the baseline measurement periodicity, i.e., 20 ms. Fig. 4.4 presents the CDF curves of these differences. The samples were split into 3 groups according to the standard deviation thresholds in Table 4.2. The brown curves are related to the case considering 80 ms as the measurement periodicity and the yellow ones are related to the case considering 160 ms as the measurement periodicity.

Considering 0.60 dB as the maximum acceptable difference, which in linear scale corresponds to a difference of 15%, in Fig. 4.4a we can see that both 80 ms and 160 ms can be used as a measurement periodicity if the samples standard deviation is lower than 0.30 dBm. Analogously, in Fig. 4.4b, we see that 160 ms should not be used as a measurement periodicity in case the standard deviation is lower than 0.80 dBm but greater than or equal to 0.30 dBm, while we can still use the value of 80 ms. Finally, Fig. 4.4c shows that neither the values of 80 ms nor 160 ms should be used as a measurement periodicity if the samples standard deviation is higher than or equal to 0.80 dBm.

Also, notice in Fig. 4.4 that the proposed method is valid not only when we have a high number of SSBs, e.g., 64, but also for the cases with low number of SSBs, e.g., 4. As shown in Fig. 4.3a, the scenario with 4 SSBs also presents cases with low RSRP standard deviation, even if they are fewer than in the scenario with more SSBs.

Figure 4.5 – Impact of mobility - 4 and 64 SSBs - sliding window.

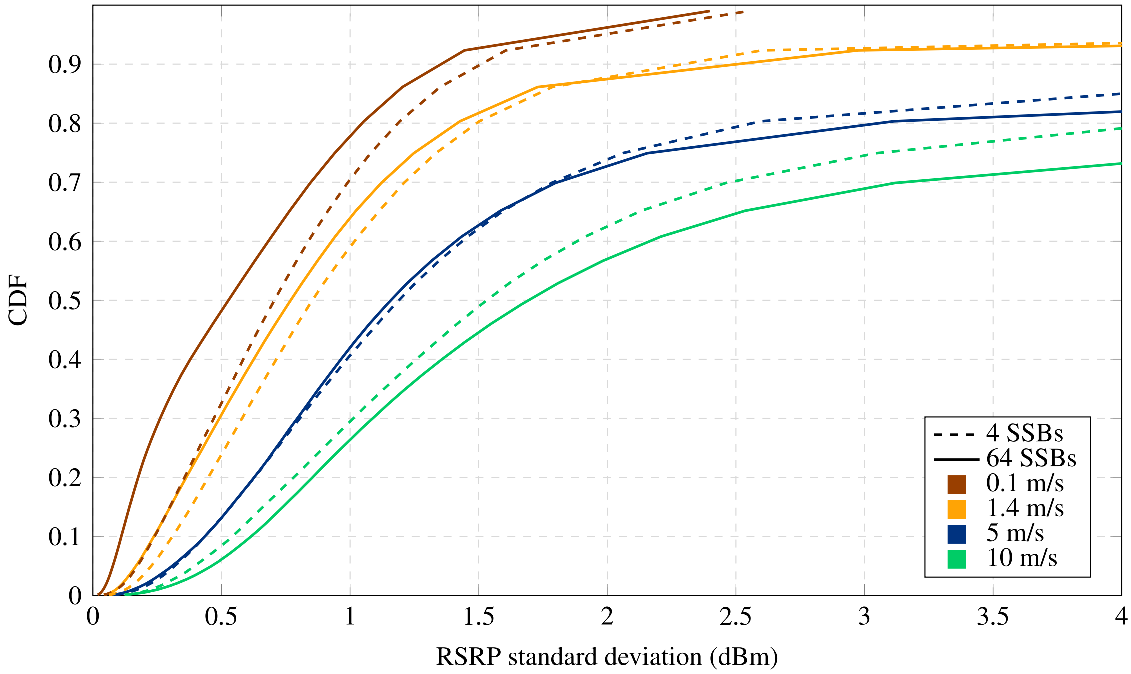

Source: Created by the author.

Figure 4.6 – Speed - Difference between RSRP measured with default periodicity and higher periodicity.

(a) Group 01 - Std < 0.30 dBm.

(b) Group 02 - 0.30 dBm ≤ std < 0.80 dBm.

(c) Group 03 - Std ≥ 0.80 dBm.

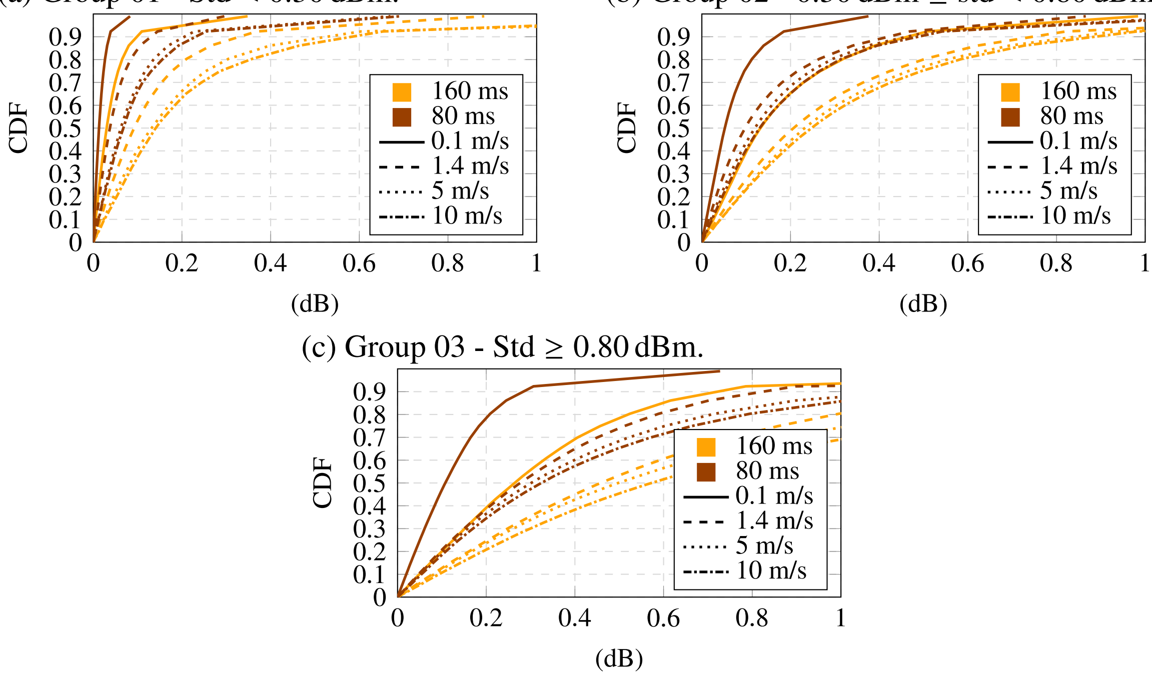

Source: Created by the author.

4.5 Mobility Impact

The impact of UE mobility on the proposed framework was also evaluated. A similar scenario to the one of the previous section was considered, the only difference is the UE speed.

As in Fig. 4.3a, Fig. 4.5 presents the CDF of standard deviation for the cases with

4 and 64 SSBs, but considering 4 different UE speeds. According to this figure, increasing the UE speed increases the channel fluctuations in both cases, i.e., 4 and 64 SSBs. Besides, remark that the mobility has a worse impact in the case with narrow beams, i.e., 64 SSBs. This is due to the fact that spatial focusing of energy provided by a narrow beam translates to a larger spatial decorrelation [44]. Thus, in a scenario with narrow beams, when moving, a UE will pass through more decorrelated beams. This result highlights the importance of beam tracking techniques in order to be able to quickly update the best beam direction to serve a UE.

Although the number of UEs subjected to channel hardening decreases when the UE speed increases, the method proposed in Section 4.2 still works as show in Fig. 4.6. Similar to Fig. 4.4, Fig. 4.6 presents the CDF of the difference between RSRP samples with baseline measurement periodicity, i.e., 20 ms, and higher measurement periodicity. For group 1, even for higher speeds, both measurement periodicities presented differences lower than 0.60 dB, i.e., 15% in linear scale, in at least 90 % of the cases. For group 2, measurement periodicity equal to 80 ms still presented differences lower than 0.60 dB in more than 90 % of the cases. These results show that, as proposed in Table 4.2, measurement periodicity equal to 160 ms can be used for group 1, even when the UEs are moving and that measurement periodicity equal to 80 ms can be used for groups 1 and 2.

4.6 Chapter Summary

The numerical results confirmed that when considering narrower SSBs and CSI-RSs (which, in this chapter, is equivalent to increasing the number of SSBs and CSI-RSs), the CH becomes more noticeable. Furthermore, the numerical evaluation presented in this chapter validated the proposed framework for CH detection and L1 measurement optimization, where the CH is detected based on the standard deviation of RSRP measurements in a sliding window and the measurement periodicity is dynamically adjusted according to the level of CH. It was also concluded that the UE mobility negatively impacts the CH, i.e., increasing the UE speed increases channel fluctuations for some UEs. Despite of this, the proposed method still works for all UEs.

5 DISTRIBUTED RRM FOR 5G MULTI-RAT NETWORKS

In the two previous chapters we investigated general aspects related to multi-RAT and CH. Now, we will address these concepts from the point-of-view of RRM. The present chapter focuses on managing radio resources in a multi-RAT scenario while the next chapter will analyze how to improve, according to the adopted RRA strategy and KPIs, the performance of a multi-RAT network in the presence of CH.

More precisely, the present chapter formulates a RRA optimization problem aiming at maximizing the minimum UE throughput in the system subject to the constraint that for each UE, its throughput must be higher than a requirement. The referred problem is non-linear and complex to solve. However, we get to transform it into a simpler form, a MILP, that can be optimally solved using standard optimization methods. This solution is categorized as a centralized solution. Thus, we propose a distributed framework to overcome the drawbacks of centralized processing, e.g., processing costs and increased signaling overhead. This framework is divided into two parts: a BS selection procedure (performed by the users) and a resource assignment algorithm (performed by the BSs). Besides, a performance evaluation is conducted, considering 4G LTE and 5G NR parameters.

5.1 Introduction

Considering the context of tight interworking between 5G NR and LTE, the traditional concept of resource can be extended from time, frequency, space and power to also include radio interfaces and access nodes. Thus, efficient RRM techniques will be even more important than they were before.

RRM techniques have already been broadly studied in the literature as it can be seen in [72], where an extensive survey on these techniques is presented for multi-user MIMO systems. However, the majority of them do not address some of the challenges presented in HetNets, as the ones presented in Section 1.1.1.

In such heterogeneous networks, UEs face different radio conditions (e.g., they may not be on the coverage area of the same RATs). Despite this, their tight requirements must be met by the operators. Satisfying all the UEs despite of the network conditions is an important task in 5G and it is the main driver of this chapter.

In this context, we consider an optimization problem that maximizes the minimum UE throughput in the system, while satisfying all the UEs, i.e., keeping their throughput higher than their requirements. In other words, while keeping all the UEs satisfied, we try to keep the throughput of the UEs in bad radio conditions as high as possible, since this can avoid dissatisfaction in case their radio conditions get worse. When other objective functions are adopted, e.g., maximize system throughput, it is harder to keep all the UEs satisfied over the time, since, usually, these functions allocate to the worst UEs only the enough amount of resources to keep them in the limit of satisfaction. However, if their radio conditions get even worse, they might enter starvation due to lack of resources.

The remainder of this chapter is organized as follows. Sections 5.2 and 5.3 introduce the network model and the problem formulation, respectively. Sections 5.4 and 5.5 present the centralized solution and the proposed distributed framework, respectively. Section 5.6 provides a practical view of our proposal, illustrating how it can be mapped into 3GPP network parameters and how they can be obtained. The proposed framework is evaluated via worst-case computational complexity analysis in Section 5.7 and via computational simulations in Section 5.8. Finally, in Section 5.9, the main conclusions of this chapter are presented.

5.2 System Model

It is considered a system with U UEs and N RATs, where the UEs and RATs are grouped in the sets $\mathcal{U}$ and $\mathcal{N}$, respectively. In RAT n there are B_n BSs grouped in the set $\mathcal{B}_n$, where $\mathcal{B} = \bigcup_{n \in \mathcal{N}} \mathcal{B}_n$ and $B = |\mathcal{B}|$.

As explained in Section 2.3, LTE and NR use different words to define the minimum allocable time-frequency chunk, however in this chapter we will use the term RB for this purpose independently of the considered RAT.

Each RB is composed of a number of adjacent subcarriers in the frequency domain and of a number of OFDM symbols spanning the duration of one Transmission Time Interval (TTI) in the time domain. Moreover, all the BSs of RAT n reuse K_n RBs arranged in the set $\mathcal{K}_n$. The set containing all RBs is defined as $\mathcal{K} = \bigcup_{n \in \mathcal{N}} \mathcal{K}_n$ and $K = |\mathcal{K}|$.

We also consider that the total transmit power available at each BS of RAT n is equal to P_n, which is equally distributed among all their RBs. Thus, the power $p_{u,k,b}$ used by BS b of RAT n through RB k to transmit to UE u is $p_{u,k,b} = P_n / K_n$.

A joint optimization of BS selection, resource assignment and power allocation would lead to a better performance. However, if an adaptive rate scheme is already implemented, the benefit of a joint optimization taking into account power allocation might be marginal when compared to the Equal Power Allocation (EPA) case, which requires lower complexity [73]. Thus, in order to achieve a good trade-off between performance and complexity, EPA with an adaptive rate scheme was adopted in the present work.

The channel coefficient $h_{u,k,b}[t]$ between BS b and UE u at TTI t is approximated by the coefficient of the first symbol of the middle subcarrier that composes RB k. Moreover, we assume that it remains constant during the period of one TTI.

Therefore, the SNR related to UE u on RB k available in BS b is given by:

$$\gamma_{u,k,b}[t] = \frac{p_{u,k,b}[t] \left| h_{u,k,b}[t] \right|^2}{\sigma^2}, \tag{5.1}$$

in which σ^2 denotes the thermal noise power.

We assume that the data transmission considers a link adaptation scheme which allows each BS to transmit with a set of possible MCSs with very low BLER. The MCS selected by a BS is a function of the SNR $\gamma_{u,k,b}[t]$.

Finally, let $x_{u,k,b}[t]$ be the assignment index indicating whether RB k, reused by BS b, is allocated to UE u at TTI t. Also, let $r_{u,k,b}[t]$ be the number of transmitted bits to UE u in RB k of BS b if this RB is allocated to UE u at TTI t, where $r_{u,k,b}[t]$ is a function of $\gamma_{u,k,b}[t]$. The mean throughput $\theta_u[t]$ of UE u between TTIs 1 and t is then defined as

$$\theta_u[t] = \frac{1}{t}\left[\sum_{j=1}^{t}\sum_{b=1}^{B}\sum_{k=1}^{K} x_{u,k,b}[j] r_{u,k,b}[j]\right]. \tag{5.2}$$

The number of received bits $g_u[t]$ by UE u until TTI t, t included, is $g_u[t] = t\theta_u[t]$, therefore (5.2) can be rewritten as

$$\theta_u[t] = \frac{1}{t}\left[\underbrace{g_u[t-1]}_{\substack{\text{received bits}\\ \text{until TTI } (t-1)}} + \underbrace{\sum_{b=1}^{B}\sum_{k=1}^{K} x_{u,k,b}[t] r_{u,k,b}[t]}_{\text{received bits at TTI } t}\right]. \tag{5.3}$$

5.3 Problem Formulation

In the following, the analyses are done TTI per TTI. Thus, in order to simplify the notation, we will replace $x_{u,k,b}[t]$ and $r_{u,k,b}[t]$ by $x_{u,k,b}$ and $r_{u,k,b}$, respectively. However, the reader should keep in mind that for different TTIs these variables assume different values, as allocation is done per TTI.

As previously mentioned, RRM techniques will play an important role in 5G systems in order to efficiently manage radio resources across different RATs. In this context, we aim at maximizing, at each TTI t, the minimum rate experienced by all UEs in the system subject to the constraint that for each UE u in $\mathcal{U}$, its throughput $\theta_u[t]$ at TTI t must be at least ψ_u.

Furthermore, the considered problem has other constraints, e.g., each BS can allocate a RB to only one UE at a time and UE u can only be connected to $l_{u,n}$ different BSs of RAT n at the same time. Moreover, consider $\omega_{k,n}$ as a binary parameter equal to one if RB k can be used by the BSs of RAT n, i.e., $k \in \mathcal{K}_n$, and zero otherwise; and $\lambda_{b,n}$ as a binary parameter equal to one if the BS b belongs to the RAT n, i.e., $b \in \mathcal{B}_n$, and zero otherwise. It is important to highlight that, it does not make sense to consider $x_{u,k,b}$ and $r_{u,k,b}$ if $\lambda_{b,n} = 1$ and $\omega_{k,n} = 0$. For these cases, consider $x_{u,k,b} = r_{u,k,b} = 0$. Taking into account these constraints, the considered optimization problem can be formulated as

$$\max_{\overline{\mathbf{X}}} \min_{u \in \mathcal{U}} \left(\frac{1}{t} \left[g_u[t-1] + \sum_{b=1}^{B} \sum_{k=1}^{K} x_{u,k,b} r_{u,k,b} \right] \right), \tag{5.4a}$$

$$\text{s.t. } \frac{1}{t} \left[g_u[t-1] + \sum_{b=1}^{B} \sum_{k=1}^{K} x_{u,k,b} r_{u,k,b} \right] \geq \psi_u, \forall u \in \mathcal{U}, \tag{5.4b}$$

$$\textstyle\sum_{u=1}^{U} x_{u,k,b} \leq 1 \text{ , } \forall k \in \mathcal{K} \text{ and } b \in \mathcal{B}, \tag{5.4c}$$

$$\sum_{b=1}^{B} \mathrm{H}\left(\sum_{k=1}^{K} x_{u,k,b}, 1 \right) \lambda_{b,n} \leq l_{u,n}, \forall u \in \mathcal{U}, \forall n \in \mathcal{N}, \tag{5.4d}$$

$$\sum_{u=1}^{U} \sum_{k=1}^{K} \sum_{b=1}^{B} x_{u,k,b} \left(1 - \sum_{n=1}^{N} \lambda_{b,n} \omega_{k,n} \right) = 0, \text{ and} \tag{5.4e}$$

$$x_{u,k,b} \in \{0, 1\}, \tag{5.4f}$$

where the elements $x_{u,k,b}$ are arranged in a multi-dimensional array $\overline{\mathbf{X}} \in \{0,1\}^{\mathcal{U} \times \mathcal{K} \times \mathcal{B}}$ and $\mathrm{H}(a,b)$ is the Heaviside function, which returns either one, if $a \geq b$, or zero, otherwise.

In (5.4a) the objective function is the minimum rate in the system, i.e., $\min_{u \in \mathcal{U}} (\theta_u[t])$, where $\theta_u[t]$ is given in (5.3). Constraint (5.4b) states that all the UEs must be satisfied, i.e., their throughput must be higher than their requirement ψ_u, while constraint (5.4c) states that none BS may allocate a RB to more than one UE at the same time.

In (5.4d), $\mathrm{H}\left(\sum_{k=1}^{K} x_{u,k,b}, 1\right)$ equals one only if BS b allocates at least one RB to UE u, otherwise it is equal to zero. Thus, the left hand side of (5.4d) represents the number of BSs of RAT n to which UE u is connected and the entire equation itself is related to the constraint on the number of connections of each UE. Also, (5.4e) means that the RB k can only be allocated by BS b, if there is $n \in [1, N]$, such that $\lambda_{b,n} \omega_{k,n} = 1$, otherwise $\left(1 - \sum_{n=1}^{N} \lambda_{b,n} \omega_{k,n}\right) = 1$, then $x_{u,k,b}$ must be equal to zero.

Notice that (5.4d) is neither a convex nor a concave function, thus in the next section we will rewrite this constraint in order to achieve a simpler instance of the problem and use it as a centralized benchmark solution.

5.4 Centralized Benchmark Solution

In this section, problem (5.4) is reformulated as a MILP, which can be solved by standard algorithms, such as the Branch and Bound (BB) method [74]. Otherwise, it would be necessary to use the brute force or exhaustive search.

The non-linear objective function (5.4a) can be linearized by introducing a slack variable μ and a new constraint, as in (5.5a) and (5.5b). We can also rewrite (5.4d) as three new linear constraints, i.e., (5.5e), (5.5f) and (5.5g), where the slack variable $\xi_{u,b} \in \{0, 1\}$ is equal to one if the UE u has any RB allocated in the BS b and zero, otherwise. These variables are arranged in the matrix $\Xi \in \{0, 1\}^{U \times B}$.

Therefore, applying these replacements in (5.4) yields

$$\max_{\mu,\overline{\mathbf{X}},\Xi} \quad \mu, \tag{5.5a}$$

$$\text{s.t. } \frac{1}{t}\left[g_u[t-1]+\sum_{b=1}^{B}\sum_{k=1}^{K}x_{u,k,b}r_{u,k,b}\right] \geq \mu, \forall u \in \mathcal{U}, \tag{5.5b}$$

$$\frac{1}{t}\left[g_u[t-1]+\sum_{b=1}^{B}\sum_{k=1}^{K}x_{u,k,b}r_{u,k,b}\right] \geq \psi_u, \forall u \in \mathcal{U}, \tag{5.5c}$$

$$\textstyle\sum_{u=1}^{U} x_{u,k,b} \leq 1 \text{ , } \forall k \in \mathcal{K} \text{ and } b \in \mathcal{B}, \tag{5.5d}$$

$$\textstyle\sum_{k=1}^{K} x_{u,k,b} \leq K\xi_{u,b}, \forall u \in \mathcal{U} \text{ and } \forall b \in \mathcal{B}, \tag{5.5e}$$

$$\textstyle\sum_{k=1}^{K} x_{u,k,b} \geq \xi_{u,b}, \forall u \in \mathcal{U} \text{ and } \forall b \in \mathcal{B}, \tag{5.5f}$$

$$\textstyle\sum_{b=1}^{B} \lambda_{b,n}\xi_{u,b} \leq l_{u,n}, \forall u \in \mathcal{U} \text{ and } \forall n \in \mathcal{N}, \tag{5.5g}$$

$$\sum_{u=1}^{U}\sum_{k=1}^{K}\sum_{b=1}^{B} x_{u,k,b}\left(1-\sum_{n=1}^{N}\lambda_{b,n}\omega_{k,n}\right) = 0, \tag{5.5h}$$

$$x_{u,k,b} \in \{0,1\} \text{ and} \tag{5.5i}$$

$$\xi_{u,b} \in \{0,1\}. \tag{5.5j}$$

If $\xi_{u,b} = 0$, UE u is not connected to BS b, and, according to (5.5e) and (5.5f), $x_{u,k,b}$ must be equal to zero $\forall k$, i.e., it can not be scheduled by this BS.

The product $\lambda_{b,n}\xi_{u,b}$ in (5.5g) is equal to one only if $\lambda_{b,n} = \xi_{u,b} = 1$, i.e., if UE u is connected to BS b and this BS belongs to RAT n. So, the left hand side of (5.5g) represents the number of BSs of RAT n to which UE u is connected and the entire equation itself is related to the constraint on the number of connections of each UE.

At this point, we introduce some concepts and definitions related to tensors. The first step is to arrange the elements $g_u[t-1]$ and ψ_u in the column vectors $\mathbf{g}[t-1]$ and $\boldsymbol{\psi}$, respectively; and the elements $\xi_{u,b}$, $\lambda_{b,n}$, $l_{u,n}$ and $\omega_{k,n}$, in the matrices Ξ, Λ, $\mathbf{L}$ and Ω, respectively. Now, we define the concept of unfolding. Considering that the elements $x_{u,k,b}$ are arranged in a multi-dimensional array $\overline{\mathbf{X}} \in \{0,1\}^{U\times K\times B}$, we denote $\mathbf{X}^{(2)} \in \{0,1\}^{K\times UB}$ as the mode-2 unfolding of $\overline{\mathbf{X}}$, where the elements $x^{(2)}$ of $\mathbf{X}^{(2)}$ are defined in function of the elements of $\overline{\mathbf{X}}$ as $x^{(2)}_{k,u+(b-1)U} = x_{u,k,b}$. Likewise, the elements $r_{u,k,b}$ form the multi-dimensional array $\overline{\mathbf{R}}$. The second concept is the vec$\{\cdot\}$ operation. It is defined as $\text{vec}\{\mathbf{Z}\} = \begin{bmatrix}\mathbf{z}_1^{\mathrm{T}} & \mathbf{z}_2^{\mathrm{T}} & \dots & \mathbf{z}_J^{\mathrm{T}}\end{bmatrix}^{\mathrm{T}}$, where $\mathbf{z}_j$ is the j-th column of matrix $\mathbf{Z}$ and $\{\cdot\}^{\mathrm{T}}$ is the transpose operation. To simplify the notation, we rename the following vectors: $\mathbf{x} = \text{vec}\left\{\mathbf{X}^{(2)^{\mathrm{T}}}\right\}$ and $\mathbf{r} = \text{vec}\left\{\mathbf{R}^{(2)^{\mathrm{T}}}\right\}$. We also consider $\mathbf{Z}\odot\mathbf{S}$ as the Hadamard product and $\mathbf{Z}\otimes\mathbf{Y}$ as the Kronecker product, where $\mathbf{S}$ and $\mathbf{Z} \in \mathbb{R}^{I\times J}$ and $\mathbf{Y} \in \mathbb{R}^{T\times R}$.

Finally, defining $\mathbf{I}_U$ as an $U \times U$ identity matrix and $\mathbf{1}_U$ as a column vector with U

ones, we can reformulate (5.5) using a tensorial notation as

$$\max_{\mu,\mathbf{x},\Xi} \quad \mu, \tag{5.6a}$$

$$\text{s.t. } \mathbf{g}[t-1]+\left[\left(\mathbf{1}_{KB}^{\mathrm{T}}\otimes\mathbf{I}_U\right)\odot\left(\mathbf{1}_U\otimes\mathbf{r}^{\mathrm{T}}\right)\right]\mathbf{x}\geq t\mu\mathbf{1}_U, \tag{5.6b}$$

$$\mathbf{g}[t-1]+\left[\left(\mathbf{1}_{KB}^{\mathrm{T}}\otimes\mathbf{I}_U\right)\odot\left(\mathbf{1}_U\otimes\mathbf{r}^{\mathrm{T}}\right)\right]\mathbf{x}\geq t\left[\left(\boldsymbol{\psi}\otimes\mathbf{1}_U^{\mathrm{T}}\right)\odot\mathbf{I}_U\right]\mathbf{1}_U, \tag{5.6c}$$

$$\left(\mathbf{I}_{KB}\otimes\mathbf{1}_U^{\mathrm{T}}\right)\mathbf{x}\leq\mathbf{1}_{KB}, \tag{5.6d}$$

$$\left(\mathbf{1}_K^{\mathrm{T}}\otimes\mathbf{I}_{UB}\right)\mathbf{x}\leq K\mathrm{vec}\left\{\Xi\right\}, \tag{5.6e}$$

$$\left(\mathbf{1}_K^{\mathrm{T}}\otimes\mathbf{I}_{UB}\right)\mathbf{x}\geq \mathrm{vec}\left\{\Xi\right\}, \tag{5.6f}$$

$$\left(\Lambda^{\mathrm{T}}\otimes\mathbf{I}_U\right)\mathrm{vec}\left\{\Xi\right\}\leq\mathrm{vec}\left\{\mathbf{L}\right\}, \tag{5.6g}$$

$$\left\{-\mathbf{1}_N^{\mathrm{T}}\left[\left(\mathbf{1}_K\otimes\Lambda\otimes\mathbf{1}_U\right)\odot\left(\Omega\otimes\mathbf{1}_{UB}\right)\right]^{\mathrm{T}}+\mathbf{1}_{UKB}^{\mathrm{T}}\right\}\mathbf{x}=0, \tag{5.6h}$$

$$\mathbf{x}\in\{0,1\}^{UKB\times 1} \text{ and} \tag{5.6i}$$

$$\mathrm{vec}\left\{\Xi\right\}\in\{0,1\}^{UB\times 1}. \tag{5.6j}$$

The equations in (5.6) are similar to their equivalents in (5.5), e.g., (5.6c) and (5.5c), the only difference is that in (5.6) we use vectors and matrices to replace the index notation. For example, (5.6c) and (5.5c) mean that all the UEs must be satisfied, i.e., their throughput must be higher than their requirement ψ_u; (5.5d) and (5.6d) mean that none BS can allocate the same RB to more than one UE at the same time; (5.6e), (5.6f), (5.6g), (5.5e), (5.5f) and (5.5g) are related to the fact that none UE can be connected to more than $l_{u,n}$ BSs of RAT n.

At this point, the variables of our problem are: μ, $\mathbf{x}$ and Ξ. To simplify even more the notation, they can be arranged into one single vector $\mathbf{w}$, in which

$$\mathbf{w}=\left[\begin{array}{c|c|c}\mu & \mathbf{x}^{\mathrm{T}} & \mathrm{vec}^{\mathrm{T}}\left\{\Xi\right\}\end{array}\right]^{\mathrm{T}}. \tag{5.7}$$

Then, considering $\mathbf{0}_{UB}$ and $\mathbf{0}_{UB\times UKB}$ as a column vector with UB zeros and a $UB\times UKB$ matrix of zeros, respectively; and defining $\mathbf{m}$, $\mathbf{A}$ and $\mathbf{B}$ as

$$\mathbf{m}=\left[\begin{array}{c|c|c}1 & \mathbf{0}_{UKB}^{\mathrm{T}} & \mathbf{0}_{UB}^{\mathrm{T}}\end{array}\right]^{\mathrm{T}}\Rightarrow\mathbf{m}^{\mathrm{T}}\mathbf{w}=\mu, \tag{5.8a}$$

$$\mathbf{A}=\left[\begin{array}{c|c|c}\mathbf{0}_{UKB} & \mathbf{I}_{UKB} & \mathbf{0}_{UKB\times UB}\end{array}\right]\Rightarrow\mathbf{A}\mathbf{w}=\mathbf{x} \text{ and} \tag{5.8b}$$

$$\mathbf{B}=\left[\begin{array}{c|c|c}\mathbf{0}_{UB} & \mathbf{0}_{UB\times UKB} & \mathbf{I}_{UB}\end{array}\right]\Rightarrow\mathbf{B}\mathbf{w}=\mathrm{vec}\left\{\Xi\right\}, \tag{5.8c}$$

we can finally rewrite the optimization problem (5.6) as

$$\max_{\mathbf{w}}\mathbf{m}^{\mathrm{T}}\mathbf{w}, \text{ s.t. } \mathbf{C}\cdot\mathbf{w}\leq\mathbf{d} \text{ and } \mathbf{e}\cdot\mathbf{w}=0, \tag{5.9}$$

where

$$\mathbf{C} = \begin{bmatrix} t\mathbf{1}_U\mathbf{m}^{\mathrm{T}} - \left[\left(\mathbf{1}_{KB}^{\mathrm{T}}\otimes\mathbf{I}_U\right)\odot\left(\mathbf{1}_U\otimes\mathbf{r}^{\mathrm{T}}\right)\right]\mathbf{A} \\ -\left[\left(\mathbf{1}_{KB}^{\mathrm{T}}\otimes\mathbf{I}_U\right)\odot\left(\mathbf{1}_U\otimes\mathbf{r}^{\mathrm{T}}\right)\right]\mathbf{A} \\ \left(\mathbf{I}_{KB}\otimes\mathbf{1}_U^{\mathrm{T}}\right)\mathbf{A} \\ \left(\mathbf{1}_K^{\mathrm{T}}\otimes\mathbf{I}_{UB}\right)\mathbf{A} - K\mathbf{B} \\ \mathbf{B} - \left(\mathbf{1}_K^{\mathrm{T}}\otimes\mathbf{I}_{UB}\right)\mathbf{A} \\ \left(\Lambda^{\mathrm{T}}\otimes\mathbf{I}_U\right)\mathbf{B} \end{bmatrix}, \tag{5.10}$$

$$\mathbf{d} = \begin{bmatrix} \mathbf{g}[t-1] \\ \mathbf{g}[t-1] - t\left\{\left[\left(\boldsymbol{\psi}\otimes\mathbf{1}_U^{\mathrm{T}}\right)\odot\mathbf{I}_U\right]\mathbf{1}_U\right\} \\ \mathbf{1}_{KB} \\ \mathbf{0}_{UB} \\ \mathbf{0}_{UB} \\ \mathrm{vec}\{\mathbf{L}\} \end{bmatrix} \text{ and} \tag{5.11}$$

$$\mathbf{e} = \left\{\mathbf{1}_{UKB}^{\mathrm{T}} - \mathbf{1}_N^{\mathrm{T}}\left[(\mathbf{1}_K\otimes\Lambda\otimes\mathbf{1}_U)\odot(\Omega\otimes\mathbf{1}_{UB})\right]^{\mathrm{T}}\right\}\mathbf{A}. \tag{5.12}$$

The solution of (5.9) allocates RBs in a way that maximizes the minimum throughput in the system and at the same time keeps all the UEs satisfied. Indirectly, it also associates UEs to BSs. To do so, it requires the knowledge of $h_{u,k,b}[t], \forall u \in \mathcal{U}, k \in \mathcal{K}$ and $b \in \mathcal{B}$ at each TTI t. As already stated, this incurs in a huge signaling overhead and is computationally intensive. Thus in the next section, we present a distributed framework in order to reduce the required complexity to allocate resources in a ultra-dense heterogeneous scenario.

5.5 Proposed Distributed Framework

The proposed framework splits (5.4) into two parts: a BS selection procedure and a resource assignment. Sections 5.5.1 and 5.5.2 describe the BS selection and the resource assignment procedures, respectively.

5.5.1 BS Selection

The BS selection procedure is sketched in the flowchart of Fig. 5.1 and its pseudo code is presented in Alg. 5.1. Each UE executes this method for each RAT in order to choose the BS that fits with its channel propagation conditions.

The first step, block (1) of Fig. 5.1 and l. 1 of Alg. 5.1, consists in selecting as candidate BSs to a handover the ones with RSRP greater than or equal to a threshold. If there is no BS satisfying this requirement, the UE will stay disconnected of this RAT, block (3.a) and l. 3. On the other hand, if this set is not empty, the UE will select as the best candidate BS to connect to, block (4) and l. 17, the BS $\hat{b}$ which maximizes the product $f_{b,1}^{\mathrm{norm}} f_{b,2}^{\mathrm{norm}}$, where $f_{b,i}^{\mathrm{norm}} = \frac{f_{b,i}}{\sum_{b\in\hat{\mathcal{B}}} f_{b,i}}, \forall i \in \{1,2\}$, $f_{b,1} = \mathrm{RSRP}_b$ and $f_{b,2} = \min(\theta_u[t-1])$, for all UE u connected to BS

Figure 5.1 – Flowchart of proposed BS selection procedure.

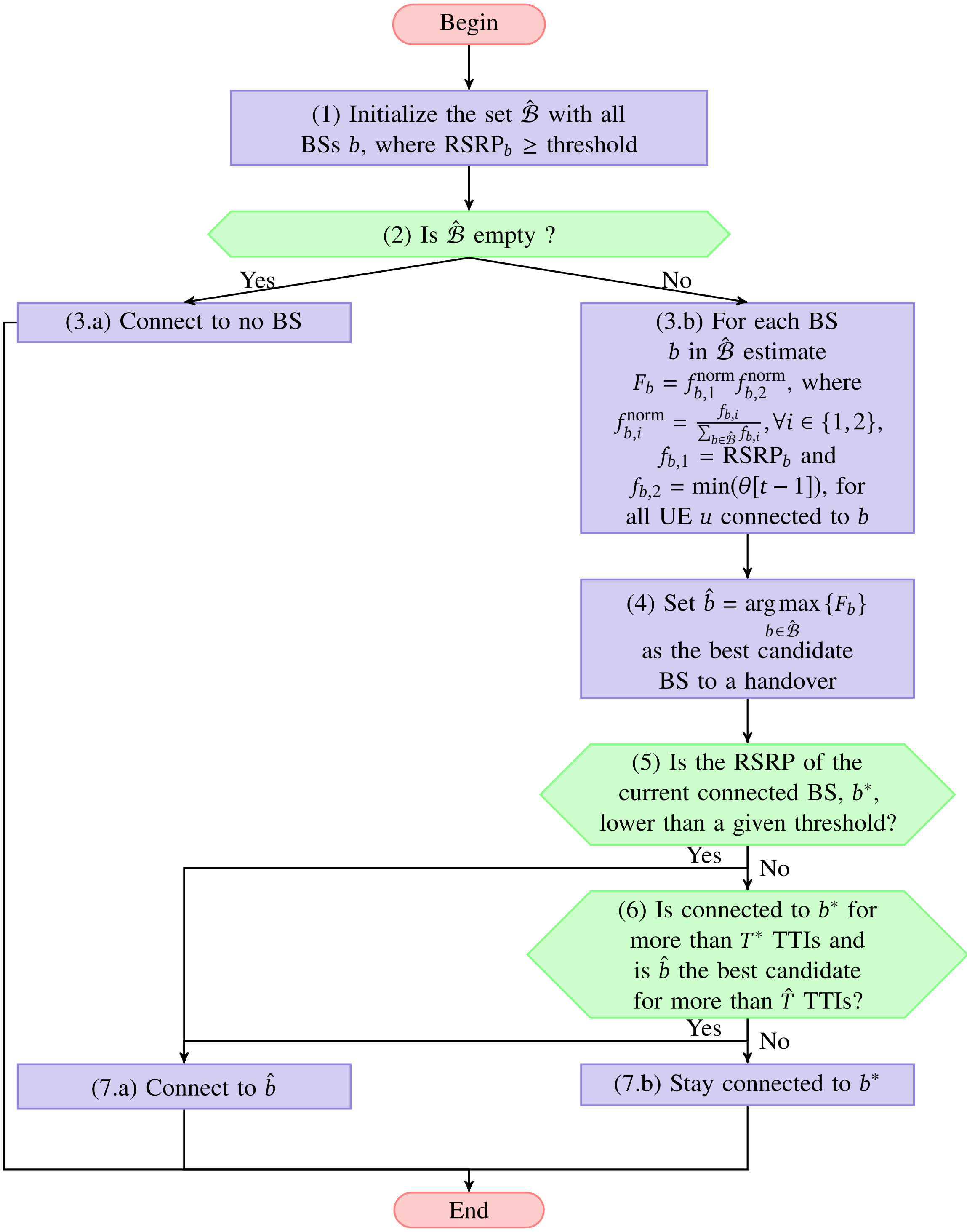

Source: Created by the author.

b. The metric $f_{b,1}$ reflects the BSs' signal strength, while $f_{b,2}$ is the lowest UE throughput among all the UEs connected to BS b.

As presented in Chapter 3, if the UEs consider only the BSs' RSRP as a criterion to connect to, the BSs with better propagation conditions will be overloaded and a high signal strength will not result in higher transmission rates. This is the reason why a UE should also take $f_{b,2}$ into account when selecting a BS. For a given BS b, if $f_{b,2}$ is low it means that at least

Algorithm 5.1 Pseudo code of proposed BS selection procedure.

1: $\hat{\mathcal{B}} \leftarrow \{b \mid b \in \mathcal{B},\ \text{RSRP}_b \geq \text{threshold}\}$
2: **if** $\hat{\mathcal{B}} = \emptyset$ **then** ▷ Test if $\hat{\mathcal{B}}$ is empty
3: $\quad \xi_{u,b} \leftarrow 0, \forall b \in \mathcal{B}$ ▷ Stay disconnected
4: **else**
5: $\quad$ **for** $b \in \hat{\mathcal{B}}$ **do**
6: $\quad\quad f_{b,1} \leftarrow \text{RSRP}_b$ ▷ $f_{b,1}$ reflects the BSs' signal strength
7: $\quad\quad f_{b,2} \leftarrow \min_{\forall \text{ UE } u \text{ connected to } b} (\theta_u [t-1])$
8: $\quad$ **end for**
9: $\quad f_1^{\text{sum}} \leftarrow \sum_{b \in \hat{\mathcal{B}}} f_{b,1}$
10: $\quad f_2^{\text{sum}} \leftarrow \sum_{b \in \hat{\mathcal{B}}} f_{b,2}$
11: $\quad$ **for** $b \in \hat{\mathcal{B}}$ **do**
12: $\quad\quad$ **for** $i \in \{1,2\}$ **do**
13: $\quad\quad\quad f_{b,i}^{\text{norm}} \leftarrow \frac{f_{b,i}}{f_i^{\text{sum}}}$ ▷ Normalization of $f_{b,i}$
14: $\quad\quad$ **end for**
15: $\quad\quad F_b = f_{b,1}^{\text{norm}} f_{b,2}^{\text{norm}}$
16: $\quad$ **end for**
17: $\quad \hat{b} \leftarrow \arg\max_{b \in \hat{\mathcal{B}}} \{F_b\}$ ▷ Best candidate to a handover
18: $\quad$ **if** $\text{RSRP}_{b^*} <$ threshold **then** ▷ Verify the RSRP of the current BS
19: $\quad\quad \xi_{u,\hat{b}} \leftarrow 1$ ▷ Connect to $\hat{b}$
20: $\quad$ **else**
21: $\quad\quad$ **if** $\left(\xi_{u,b^*}[i] = 1, \forall i \in [t-T^*, t-1]\right)$ & $\left(\hat{b}[i] = \hat{b}, \forall i \in [t-\hat{T}+1, t-1]\right)$ **then**
22: $\quad\quad\quad \xi_{u,\hat{b}} \leftarrow 1$ ▷ Connect to $\hat{b}$
23: $\quad\quad$ **else**
24: $\quad\quad\quad \xi_{u,b^*} \leftarrow 1$ ▷ Stay connected to the current BS, b^*
25: $\quad\quad$ **end if**
26: $\quad$ **end if**
27: **end if**

one UE connected to BS b has a low throughput. This may indicate for a UE looking for a BS to connect to that if it tries to handover to BS b it may also experience a low throughput. On the other hand, if $f_{b,2}$ is high, it means that all the UEs connected to it have high throughput. Thus, this BS may be a good candidate in order to get a high throughput.

Before a handover, a UE must stay connected to the current BS b^* for at least T^* TTIs, and the candidate BS to the handover, $\hat{b}$, must have been selected as the best candidate for at least $\hat{T}$ consecutive TTIs, block (6) and l. 21. Otherwise, it must stay connected to b^*, block (7.b) and l. 24. However, if the RSRP of b^* is lower than a given threshold, block (5) and l. 18, an UE is allowed to connect to $\hat{b}$ even if the constraints in block (6) and l. 21 are not satisfied.

5.5.2 Resource Assignment

The proposed resource assignment is described in the flowchart of Fig. 5.2 and its pseudo code is presented in Alg. 5.2. This algorithm should be executed independently by each BS. Its main idea is first to keep all the UEs satisfied and after, if there is still available RBs, allocate them to the UEs with lower throughput in order to increase the minimum throughput in the system. It is divided into three parts:

Algorithm 5.2 Pseudo code of resource assignment procedure.

1: $\mathbf{X} \leftarrow \mathbf{0}_{\mathcal{U}_b \times K_n}$ ▹ Initialize the allocation matrix
2: $\text{RB}_{\text{free}} \leftarrow K_n$ ▹ Initialize the number of unassigned RBs
3: $\mathcal{U}_b \leftarrow \{u \mid u \in \mathcal{U},\ \xi_{u,b} = 1\}$
4: **for** $u \in \mathcal{U}_b$ **do**
5: **if** $\theta_u[t] \geq \psi_u$ **then**
6: $\mathcal{U}_b \leftarrow \mathcal{U}_b \setminus \{u\}$ ▹ Remove UE u from $\mathcal{U}_b$
7: **end if**
8: **end for**
9: **while** $(\mathcal{K}_n \neq \emptyset \ \&\ \mathcal{U}_b \neq \emptyset)$ **do**
10: $(\widehat{u}, \widehat{k}) \leftarrow \underset{u \in \mathcal{U}_b, k \in \mathcal{K}_n}{\arg\max} \{r_{u,k,b}\}$
11: $x_{\widehat{u},\widehat{k},b} \leftarrow 1$ ▹ Assign RB $\widehat{k}$ to UE $\widehat{u}$
12: $\theta_{\widehat{u}}[t] \leftarrow \frac{t\theta_{\widehat{u}}[t] + r_{\widehat{u},\widehat{k},b}}{t}$ ▹ Update the throughput of UE $\widehat{u}$
13: $\mathcal{K}_n \leftarrow \mathcal{K}_n \setminus \{\widehat{k}\}$ ▹ Remove RB $\widehat{k}$ from the set of RBs, $\mathcal{K}_n$
14: **if** $\theta_{\widehat{u}}[t] \geq \psi_{\widehat{u}}$ **then** ▹ Test if UE $\widehat{u}$ is satisfied
15: $\mathcal{U}_b \leftarrow \mathcal{U}_b \setminus \{u\}$ ▹ Remove UE $\widehat{u}$ from $\mathcal{U}_b$
16: **end if**
17: **end while**
18: **if** $\mathcal{K} \neq \emptyset$ **then**
19: $\mathcal{U}_b \leftarrow \{u \mid u \in \mathcal{U},\ \xi_{u,b} = 1\}$ ▹ Reinitialize the set $\mathcal{U}_b$ with all UEs connected to BS b
20: **while** $\mathcal{K}_n \neq \emptyset$ **do**
21: $u^* \leftarrow \underset{u \in \mathcal{U}_b}{\arg\min} \{\theta_u[t]\}$
22: $k^* \leftarrow \underset{k \in \mathcal{K}_n}{\arg\max} \{r_{u^*,k,b}\}$
23: $x_{u^*,k^*,b} \leftarrow 1$ ▹ Assign RB k^* to UE u^*
24: $\theta_{u^*}[t] \leftarrow \frac{t\theta_{u^*}[t] + r_{u^*,k^*,b}}{t}$ ▹ Update the throughput of UE $\widehat{u}$
25: $\mathcal{K}_n \leftarrow \mathcal{K}_n \setminus \{k^*\}$ ▹ Remove RB k^* from $\mathcal{K}_n$
26: **end while**
27: **end if**

1. Exclude satisfied UEs, blocks (1)-(3) and ll. 4-8;

2. Satisfy UEs, blocks (4)-(9) and ll. 9-17; and

3. Max. min. throughput, blocks (10)-(13) and ll. 18-27.

The first part consists in excluding the UEs that are already satisfied, i.e., $\theta_u[t] \geq \psi_u$. For this, each UE must inform the BSs to which it is connected (it may be more than one, e.g., one per RAT), its current throughput. The UE must take into account all the data that it has already received, no matter the RAT from which it came from.

The second part tries to satisfy the UEs not yet satisfied. It works in a loop, allocating RBs to the UEs with highest transmit rate on each RB, blocks (4)-(5) and ll. 10-11. When a UE gets satisfied, it is removed, block (7) and ll. 14-16. This loop continues until all the RBs have been allocated, block (8), or all the UEs are satisfied, block (9) and l. 9.

In the last part, the remaining RBs are allocated to the UEs with lowest throughput, block (11) and l. 21, aiming at maximizing the minimum throughput.

Figure 5.2 – Flowchart of proposed resource assignment procedure.

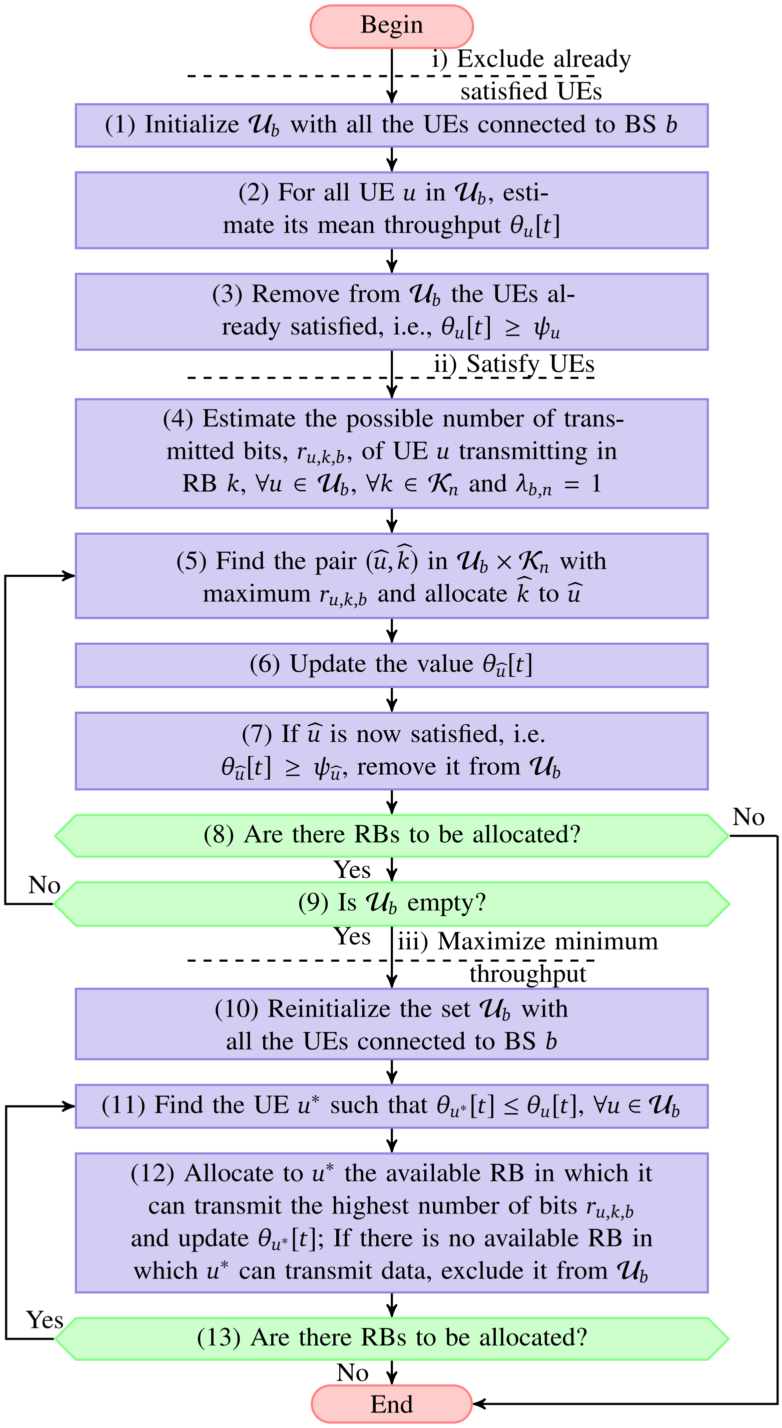

Source: Created by the author.

5.6 Practical Implementation Considerations

In order to provide to the readers a practical view of our proposal, we illustrate how our framework can be mapped into 3GPP network parameters and how they can be obtained.

In order to execute a BS selection, each UE needs to know:

- **RSRP of candidate BSs** — The UE can locally monitor the signal strength. This procedure is already standardized in LTE and in 5G NR;

- **Lowest UE throughput in each BS** — Each UE must periodically inform its throughput to the BSs to which it is connected, and, after that, each BS must broadcast the lowest throughput among the UEs connected to it.

  Regarding the resource allocation procedure, each BS needs:

- **Throughput requirement of UEs connected to it** — From the network operators' point of view, usually the throughput requirement of a UE is associated with the service it is using and/or its data plan, which can be available for the BSs, since the operators have access to these information;

- **Throughput of UEs connected to it** — This information was already listed as a requirement in order to execute the BS selection and must be informed by the UEs to the BSs to which they are connected;

- **CQI of UE connected to it** — In LTE, this information is already standardized. The UEs monitor the received signal strength of the connected BSs and report back the measured CQI.

5.7 Complexity Analysis

In this section, we provide the worst-case computational complexity of the centralized benchmark and of the proposed framework. It gives an upper bound on the computational resources required by an algorithm and is represented by the asymptotic notation $O(\cdot)$. As in [75], we consider summations, multiplications and comparisons as the most relevant and time-consuming operations.

The solution of (5.9) can be obtained using the Branch and Bound (BB) algorithm. According to [76], to solve a linear programming problem with c constraints and v integer variables, the number of required operations is $2(v+c)(2vc+v-3c)\sqrt{2^v}$. In (5.9), $v = 1 + UKB + UB$ and $c = 2U + KB + 2UB + UN + 1$, thus its complexity is $O\Big([U^2K^2B^2(UB + UN + KB) + U^3KBN^2]\sqrt{2^{1+UB(K+1)}}\Big)$. On the other hand, the complexity of the proposed framework is $O\left(UK^2\right)$. The detailed analysis to obtain this value is presented in Appendix A. Comparing both complexities, it can be concluded that the proposed framework can better handle large-scale scenarios, which is a key feature of 5G multi-RAT multi-connectivity systems.

5.8 Performance Evaluation

In this section, the performance of the proposed distributed framework is evaluated via simulation. Subsection 5.8.1 presents the considered scenario and the benchmark solutions. Subsection 5.8.2 presents and discusses the results.

Figure 5.3 – Illustration of a 5G multi-RAT multi-connectivity scenario, where the LTE BS acts as an umbrella cell and NR BSs act as hotspots. The BSs are connected to a centralized processing unit, which is responsible for coordinating the resource usage by the BSs. UEs with DC capability may simultaneously connect to BSs of both RATs when inside their coverage area.

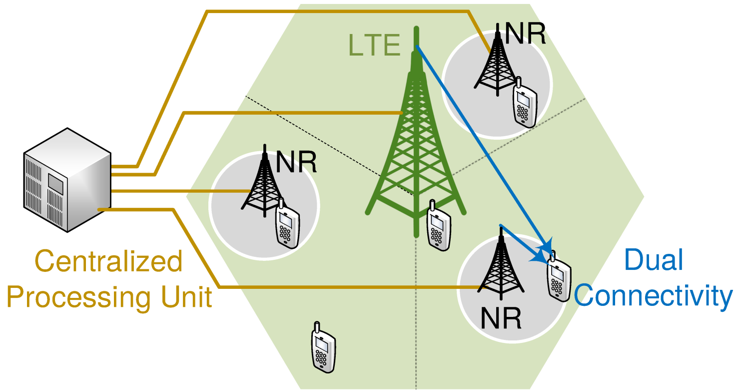

Source: Created by the author.

5.8.1 Simulation Assumptions

The scenario considered in the performance evaluation was aligned with the 3GPP specifications. More specifically, we considered a downlink 5G multi-RAT network based on the dense urban scenario proposed in [70]. It focused on macro LTE BSs with micro NR BSs. The LTE BSs were deployed in a hexagonal grid with 3 sectors per site, while the NR BSs were randomly deployed (one NR BS per LTE sector). The LTE BSs acted as umbrella cells ensuring coverage to the system, while the NR BSs acted as hotspots ensuring high values of throughput, as illustrated in Fig. 5.3. For this purpose, the chosen LTE carrier frequency was 3.50 GHz with 20 MHz of system bandwidth and 49 dBm of transmit power [77]. On the other hand, the chosen NR carrier frequency was 28 GHz with 100 MHz of system bandwidth and 35 dBm of transmit power [71].

Concerning the NR physical layer, as in LTE, the NR RB consisted of 12 subcarriers and 14 OFDM symbols. However, the subcarrier spacing and the TTI were different. In LTE they were equal to 15 kHz and 1 ms, respectively, while in NR, they were equal to 60 kHz and 0.25 ms, respectively [56].

The QUAsi Deterministic RadIo channel GenerAtor (QuaDRiGa) [78] was used for the generation of channel samples. It generates 3D spatial and temporal consistent channel samples considering large and small-scale fading. The LTE channel samples were generated according to the model standardized in [77]. Concerning the NR channel model, it was adopted the one proposed by the mmMAGIC project in [79]. As in [80], for NR, it was considered 3D antenna beamforming with high directive gain, 24.50 dB, and narrow beam width, 10.90° Half Power Beamwidth (HPBW) in the azimuth plane. Ideal beam selection and beam tracking procedures were assumed. Tables 5.1 and 5.2 present an extensive list of the adopted simulation parameters.

The solution of (5.9) was used as an upper bound and was obtained with the IBM ILOG CPLEX Optimizer [83]. Only its feasible snapshots were considered.

The cross-carrier Proportional Fairness (PF) [84] was also used as benchmark. It tries to maximize the system throughput, while allowing all UEs to have at least a minimal throughput. The scheduled UE $u^\star$ on RB k in BS b at TTI t is determined as:

$$u^\star = \arg\max_{u \in \mathcal{U}_b} \left\{ \frac{r_{u,k,b}[t]}{g_u[t-1]} \right\}. \tag{5.13}$$

5.8.2 Numerical Results

First of all, in order to analyze the coverage of LTE and NR BSs, for each UE and RAT, we considered the strongest SNR among all the possible UE-BS links. We highlight that, even the UEs that were not connected to a BS of a given RAT, because even their best link to a BS of this RAT was lower than a given threshold, were considered in this analysis. Fig. 5.4 presents the CDF of these values. Considering −5 dB as the minimum SNR allowing a UE to connect to a BS, according to the MCSs curves in [67], we can see that all the UEs were covered by a LTE BS, since, for all UEs, their best link was higher than −5 dB. On the other hand, for 20 % of the UEs, even their best link to a NR BS was not enough to connect them to a NR BS, i.e., 20 % of the UEs were not inside a NR BS coverage area. This validates the scenario as a macro layer, LTE RAT, acting as an umbrella and the micro layer, NR RAT, as hotspots.

Fig. 5.5 presents the impact of the number of UEs on the minimum throughput. For $U > 30$, there were no feasible solutions for the centralized benchmark, thus the presented results concern $U \leq 30$.

For $U \leq 20$, the proposed distributed framework performed nearly equal to the centralized solution requiring less computational effort and signaling overhead. By interpolation, we find that, for $U > 16$, PF was not able to keep all the UEs satisfied, i.e., with a throughput higher than 20 Mbps, while our proposal was able to keep at least 21 UEs simultaneously satisfied.

Table 5.1 – Common simulation parameters for both RATs.

Parameter	Value
UE distribution	Uniform in the macro layer
UE height	1.50 m
UE speed	5 km/h
UE service profile	Full buffer
UE requirement (ψ_u)	20 Mbps
UE capabilities ($l_{u,n}$)	1 LTE Rx and 1 NR Rx
Min. num. of snapshots	35
Confidence interval	95 %

Source: Created by the author.

Table 5.2 – Simulation parameters for LTE and NR.

Parameter	**LTE**	**NR**	**Ref.'s**[a]
Layout	Macro layer: 1 hexagonal site with 3 sectors	Micro layer: 1 randomly dropped NR BS per LTE sector	[70]
Scenario	3GPP 3D Urban Macro	mmMAGIC initial Urban Micro 10-80	[77], [79]
Inter-site distance	500 m	–	[77]
BS height	25 m	10 m	[77], [71]
Carrier frequency	3.50 GHz	28 GHz	[77], [71]
System bandwidth	20 MHz	100 MHz	[77], [71]
Subcarrier spacing	15 kHz	60 kHz	[81], [56]
Num. of RBs (K_n)	100	125	[82], [56]
TTI	1 ms	0.25 ms	[81], [56]
Noise figure	9 dB	9 dB	[71]
BS Tx power (P_n)	49 dBm	35 dBm	[77], [71]
Tx antenna type	3GPP 3D	Narrow beam (HPBW = 10.90° and directivity gain = 24.50 dB)	[77], [80]

[a] Whenever two references appear, the first refers to LTE and the second to NR. Also, only one reference refers to both RATs.

Source: Created by the author.

Figure 5.4 – SNR of the UEs' best link. For each RAT, we considered the strongest SNR among all the possible UE-BS links. Notice, in the NR curve, that 20 % of the cases were lower than −5 dB meaning that for 20 % of the UEs, even their best link was not enough to connect them to a NR BS, i.e., 20 % of the UEs were not inside a NR BS coverage area.

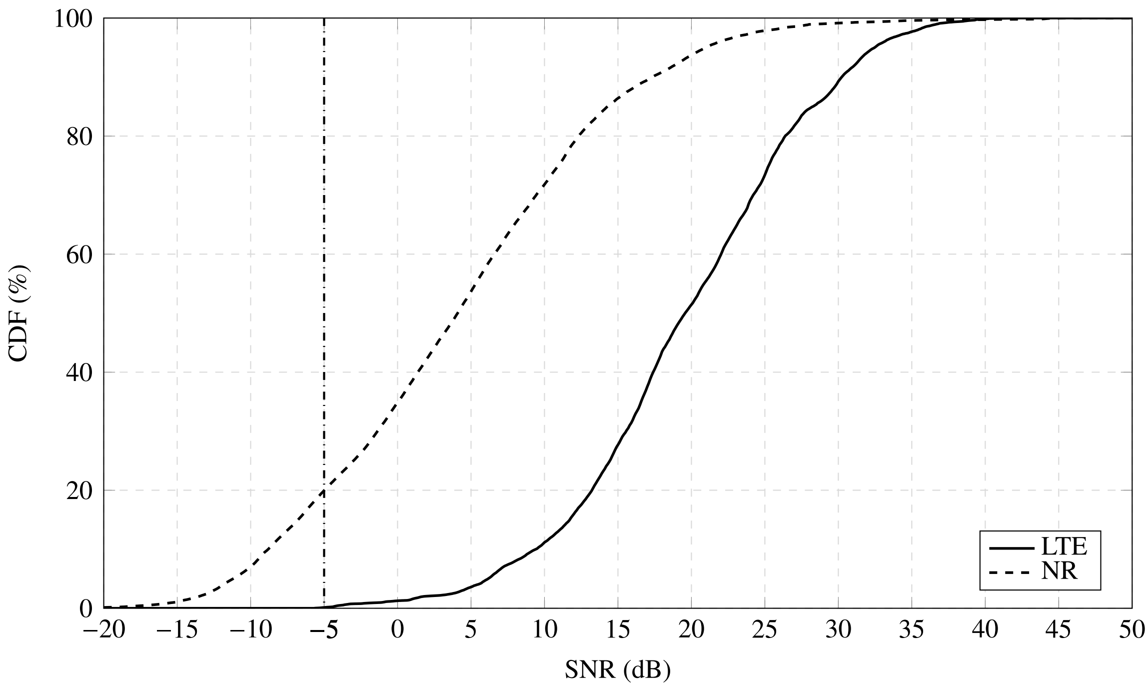

Source: Created by the author.

Figure 5.5 – Minimum UE throughput.

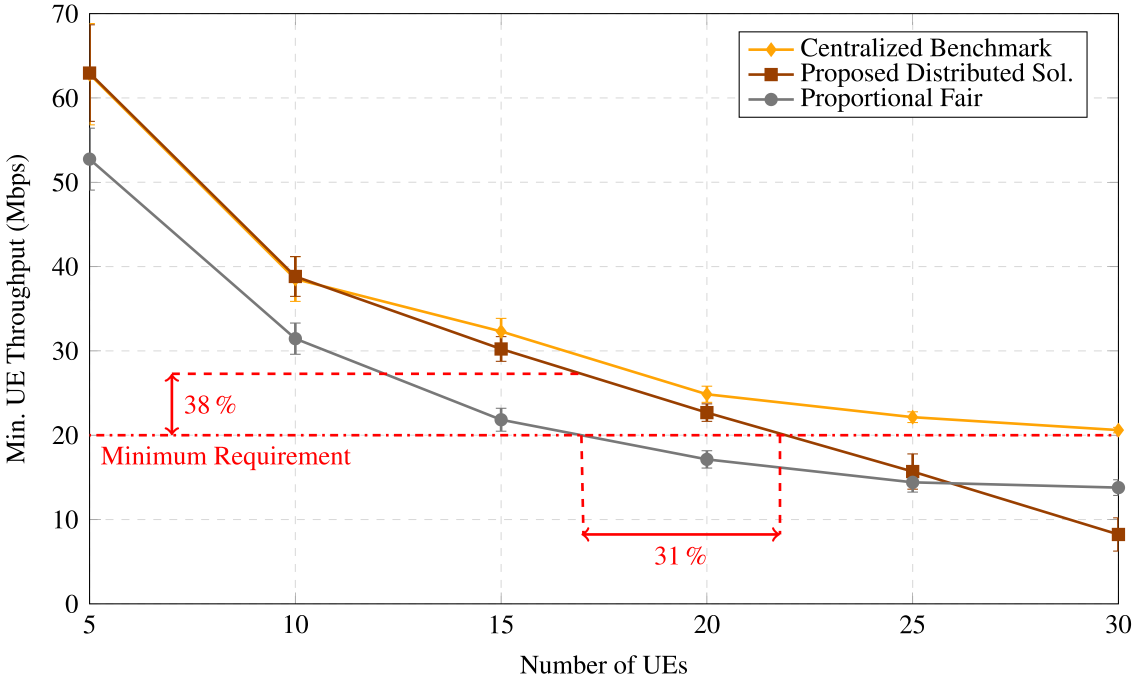

Source: Created by the author.

This means an increase of 31 % in the system's capacity. For $U = 16$, our proposal increased the minimum UE throughput in 38 %, from 20.80 Mbps to 28.70 Mbps.

Note that, the proposed resource assignment, Fig. 5.2, tries to satisfy all the UEs before maximizing the minimum throughput. Thus, when it can not satisfy all the UEs, it prioritizes satisfying as much UEs as possible rather than maximizing the minimum throughput. Therefore, for $U > 25$, our proposal has lower minimum throughput than the PF. This is a trade-off that needs to be implemented in scenarios with high number of UEs.

This trade-off can also be seen in Fig. 5.6. It presents the outage and the Jain's index in function of the number of UEs, where the outage is the percentage of not satisfied UEs and the Jain's fairness index measures the fairness among the UEs throughput, i.e., $\Delta = \frac{(\sum_{u=1}^{U} \theta_u)^2}{U \sum_{u=1}^{U} (\theta_u)^2}$. The outage of PF is always higher than the one of the proposed framework, even for $U > 25$ (when its minimum throughput is lower), this is due to the trade-off already explained.

Sometimes it is difficult to keep the throughput of UEs only connected to LTE BSs as high as that of UEs connected to both RATs. When the number of UEs increased from 5 to 20, the Jains' index of the proposed framework also raised, since this increased the competition for NR RBs, decreasing the throughput of UEs in DC and approximating it to the one achieved by the UEs only connected to LTE. For these loads, the Jains' index of the centralized benchmark was equal to 100 %. The Jains' index of the proposed framework was close to this value, but not equal, since not all UEs were satisfied.

Concerning the Jains' index of the PF, it was clearly lower than the one of our proposal. Ideally, it should exploit multi-user diversity while maintaining fairness. However, the fairness is not achieved. This problem is highlighted in Fig. 5.7, which presents the 50 %-ile

Figure 5.6 – Outage and Jain's index.

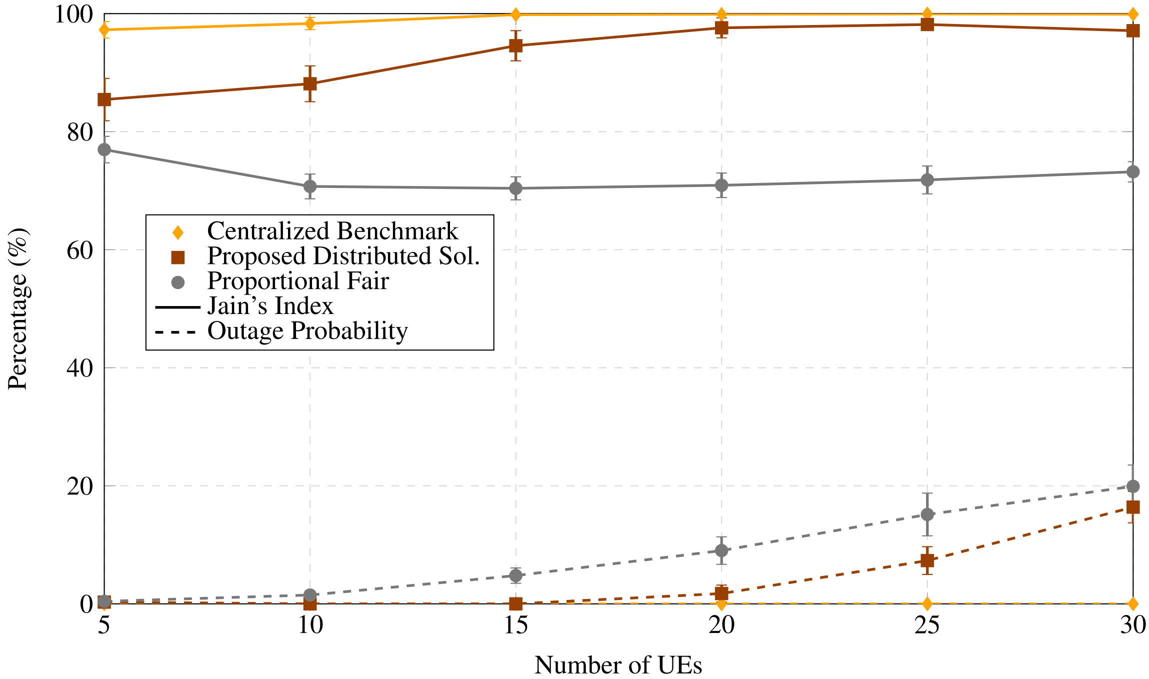

Source: Created by the author.

and 90 %-ile UEs throughput. The unfair scheduling of PF can be seen in the high difference between the throughput of these percentiles, even when the system is overloaded ($U = 30$).

5G networks are expected to be deployed in high frequencies, where the propagation conditions are challenging, e.g., higher path loss and lower diffraction. Thus, the UEs may experience channels with very different quality, as shown in Fig. 5.4, where the NR SNR varies from −20 dB to 30 dB (from a very poor to a very good quality). In such scenarios, since PF is opportunistic, it may schedule UEs with better channel quality even if they have high throughput, keeping UEs with poor channel quality in starvation. In other words, for PF, the good channel experienced by some UEs compensates their high throughput in (5.13), given to them priority to be scheduled. That is why, in Fig. 5.7, we have the large difference between the 50 %-ile and the 90 %-ile throughput.

The behavior of PF not scheduling the UEs with worst channel in NR is illustrated in Fig. 5.8. This figure presents the CDF of the SNR related to the scheduled UEs in each RAT. In NR, we can see that centralized benchmark and our proposal were able to schedule UEs in a larger range of SNR than PF. Regarding LTE, the behavior of PF was similar to the one of the centralized benchmark and of our proposal, allocating all UEs. This is due to the fact that, in LTE, the difference of channel quality among the UEs is not so large as it is in NR, as it can be seen in Fig. 5.4.

In Chapter 3, it was concluded that it might be interesting to consider frameworks that could select between single connection and DC according to the system load. When the load is high and the UEs try to connect to more than one BS at the same time, the network becomes highly interference-limited and the system performance decreases very fast. Thus, not all the

Figure 5.7 – 50 %-ile and 90 %-ile of UEs' throughput.

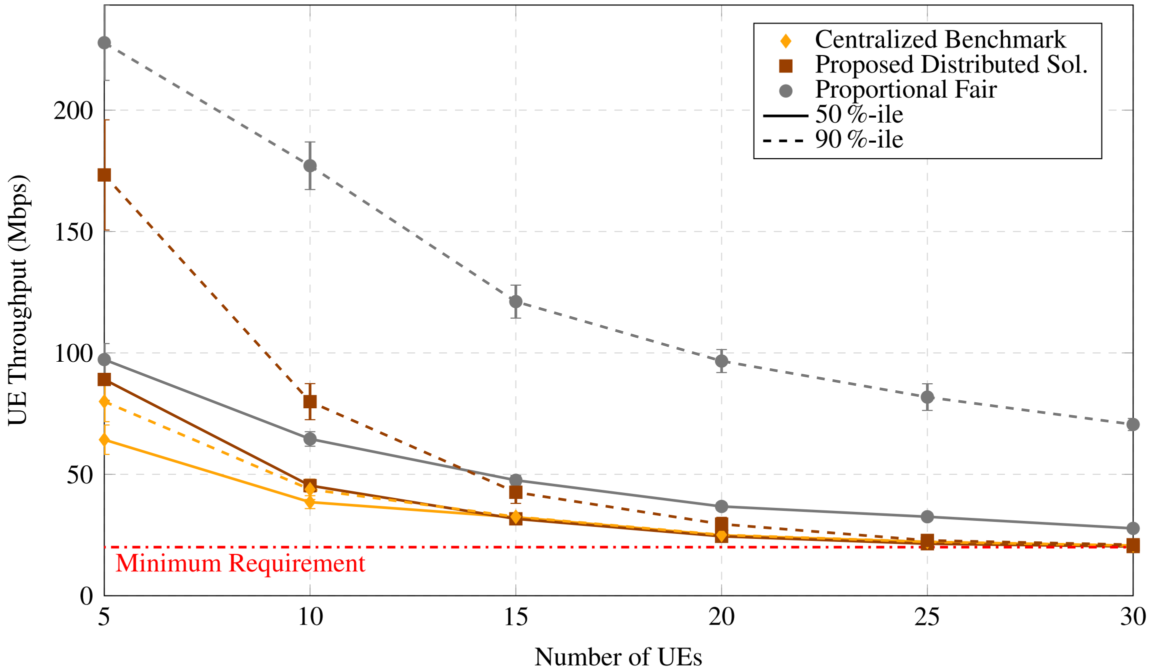

Source: Created by the author.

Figure 5.8 – SNR of scheduled UEs per RAT.

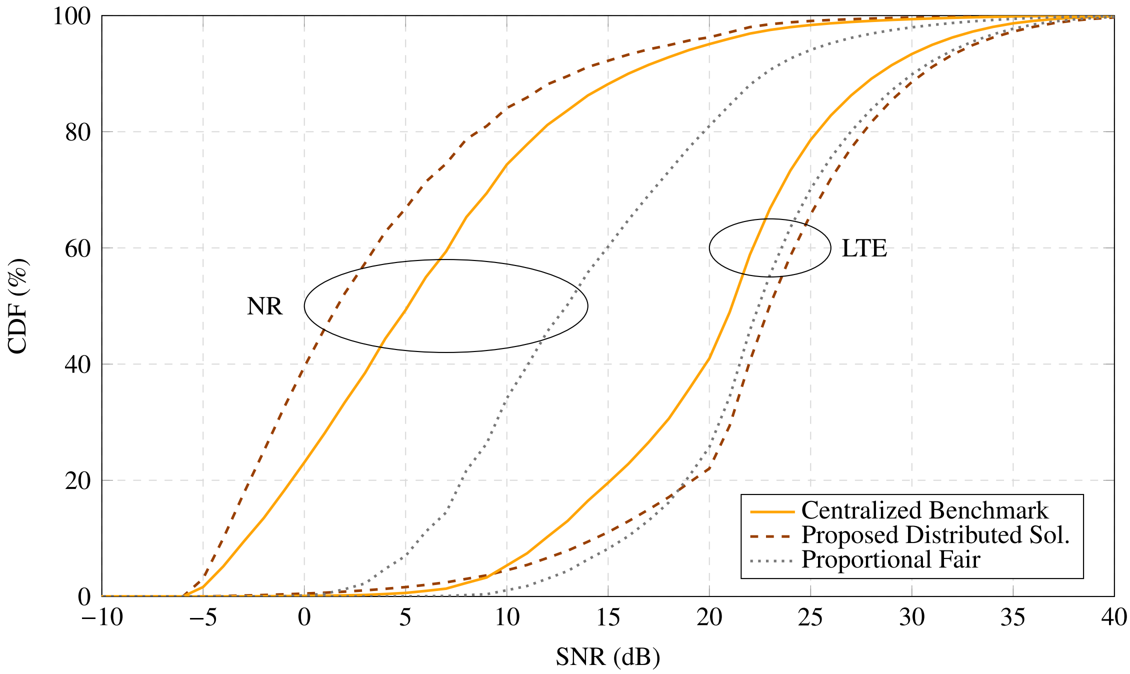

Source: Created by the author.

Figure 5.9 – Percentage of connected UEs in DC.

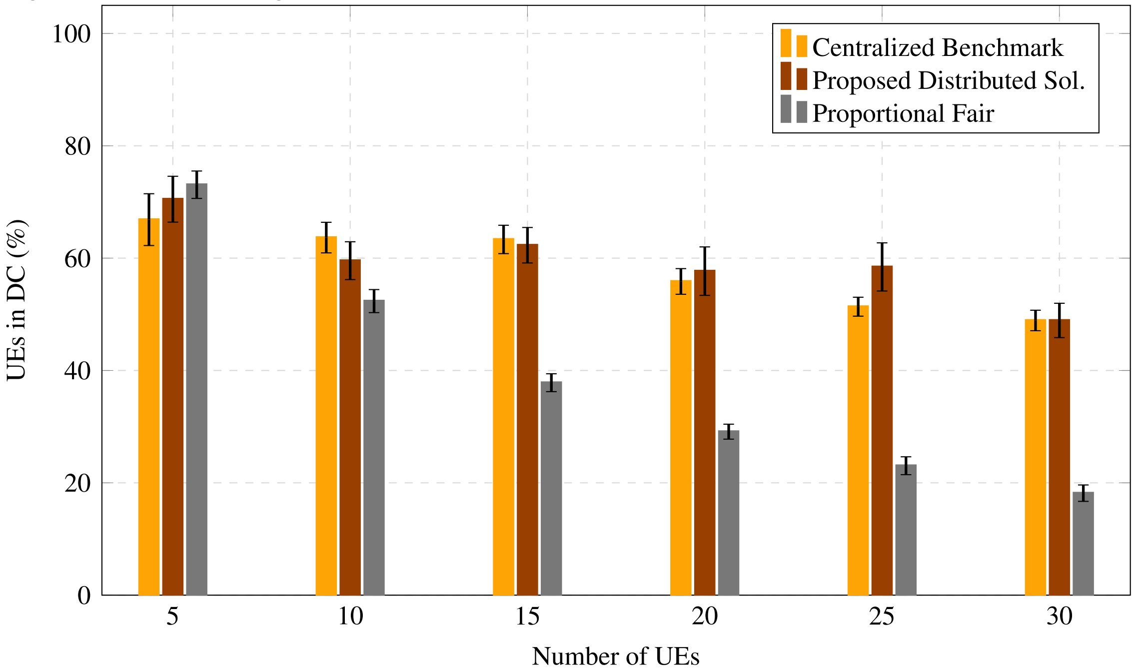

Source: Created by the author.

UEs will benefit from the larger transmission bandwidth offered by DC. A balance between load and number of UEs in DC needs to be found.

Our proposed framework already takes this balance into account, as it can be seen in Fig. 5.9. This figure presents the percentage of connected UEs which were in DC as a function of the number of UEs in the system. The complementary of this percentage represents the UEs in single connection. In low loads, the majority of the UEs were in DC mode. The single connection UEs were mainly the ones which were not in the coverage area of a NR BS. When the load increased, in order to maintain the system's performance, the percentage of UEs in DC decreased for the three considered solutions. However, for PF this reduction was higher than for the others. It decreased more than the necessary, if we consider the behavior of the centralized benchmark as the optimal one.

5.9 Chapter Summary

The present chapter focused on managing radio resources in a multi-RAT scenario. More specifically, an optimization problem was formulated in order to maximize the minimum UE throughput in the system subject to the constraint that all users must be satisfied. The referred problem is non-linear and hard to solve. However, we got to transform it into a simpler form, a MILP, that can be optimally solved using standard numerical optimization methods. It was also proposed a distributed framework to overcome the drawbacks of centralized processing. It is divided into two parts: a BS selection procedure (performed independently by each UE) and a resource assignment algorithm (performed independently by each BS). Besides, a performance evaluation was conducted, considering Fourth Generation (4G) LTE and 5G NR system parameters.

The proposed solution outperforms a cross-carrier PF, as well as, it performs close to the benchmark solution. Compared to PF, our proposal improves by 31 % the system's capacity and by up to 38 % the minimum throughput in the system. Regarding the benchmark solution, our proposal requires less computation effort and less signaling overhead. The analyses also showed that the proposed framework tries to avoid the system overload by decreasing the percentage of UEs in DC mode when the number of UEs increases.

6 RESOURCE ALLOCATION IN 5G: COMPLEXITY AND RELIABILITY ASPECTS

Continuing the study of 5G multi-RAT scenarios and CH occurrence, the present chapter focuses on the implications of these topics on the adopted KPIs and RRA algorithms.

More specifically, three different RRAs and three different KPIs were considered in the analyses. Regarding reliability, DC and FS performances were compared. Concerning complexity, it was evaluated a proposed method that optimizes CQI measurements and reporting based on the occurrence of CH.

Before addressing the evaluations themselves, next section presents the proposed method for CQI measurement and reporting optimization.

6.1 CQI Measurement and Reporting Optimization Based on CH Occurrence

As already presented, due to the higher diversity of possible links (Tx-Rx beam pairs) over a wider bandwidth, the amount of CQIs being reported by the UEs might increase the complexity of RRA. Thus, new approaches need to be adopted to avoid the increase in RRA complexity as the number of antennas increases and the bandwidth enlarges.

Since CH may reduce channel fluctuations, CQI RBs may have similar values. Thus, it will not be worth the effort to measure and report all of them. In this context, we propose a method in which is up to the UE to identify when CH is happening and inform this to its serving BS, so it can take advantage of it.

The first step of the proposed method is illustrated in Fig. 6.1. A UE performs measurements to derive the channel quality in all configured pairs of RBs and beams (the colored squares in the figure). Then, the UE estimates the correlation of these pairs. If the correlation is high for a subset of beams and RBs (squares with the same color in the figure), meaning that the channel has been hardened in this subset, the UE will select a pair beam-RB as representative of the subset and will report to the BS only the CQI of this pair. Besides, it needs to report a single bit indicating that there is CH along with the bits informing the list of beams and RBs to which this report corresponds.

As illustrated in Fig. 6.2, for each set of pairs beam-RB in which the UE detects the CH, the UE will still measure the CQI of all pairs beam-RB of these sets during the next X' measurement periods. If CH is detected during these X' measurement periods, for the next measurement periods, the UE is allowed to measure only the CQI of the representative pair. The other pairs will still be measured, but with a longer periodicity to verify whether CH is still happening or not.

Figure 6.1 – Proposed CQI reporting optimization based on CH occurence.

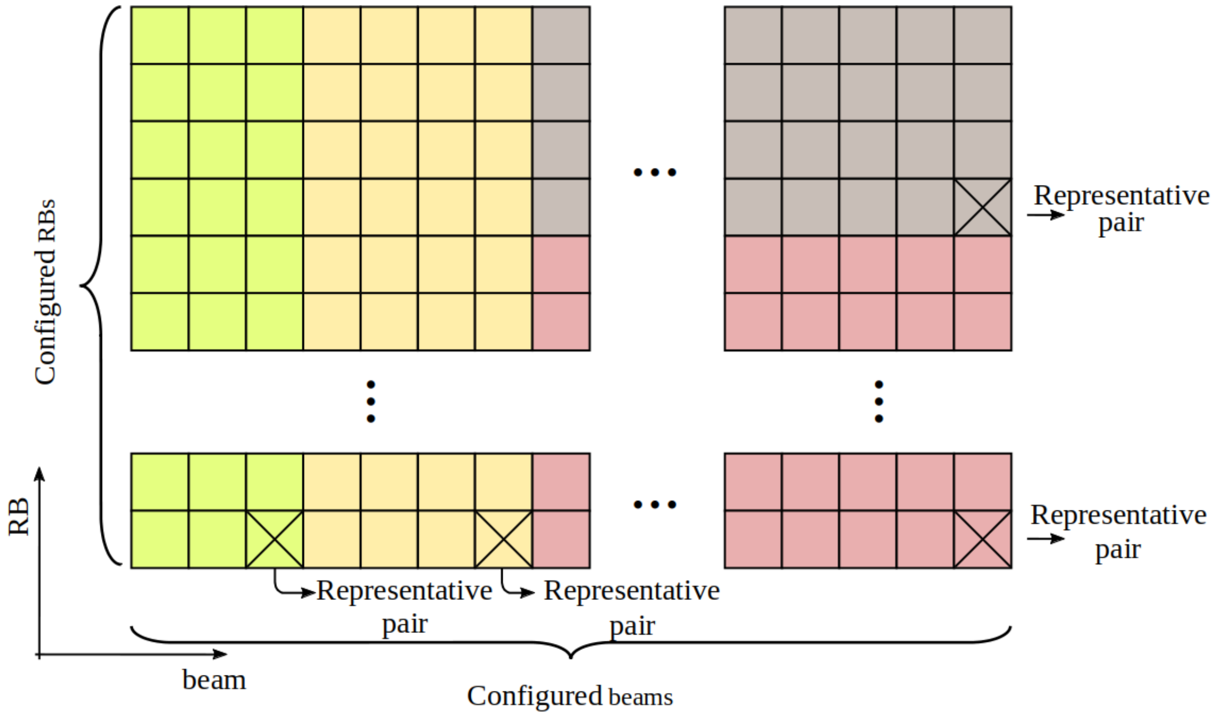

Source: Created by the author.

Figure 6.2 – Proposed CQI measurement optimization based on CH occurence.

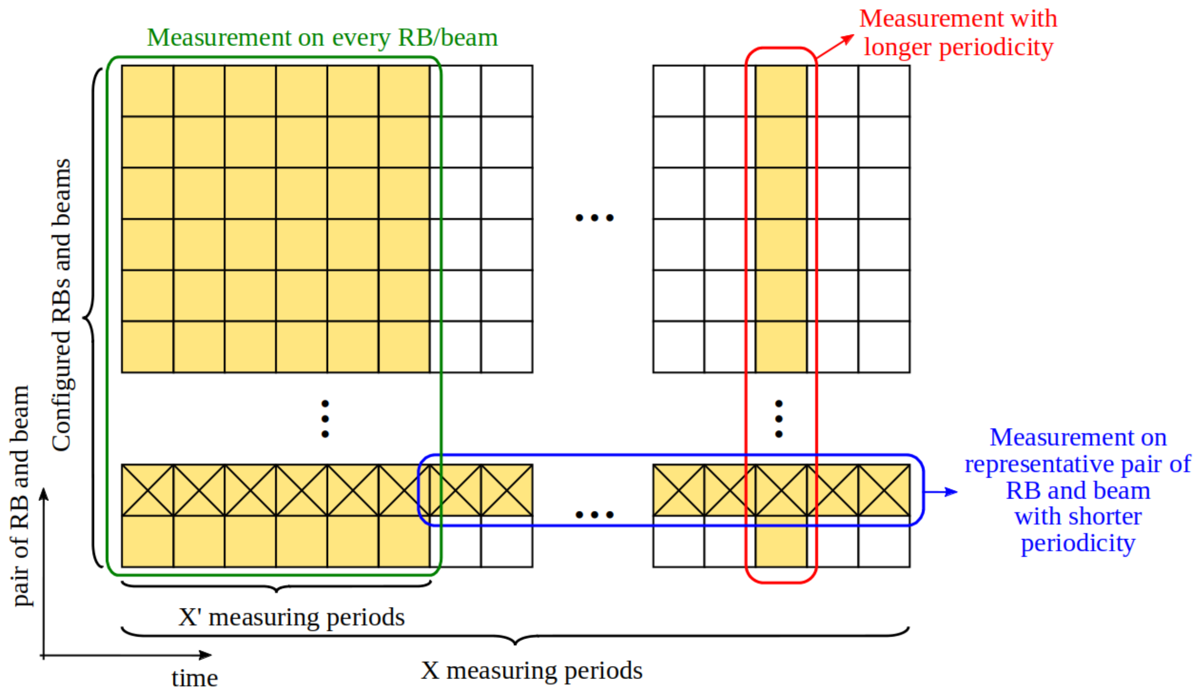

Source: Created by the author.

Figure 6.3 – 5G multi-RAT scenario.

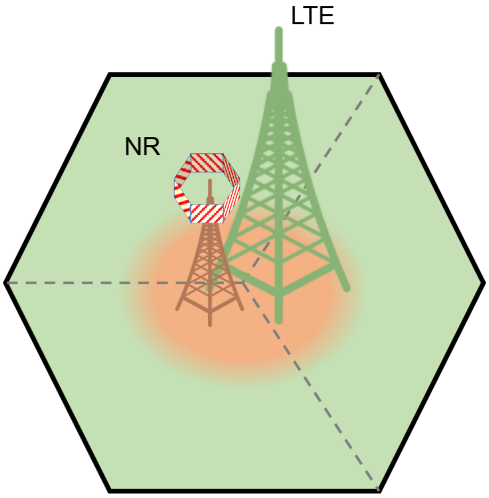

Source: Created by the author.

6.2 Performance Evaluation

6.2.1 Simulation Assumptions

As illustrated in Fig. 6.3, this chapter considers co-sited LTE and NR BSs. When not explicitly defined, the LTE antennas cover areas of 120°, while six 8×8 NR antenna arrays cover areas of 60° each. Besides, each NR antenna array is connected to one analog beamformer. The LTE and NR RATs are responsible for ensuring coverage and high throughput, respectively. To this purpose, the chosen LTE carrier frequency is 2 GHz with 10 MHz of system bandwidth and 46 dBm of transmit power. On the other hand, the chosen NR carrier frequency is 28 GHz with 20 MHz of system bandwidth and 28 dBm of transmit power.

Concerning the physical layer, the configuration presented in Section 2.3 was adopted. In LTE, the minimum scheduling unit is a subframe consisting of two RBs, i.e., 14 OFDM symbols spanning over 1 ms and 12 subcarriers with subcarrier spacing equal to 15 kHz. In NR, the minimum scheduling unit is a slot, also consisting of 14 OFDM symbols and 12 subcarriers, but spanning over 0.25 ms and with subcarrier spacing equal to 60 kHz. Tables 6.1 and 6.2 present an extensive list of the adopted simulation parameters.

As presented in [72], different scheduling criteria have already been considered in the literature. They have pros and cons. Thus, three different scheduling criteria were chosen in order to analyze the possible impacts of the solutions used to address the challenges presented in the previous section. They are:

- *Max-rate*: maximizes the system throughput;
- *PF*: schedules the UE that maximizes the ratio between CQI and the amount of already received bits;
- *Satisfaction oriented*: first maximizes the number of satisfied UEs, and, after, allocates remaining unscheduled resources to the UEs with minimum throughput.

Table 6.1 – Simulation parameters for LTE and NR.

Parameter	**LTE**	**NR**	**Ref.'s**[b]
Layout	Macro layer: 1 site with 3 sectors	Micro layer: 1 site with 6 sectors	[70]
Scenario	3GPP 3D Urban Macro	mmMAGIC initial Urban Micro 10-80	[77], [79]
Inter-site distance	200 m	–	[77]
BS height	25 m	10 m	[77], [71]
Carrier frequency	2 GHz	28 GHz	[77], [71]
System bandwidth	10 MHz	20 MHz	[77], [71]
Subcarrier spacing	15 kHz	60 kHz	[81], [56]
Num. of RBs	50	25	[82], [85]
Subframe (LTE) \ Slot (NR) time duration	1 ms	0.25 ms	[81], [56]
Noise figure	9 dB	9 dB	[71]
BS Tx power	46 dBm	28 dBm	[77], [71]
Tx antenna type	3GPP 3D	3GPP 3D	[77]

[b] Whenever two references appear, the first refers to LTE and the second to NR. Also, only one reference refers to both RATs.
Source: Created by the author.

Table 6.2 – Common simulation parameters for both RATs.

Parameter	**Value**
UE distribution	Uniform in the macro layer
UE height	1.50 m
UE speed	5 km/h
UE service profile	Full buffer
UE requirement	15 Mbps
Min. num. of snapshots	35
Confidence interval	95 %

Source: Created by the author.

In this chapter, the joint beam-frequency multiuser scheduler framework proposed in [86] was adopted. For each analog beamformer in the system, it finds the optimal beam direction in order to maximize the scheduling metric. Then, for each selected beam, the scheduler allocates the RBs to the UEs that maximizes the contribution to the target scheduling metric. Each UE reports a set of preferred beams indices and a CQI vector for all the RBs over these beams.

This framework was adopted in two different ways:

- *Centralized*: a central unit is responsible for choosing which BS, beam and frequency RBs will be used to serve each UE;
- *Decentralized*: each BS individually allocates its own resource (without coordination among them), while the UEs are responsible for choosing the best BS for them.

Max-rate and PF schedulers were implemented as centralized solutions while the satisfaction oriented scheduler was implemented as a decentralized solution. This way, we could also analyze

Figure 6.4 – SNR of the UEs' best link. For each RAT, we considered the strongest SNR among all the possible UE-BS links. Considering −5 dB as the minimum SNR allowing a UE to connect to a BS, notice that all the UEs were covered by a LTE BS. On the other hand, considering NR 8×8 arrays, the UE-NR best links of 20 % of the UEs were not good enough to connect them to a NR BS, i.e., 20 % of the UEs were not inside a NR BS coverage area. This validates the scenario as a macro layer, LTE, acting as an umbrella and a micro layer, NR, as hotspots.

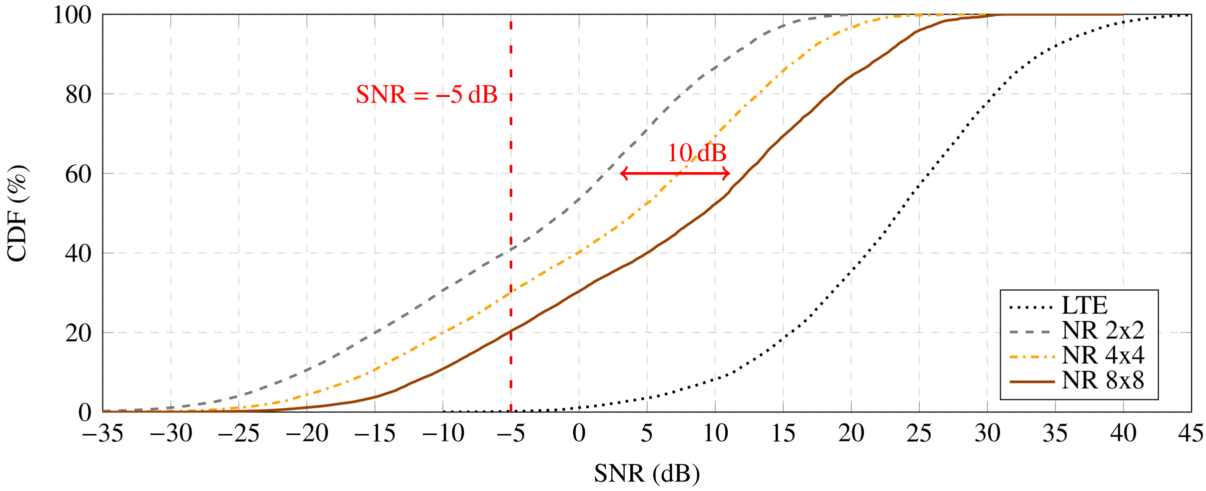

Source: Created by the author.

these two different implementation approaches.

6.2.2 Numerical Results

First, we analyzed the coverage of LTE and NR BSs. As in the previous chapter, for each UE and RAT, we considered the link with the strongest SNR among all possible UE-BS links. Fig. 6.4 presents the CDF of these values. Assuming −5 dB as the minimum SNR allowing a UE to connect to a BS, notice that all the UEs were covered by a LTE BS. On the other hand, considering NR 8×8 arrays, the UE-NR best links of 20 % of the UEs were not good enough to connect them to a NR BS, i.e., 20 % of the UEs were not inside a NR BS coverage area. This validates the scenario as a macro layer, LTE, acting as an umbrella and a micro layer, NR, as hotspots. Also, notice the difference of 10 dB between the curves of 2×2 and 8×8 antenna arrays. Fig. 6.5 complements Fig. 6.4 by presenting the SNR heat map. When deployed with smaller arrays, the coverage of NR was even smaller.

6.2.2.1 Complexity

As aforementioned, the CH effect may simplify RRA in the frequency domain. Thus, in this section we investigate how to take advantage of this and we analyze its main impact on system's KPIs.

Fig. 6.6 presents the standard deviation of RBs SNR. The obtained result confirms the existence of CH. That is, the fluctuations of RBs SNR around the mean SNR decrease as the number of antennas increases. This suggests that choosing the central RB as a representative

Figure 6.5 – SNR heat map snapshot inside a circle of radius 133.33 m.

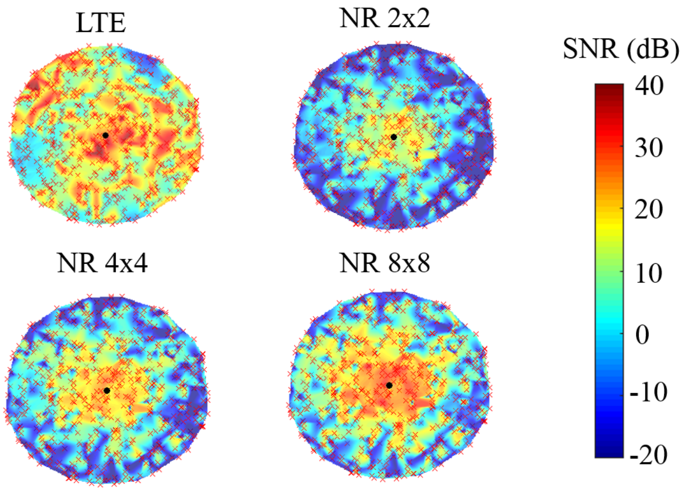

Source: Created by the author.

Figure 6.6 – CDF of standard deviation of RBs SNR. Increasing the number of antennas, the standard deviation decreases, i.e., the fluctuations of RBs SNR around the mean SNR decrease, which confirms the existence of CH in the considered scenario.

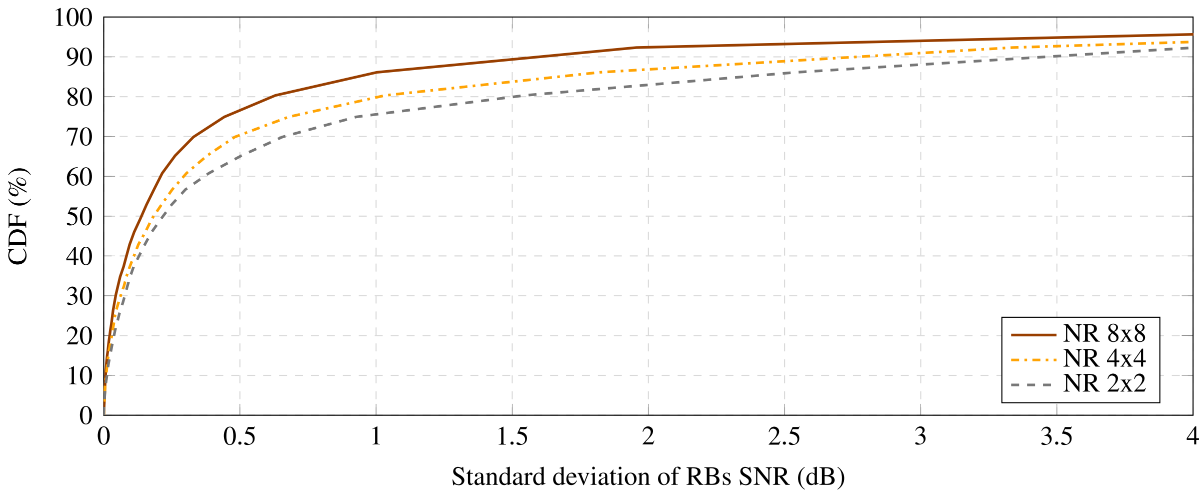

Source: Created by the author.

RB, reporting only its CQI and considering the others RBs CQI equal to the reported value may not strongly harm the system's performance. Thus, we investigated the impact of this strategy on system's performance when using the previously presented schedulers (max rate, PF and satisfaction oriented).

Fig. 6.7 presents three system's KPIs: the percentage of satisfied UEs, the system throughput and the Jain's fairness index. Solid lines represent the case where the schedulers had knowledge of all RBs CQI, while dashed lines represent the case where the central RB was used as representative and the schedulers considered the RBs CQIs equal to the central RB CQI. Notice that all the dashed lines are very close to their equivalent solid lines. Considering the confidence interval of 95 %, one could say that they are equal in many cases.

Figure 6.7 – Impact on system KPIs of two different CQI reporting strategies. It was considered 8x8 NR antenna arrays.

(a)

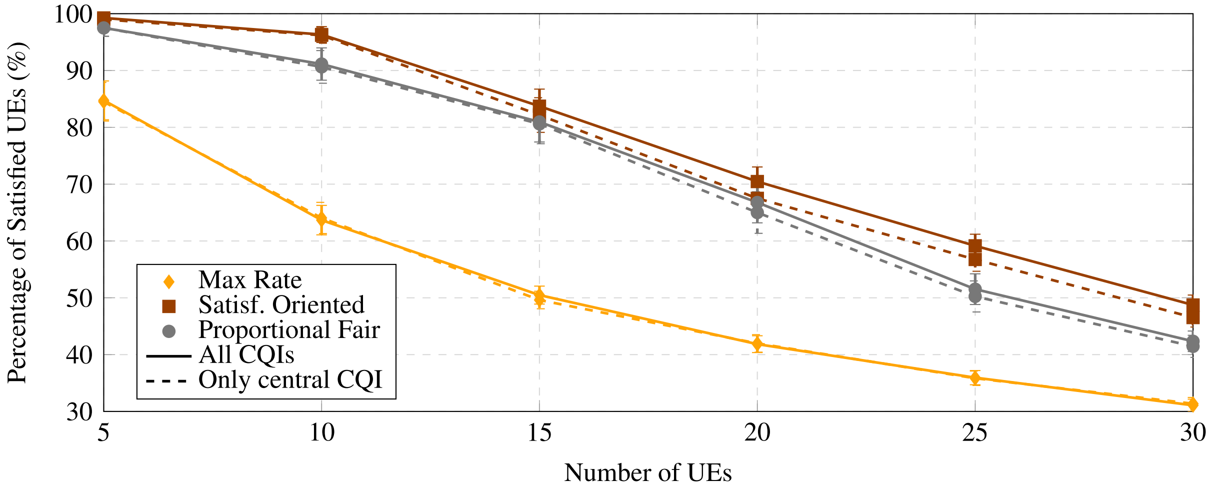

(b)

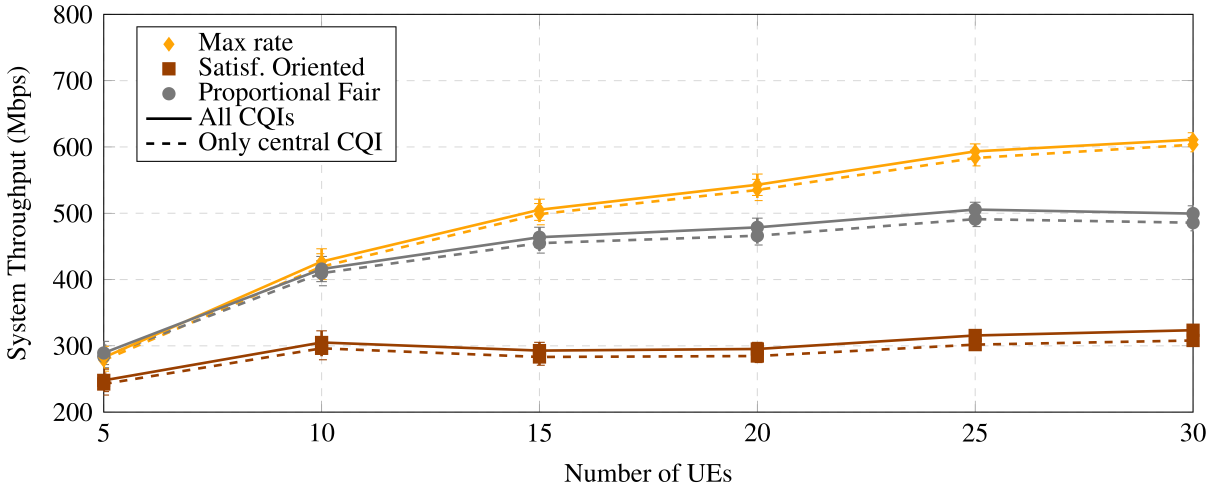

(c)

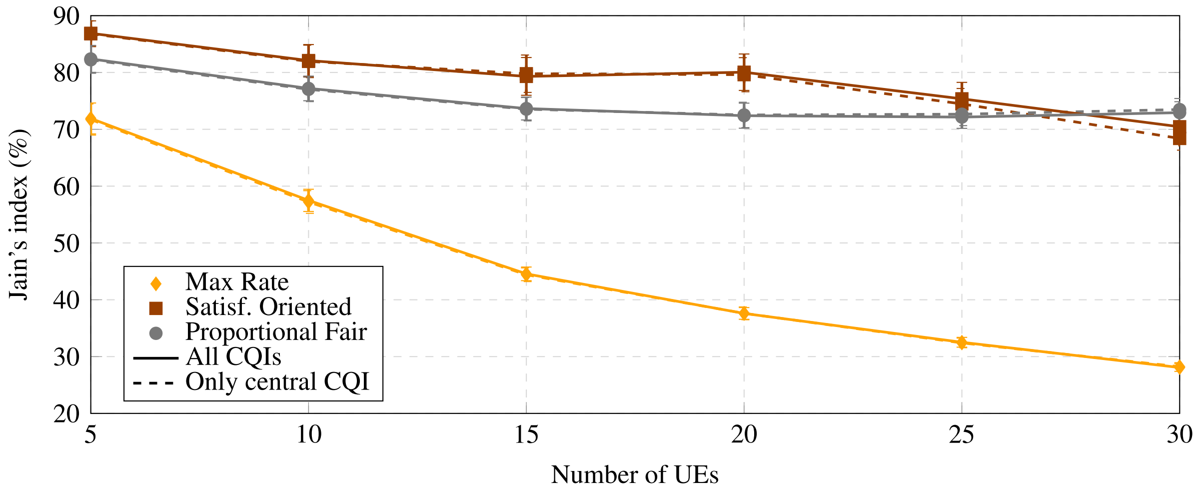

Source: Created by the author.

It is clear that the proposed strategy does not strongly harm the system's performance, while it reduces signaling overhead and RRA complexity. Since frequency selective fading is mitigated by the CH, there is no need for performing complex frequency selective RRA.

6.2.2.2 Reliability

As already mentioned, LTE is expected to be used together with 5G as a reliable link. The UE will be either simultaneously connected to both RATs or it will be able to fast switch to LTE when NR quality decreases. The effects of these two approaches may differ according to the adopted scheduler, as we show in this section.

Fig. 6.8 presents three system's KPIs. Solid lines represent results considering the DC approach, while dashed lines concerns the results of the FS.

Regarding the max rate scheduler, when considering FS, instead of DC, the UEs in poor coverage have higher chances to be scheduled, since UEs with high channel gain are scheduled in only one RAT. Therefore, for the max rate criterion, FS has higher percentage of satisfied UEs and higher Jain's fairness index, but DC has higher system throughput.

The satisfaction oriented assumes no coordination between the BSs. As a consequence, in DC, both RATs try to satisfy the same UEs first (the easiest ones). Therefore, there are more UEs with low throughput in DC than in FS, which means higher fairness but less satisfied UEs.

On the other hand, PF assumes coordination between the BSs. Therefore, in DC there is more diversity to schedule the UEs than in FS, so higher chances to increase the fairness and to satisfy more UEs. However, there is a trade-off between satisfying UEs with low channel gains and having high system throughput, so DC has lower system throughput than FS.

As one can see, it is important to take into account the scheduler being used in the BSs and the KPIs of interest when enabling DC or FS mode in the UEs, since the selected mode may have a different impact on system performance according to the adopted scheduler.

6.3 Chapter Summary

Concerning the RRA complexity, it was concluded that it can be reduced with almost no loss of performance by taken into account the CH effect. Since CH occurrence means that the channel fluctuations over the frequency become negligible, the UEs could report the CQI of just one RB-beam pair that represent the set of pairs where CH occurs. Thus, in this case, the RRA may be simplified, since there is no frequency selectivity.

Regarding the 5G reliability, DC and FS can be used to improve it. However, despite of what one could expect, it was concluded that DC is not always better than FS. DC and FS performances are impacted by the adopted RRA strategy. For example, while a max rate strategy with DC satisfies less UEs than with FS, PF presented an opposite behavior.

Figure 6.8 – Impact of FS and DC on system KPIs considering 3 different schedulers. It was considered 8x8 NR antenna arrays.

(a)

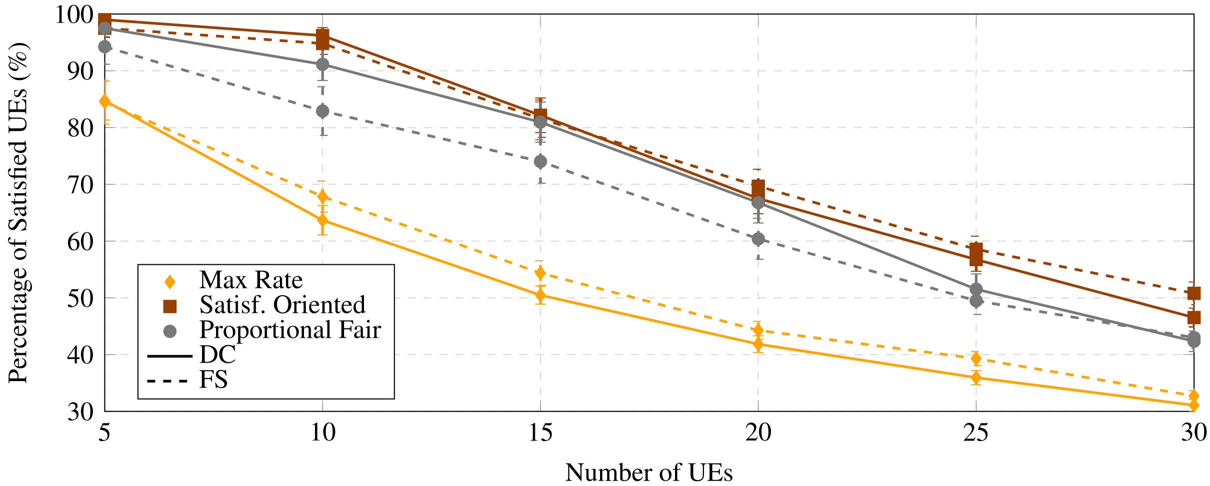

(b)

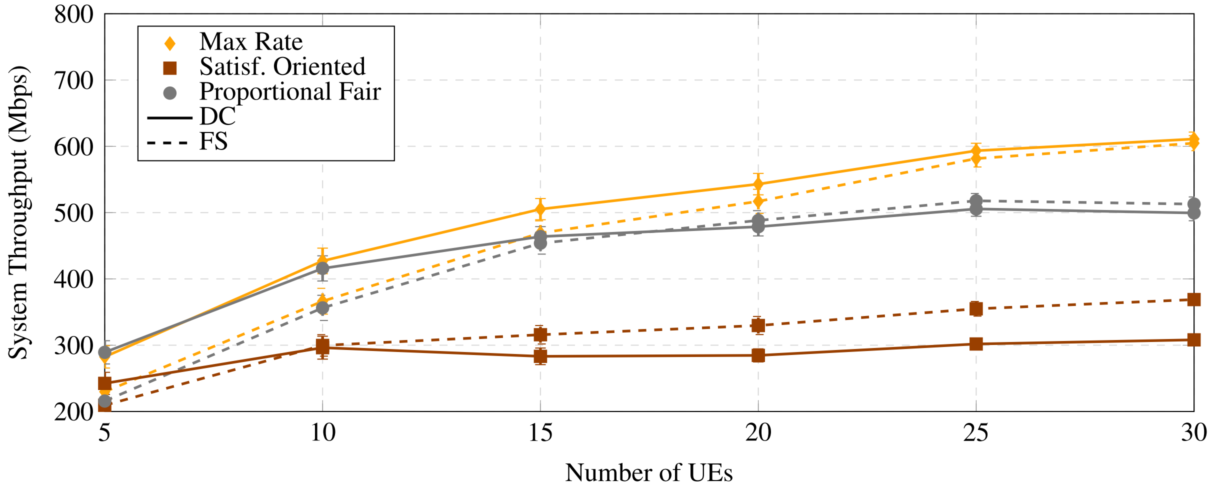

(c)

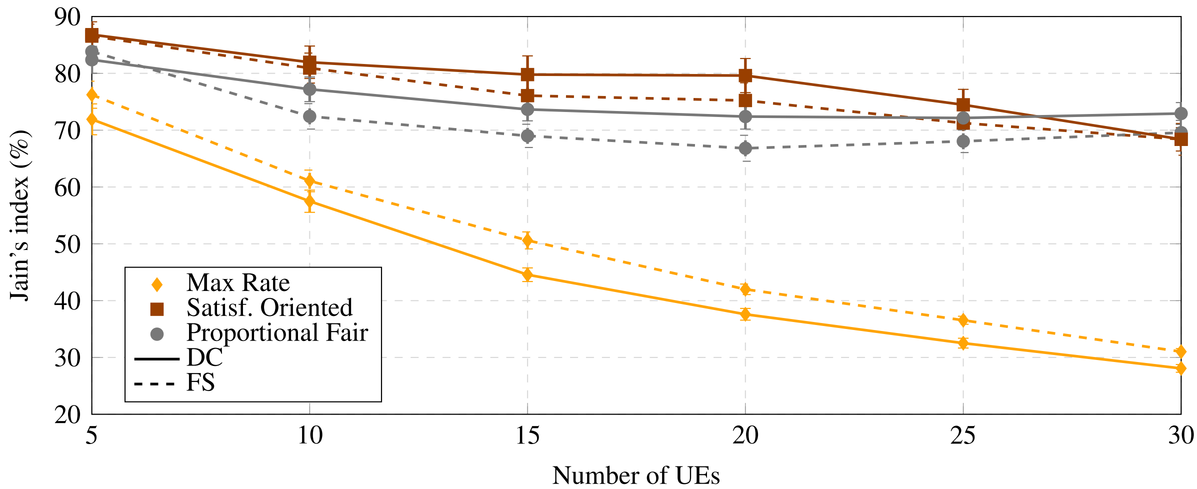

Source: Created by the author.

7 CONCLUSIONS

As presented in Chapter 1, the main purposes of this thesis was to study solutions based on DC and CH occurrence to address the problems of reliability and complexity in 5G.

The literature review presented in Chapters 1 and 2 showed a better understanding of both concepts. Concerning DC, we identified some challenges related to HetNet scenarios, e.g., RAT selection, and the standardized architectures, which gave us an idea of the degrees of freedom related to new proposals. For example, since a non-ideal backhaul interface is expected to connect BSs of different RAT, the new solutions can not rely on heavy communications between them. Furthermore, we also identified alternative solutions to DC, e.g., FS, since DC is not expected to have the best performance in all scenarios. Regarding the CH, the literature review helped us to identify possible causes of CH, e.g., higher number of antennas and narrower beams. Besides, the technical background regarding measurement related tasks, e.g., mobility management, and NR reference signals, such as SSB and CSI-RS, helped us to determine which upper layer functions could take advantage of CH, e.g., SSB is associated with cell RSRP measurements (handover) and CSI-RS is associated with CQI measurements (scheduling).

With respect to the numerical results, on one hand, Chapters 3 and 4 presented general analyses related to DC and CH occurrence, respectively. On the other hand, Chapters 5 and 6 addressed these concepts from the perspective of RRA.

In Chapter 3, it was concluded that, in multi-RAT scenarios, metrics related to signal quality, e.g. RSRQ, should be prioritized instead of metrics only related to the signal strength, e.g., RSRP. Decision criteria only based on signal strength tend to overload the RAT with better propagation conditions. It was also concluded that, in 5G, it should be considered shorter time between consecutive RAT scheduling evaluations, which can vary according to the system conditions, e.g., the UE speed. Finally, it was showed that while DC performs better than FS for low loads, FS can present higher gains than DC for high loads.

In Chapter 4, the numerical results confirmed that when deploying narrow beams (in that case, it was the same as increasing the number of SSBs and CSI-RSs), the CH becomes more noticeable. Furthermore a framework for CH detection and L1 measurement optimization was proposed and validated. The proposed solution calculates the standard deviation of RSRP measurements in a sliding window in order to measure the level of CH and, based on this, the measurement periodicity is dynamically adjusted. It was also concluded that the UE mobility negatively impacts the CH, i.e., increasing the UE speed increases channel fluctuations for some UEs. Despite of this, the proposed method still works for all UEs.

In Chapter 5, we took into account the conclusions of Chapter 3 and we proposed a decentralized framework for radio resource managing. It is divided into two parts: a BS selection procedure (performed independently by each UE) and a resource assignment algorithm (performed independently by each BS). As suggested in Chapter 3, the proposed BS selection procedure takes into account not only the signal strength, but also the state of the UEs already connected to the target BS. Besides, as also suggested in Chapter 3, the balance between UEs in DC and single connection is also taken into account.

Finally, Chapter 6 focused on the implications of DC and CH occurrence on the adopted KPIs and RRA algorithm. Concerning the RRA complexity, it was concluded that it can be reduced with almost no loss of performance by taken into account the CH effect. Since CH occurrence means that the channel fluctuations over the frequency become negligible, the UEs could report the CQI of just one subband-beam pair that represent the set of pairs where CH occurs. Thus, in this case, the RRA may be simplified, since there is no frequency selectivity. Regarding multi-RAT connectivity, it was concluded that DC and FS performances are impacted by the adopted RRA strategy. For example, while a max rate strategy with DC satisfies less UEs than with FS, PF presented an opposite behavior.

REFERENCES

1 ITU-R. **IMT vision – Framework and Overall Objectives of the Future Development of IMT for 2020 and Beyond**. [S.l.], Sept. 2015. Available from: <https://www.itu.int/rec/R-REC-M.2083>. Visited on: 19 Oct. 2018.

2 ________. **Minimum Requirements Related to Technical Performance for IMT - 2020 Radio Interface(s)**. [S.l.], Feb. 2017. Available from: <https://www.itu.int/pub/R-REP-M.2410-2017>. Visited on: 19 Oct. 2018.

3 3GPP. **3GPP Specification Serie 38**. 2016. Available from: <http://www.3gpp.org/DynaReport/38-series.htm>. Visited on: 19 Oct. 2018.

4 ________. **3GPP Release 15**. July 2018. Available from: <http://www.3gpp.org/release-15>. Visited on: 18 Oct. 2018.

5 MARSCH, P. et al. 5G Radio Access Network Architecture: Design Guidelines and Key Considerations. **IEEE Communications Magazine**, v. 54, n. 11, p. 24–32, Nov. 2016. DOI: 10.1109/MCOM.2016.1600147CM.

6 LIN, X. et al. 5G New Radio: Unveiling the Essentials of the Next Generation Wireless Access Technology. **CoRR**, June 2018. Available from: <https://arxiv.org/abs/1806.06898>. Visited on: 5 July 2018.

7 BOGALE, T. E.; LE, L. B. Massive MIMO and mmWave for 5G Wireless HetNet: Potential Benefits and Challenges. **IEEE Vehicular Technology Magazine**, v. 11, n. 1, p. 64–75, Mar. 2016. DOI: 10.1109/MVT.2015.2496240.

8 SUN, S. et al. MIMO for Millimeter-Wave Wireless communications: Beamforming, Spatial Multiplexing, or Both? **IEEE Communications Magazine**, v. 52, n. 12, p. 110–121, 2014. DOI: 10.1109/MCOM.2014.6979962.

9 DONG, M.; KIM, T. **Reliability of an Urban Millimeter Wave Communication Link with First-Order Reflections**. In: PROCEEDINGS of the IEEE Global Telecommunications Conference (GLOBECOM). [S.l.: s.n.], Dec. 2016. p. 1–6. DOI: 10.1109/GLOCOM.2016.7842213.

10 3GPP. **Beam Measurement Quantity Reporting**. [S.l.], Oct. 2017. Available from: <http://www.3gpp.org/ftp/tsg_ran/wg2_rl2/TSGR2_99bis/Docs/>. Visited on: 19 Oct. 2018.

11 ________. **NR; NR and NG-RAN Overall Description; Stage 2**. [S.l.], Oct. 2018. v.15.3.1. Available from: <http://www.3gpp.org/ftp/Specs/html-info/38300.htm>. Visited on: 15 Oct. 2018.

12 3GPP. **Evolved Universal Terrestrial Radio Access (E-UTRA) and Evolved Universal Terrestrial Radio Access Network (E-UTRAN); Overall description; Stage 2**. [S.l.], Oct. 2018. Available from: <`http://www.3gpp.org/ftp/Specs/html-info/36300.htm`>. Visited on: 17 Oct. 2018.

13 BJORNSON, E.; LARSSON, E. G.; MARZETTA, T. L. Massive MIMO: Ten Myths and One Critical Question. **IEEE Communications Magazine**, v. 54, n. 2, p. 114–123, Feb. 2016. DOI: `10.1109/MCOM.2016.7402270`.

14 ANDREWS, J. G. Seven Ways that HetNets are a Cellular Paradigm Shift. **IEEE Communications Magazine**, v. 51, n. 3, p. 136–144, 2013. DOI: `10.1109/MCOM.2013.6476878`.

15 WANG, L.; KUO, G. S. G. S. Mathematical Modeling for Network Selection in Heterogeneous Wireless Networks - A Tutorial. **IEEE Communications Surveys and Tutorials**, v. 15, n. 1, p. 271–292, 2013. DOI: `10.1109/SURV.2012.010912.00044`.

16 PARK, S. Y.; KIM, J. H.; LEE, H. **Dynamic inter-RAT Handover Decision for Offloading Heavy Traffic in Heterogeneous Networks**. In: INTERNATIONAL Conference on Ubiquitous and Future Networks (ICUFN). [S.l.: s.n.], July 2014. p. 466–471. DOI: `10.1109/ICUFN.2014.6876834`.

17 3GPP. **Study on Small cell enhancements for E-UTRA and E-UTRAN - Higher layer aspects**. [S.l.], Jan. 2014. Available from: <`http://www.3gpp.org/dynareport/36842.htm`>. Visited on: 17 Sept. 2018.

18 WANG, R.; HU, H.; YANG, X. Potentials and Challenges of C-RAN Supporting Multi-RATs Toward 5G Mobile Networks. **IEEE Access**, v. 2, p. 1187–1195, 2014. DOI: `10.1109/ACCESS.2014.2360555`.

19 GIORDANI, M. et al. **Multi-connectivity in 5G mmWave Cellular Networks**. In: 2016 Mediterranean Ad Hoc Networking Workshop (Med-Hoc-Net). [S.l.: s.n.], June 2016. p. 1–7. DOI: `10.1109/MedHocNet.2016.7528494`.

20 PENG, M. et al. Fronthaul-Constrained cloud Radio Access Networks: Insights and Challenges. **IEEE Wireless Communications Magazine**, v. 22, n. 2, p. 152–160, Apr. 2015. DOI: `10.1109/MWC.2015.7096298`.

21 WU, Y. et al. Secrecy-Based Energy-Efficient Data Offloading via Dual Connectivity Over Unlicensed Spectrums. **IEEE Journal on Selected Areas in Communications**, v. 34, n. 12, p. 3252–3270, Dec. 2016. DOI: `10.1109/JSAC.2016.2611979`.

22 3GPP. **Evolved Universal Terrestrial Radio Access (E-UTRA) and NR; Multi-connectivity; Stage 2**. [S.l.], Sept. 2018. Available from: <`http://www.3gpp.org/ftp/Specs/html-info/37340.htm`>. Visited on: 1 Oct. 2018.

23 METIS-II. **Refined Scenarios and Requirements, Consolidated Use Cases, and Qualitative Techno-economic feasibility Assessment**. [S.l.], Jan. 2016. Available from: <https://metis-ii.5g-ppp.eu/wp-content/uploads/deliverables/METIS-II_D1.1_v1.0.pdf>. Visited on: 17 Sept. 2018.

24 ZAKRZEWSKA, A. et al. **Dual Connectivity in LTE HetNets with Split Control- and User-plane**. In: 2013 IEEE Globecom Workshops. [S.l.: s.n.], Dec. 2013. p. 391–396. DOI: 10.1109/GLOCOMW.2013.6825019.

25 MARTIKAINEN, H. et al. **Mobility and Reliability in LTE-5G Dual Connectivity Scenarios**. In: PROCEEDINGS of the IEEE Vehicular Technology Conference (VTC). [S.l.: s.n.], Sept. 2017. p. 1–7. DOI: 10.1109/VTCFall.2017.8288056.

26 3GPP. **0 ms interruption support during handover procedure in NR**. [S.l.], Oct. 2017. Available from: <http://www.3gpp.org/ftp/tsg_ran/wg2_rl2/TSGR2_99bis/Docs/>. Visited on: 19 Oct. 2018.

27 RAO, J.; VRZIC, S. **Packet Duplication for URLLC in 5G Dual Connectivity Architecture**. In: PROCEEDINGS of the IEEE Wireless Communications and Networking Conference (WCNC). [S.l.: s.n.], Apr. 2018. p. 1–6. DOI: 10.1109/WCNC.2018.8377054.

28 MOHAMED, A. et al. Memory-Full Context-Aware Predictive Mobility Management in Dual Connectivity 5G Networks. **IEEE Access**, v. 6, p. 9655–9666, 2018. DOI: 10.1109/ACCESS.2018.2796579.

29 CHAE, S. H.; HONG, J. P.; CHOI, W. Optimal Access in OFDMA Multi-RAT Cellular Networks With Stochastic Geometry: Can a Single RAT Be Better? **IEEE Transactions on Wireless Communications**, v. 15, n. 7, p. 4778–4789, July 2016. DOI: 10.1109/TWC.2016.2546239.

30 LEE, W. C. Y. Preliminary Investigation of Mobile Radio Signal Fading Using Directional Antennas on the Mobile Unit. **IEEE Transactions on Vehicular Communications**, v. 15, n. 2, p. 8–15, Oct. 1966. DOI: 10.1109/TVC.1966.33033.

31 CLARKE, R. H. A Statistical Theory of Mobile-radio Reception. **The Bell System Technical Journal**, v. 47, n. 6, p. 957–1000, July 1968. DOI: 10.1002/j.1538-7305.1968.tb00069.x.

32 HOCHWALD, B. M.; MARZETTA, T. L.; TAROKH, V. Multiple-Antenna Channel Hardening and its Implications for Rate Feedback and Scheduling. **IEEE Transactions on Information Theory**, v. 50, n. 9, p. 1893–1909, Sept. 2004. DOI: 10.1109/TIT.2004.833345.

33 NGO, H. Q.; LARSSON, E. G. No Downlink Pilots Are Needed in TDD Massive MIMO. **IEEE Transactions on Wireless Communications**, v. 16, n. 5, p. 2921–2935, May 2017. DOI: 10.1109/TWC.2017.2672540.

34 CHIEN, T. V.; BJORNSON, E.; LARSSON, E. G. **Multi-cell Massive MIMO Performance with Double Scattering Channels**. In: 2016 IEEE 21st International Workshop on Computer Aided Modelling and Design of Communication Links and Networks (CAMAD). [S.l.: s.n.], Oct. 2016. p. 231–236. DOI: `10.1109/CAMAD.2016.7790363`.

35 GAO, X. et al. Massive MIMO in Real Propagation Environments: Do All Antennas Contribute Equally? **IEEE Transactions on Communications**, v. 63, n. 11, p. 3917–3928, Nov. 2015. DOI: `10.1109/TCOMM.2015.2462350`.

36 BJORNSON, E.; HOYDIS, J.; SANGUINETTI, L. Massive MIMO Networks: Spectral, Energy, and Hardware Efficiency. **Foundations and Trends in Signal Processing**, v. 11, n. 3-4, p. 154–655, 2017. DOI: `10.1561/2000000093`.

37 ROY, M. et al. MIMO Channel Hardening: A Physical Model based Analysis. **CoRR**, abs/1804.07491, May 2018. Available from: <`http://arxiv.org/abs/1804.07491`>. Visited on: 18 June 2018.

38 SAUNDERS, S. R.; ZAVALA, A. A. **Antennas and Propagation for Wireless Communication Systems**. [S.l.]: John Wiley & Sons, 2007. ISBN 9780470848791.

39 RAPPAPORT, T. S. **Wireless Communications: Principles and Practice**. [S.l.]: Prentice Hall PTR, 2002. ISBN 9780130422323.

40 NORKLIT, O.; VAUGHAN, R. G. **Reducing the Fading Rate with Antenna Arrays**. In: IEEE GLOBECOM 1998. [S.l.: s.n.], 1998. p. 3187–3192. DOI: `10.1109/GLOCOM.1998.775685`.

41 MARTINEZ, A. O.; CARVALHO, E. D.; NIELSEN, J. O. **Massive MIMO Properties Based on Measured Channels: Channel Hardening, User Decorrelation and Channel Sparsity**. In: 2016 50th Asilomar Conference on Signals, Systems and Computers. [S.l.: s.n.], Nov. 2016. p. 1804–1808. DOI: `10.1109/ACSSC.2016.7869694`.

42 ZHANG, B. et al. Multi-User Channels With Large-Scale Antenna Arrays in a Subway Environment: Characterization and Modeling. **IEEE Access**, v. 5, p. 23613–23625, 2017. DOI: `10.1109/ACCESS.2017.2764621`.

43 GUNNARSSON, S. et al. Channel Hardening in Massive MIMO - A Measurement Based Analysis. **CoRR**, abs/1804.01690, May 2018. Available from: <`http://arxiv.org/abs/1804.01690`>. Visited on: 18 June 2018.

44 HARRIS, P. et al. Performance Characterization of a Real-Time Massive MIMO System With LOS Mobile Channels. **IEEE Journal on Selected Areas in Communications**, v. 35, n. 6, p. 1244–1253, June 2017. DOI: `10.1109/JSAC.2017.2686678`.

45 HARRIS, P. et al. **An Overview of Massive MIMO Research at the University of Bristol**. In: RADIO Propagation and Technologies for 5G (2016). [S.l.: s.n.], Oct. 2016. p. 1–5. DOI: `10.1049/ic.2016.0064`.

46 BLANDINO, S. et al. **Link Adaptation in Massive MIMO: Throughput-Fairness Trade-off**. In: 2017 IEEE Symposium on Communications and Vehicular Technology (SCVT). [S.l.: s.n.], Nov. 2017. p. 1–6. DOI: `10.1109/SCVT.2017.8240314`.

47 LARSSON, E. G.; POOR, H. V. Joint Beamforming and Broadcasting in Massive MIMO. **IEEE Transactions on Wireless Communications**, v. 15, n. 4, p. 3058–3070, Apr. 2016. DOI: `10.1109/TWC.2016.2515598`.

48 NARASIMHAN, T. L.; CHOCKALINGAM, A. Channel Hardening - Exploiting Message Passing (CHEMP) Receiver in Large-Scale MIMO Systems. **IEEE Journal of Selected Topics in Signal Processing**, v. 8, n. 5, p. 847–860, 2014. DOI: `10.1109/JSTSP.2014.2314213`.

49 BJORNSON, E. et al. A Random Access Protocol for Pilot Allocation in Crowded Massive MIMO Systems. **IEEE Transactions on Wireless Communications**, v. 16, n. 4, p. 2220–2234, Apr. 2017. DOI: `10.1109/TWC.2017.2660489`.

50 LI, J. et al. Benefits of Beamforming Training Scheme in Distributed Large-Scale MIMO Systems. **IEEE Access**, v. 6, p. 7432–7444, 2018. DOI: `10.1109/ACCESS.2018.2793845`.

51 CHEN, Z.; BJOERNSON, E. **Can We Rely on Channel Hardening in Cell-Free Massive MIMO?** In: 2017 IEEE GLOBECOM WORKSHOPS (GC WKSHPS). [S.l.: s.n.], Dec. 2017. p. 1–6. DOI: `10.1109/GLOCOMW.2017.8269162`.

52 ROTTENBERG, F. et al. Performance Analysis of Linear Receivers for Uplink Massive MIMO FBMC-OQAM Systems. **IEEE Transactions on Signal Processing**, v. 66, n. 3, p. 830–842, Feb. 2018. DOI: `10.1109/TSP.2017.2778682`.

53 QI, Y.; QIAN, R. Distance Hardening in Large MIMO Systems. **IEEE Transactions on Communications**, v. 66, n. 4, p. 1452–1466, Apr. 2018. DOI: `10.1109/TCOMM.2017.2782343`.

54 QUALCOMM. **Understanding 3GPP – Starting with the Basics**. [S.l.: s.n.]. Available from: <`https://www.qualcomm.com/news/onq/2017/08/02/understanding-3gpp-starting-basics`>. Visited on: 19 Oct. 2018.

55 DA SILVA, I. et al. **Tight Integration of New 5G Air Interface and LTE to Fulfill 5G Requirements**. In: PROCEEDINGS of the IEEE Vehicular Technology Conference (VTC). [S.l.: s.n.], May 2015. p. 1–5. DOI: `10.1109/VTCSpring.2015.7146134`.

56 3GPP. **NR; Physical channels and modulation**. [S.l.], Sept. 2018. Available from: <`http://www.3gpp.org/ftp/Specs/html-info/38211.htm`>. Visited on: 1 Oct. 2018.

57 DAHLMAN, E.; PARKVALL, S.; SKOLD, J. **5G NR: The Next Generation Wireless Access Technology**. [S.l.]: Elsevier, 2018. ISBN 9780128143230.

58 ________. **4G LTE/LTE-Advanced for Mobile Broadband**. [S.l.]: Elsevier, 2014. ISBN 9780124199859.

59 3GPP. **NR; Radio resource control (RRC) protocol specification**. [S.l.], Sept. 2018. Available from: <`http://www.3gpp.org/ftp/Specs/html-info/38331.htm`>. Visited on: 1 Oct. 2018.

60 LIU, J. et al. Initial Access, Mobility, and User-Centric Multi-Beam Operation in 5G New Radio. **IEEE Communications Magazine**, v. 56, n. 3, p. 35–41, Mar. 2018. DOI: `10.1109/MCOM.2018.1700827`.

61 MARSCH, P. et al. **5G System Design - Architectural and Functional Considerations and Long Term Research**. [S.l.]: J. Wiley & Sons, 2018. ISBN 9781119425120.

62 GIORDANI, M. et al. A Tutorial on Beam Management for 3GPP NR at mmWave Frequencies. **CoRR**, abs/1804.01908, May 2018. Available from: <`https://arxiv.org/abs/1804.01908`>. Visited on: 4 July 2018.

63 3GPP. **NR; Physical layer procedures for data**. [S.l.], Oct. 2018. Available from: <`http://www.3gpp.org/ftp/Specs/html-info/38214.htm`>. Visited on: 15 Oct. 2018.

64 ________. **NR; Physical layer procedures for control**. [S.l.], Oct. 2018. v.15.3.0. Available from: <`http://www.3gpp.org/ftp/Specs/html-info/38213.htm`>. Visited on: 15 Oct. 2018.

65 ________. **NR; Physical layer measurements**. [S.l.], Sept. 2018. Available from: <`http://www.3gpp.org/ftp/Specs/html-info/38215.htm`>. Visited on: 15 Oct. 2018.

66 FANTACCI, R. et al. Adaptive Modulation and Coding Techniques for OFDMA Systems. **Wireless Communications, IEEE Transactions on**, v. 8, n. 9, p. 4876–4883, Sept. 2009. DOI: `10.1109/TWC.2009.090253`.

67 MEHLFÜHRER, C. et al. **Simulating the Long Term Evolution Physical Layer**. In: PROCEEDINGS of the European Signal Processing Conference. Glasgow, Scotland: [s.n.], Aug. 2009. p. 1471–1478.

68 METIS-II. **Final Considerations on Synchronous Control Functions and Agile Resource Management for 5G**. [S.l.], Mar. 2017. Available from: <`https://metis-ii.5g-ppp.eu/wp-content/uploads/deliverables/METIS-II_D5.2_V1.1.pdf`>. Visited on: 5 Dec. 2018.

69 3GPP. **Evolved Universal Terrestrial Radio Access (E-UTRA); Requirements for support of radio resource management**. [S.l.], Mar. 2016. Available from: <`http://www.3gpp.org/ftp/Specs/html-info/36133.htm`>. Visited on: 15 Oct. 2018.

70 ________. **Study on Scenarios and Requirements for Next Generation Access Technologies**. [S.l.], Aug. 2017. Available from: <`http://www.3gpp.org/DynaReport/38913.htm`>. Visited on: 3 Aug. 2017.

71 ________. **Study on Channel Model for Frequencies from 0.5 to 100 GHz**. [S.l.], Sept. 2017. Available from: <`http://www.3gpp.org/DynaReport/38901.htm`>. Visited on: 26 Sept. 2017.

72 CASTANEDA, E. et al. An Overview on Resource Allocation Techniques for Multi-User MIMO Systems. **IEEE Communications Surveys and Tutorials**, v. 19, n. 1, p. 239–284, Firstquarter 2017. DOI: 10.1109/COMST.2016.2618870.

73 LIMA, F. R. M. et al. Resource Assignment for Rate Maximization with QoS Guarantees in Multiservice Wireless Systems. **IEEE Transactions on Vehicular Technology**, v. 61, n. 3, p. 1318–1332, Mar. 2012. DOI: 10.1109/TVT.2012.2183905.

74 NEMHAUSER, G.; WOSLEY, L. **Integer and Combinatorial Optimization**. [S.l.]: John Wiley & Sons, 1999.

75 ZHANG, Y. J.; LETAIEF, K. B. Multiuser Adaptive Subcarrier-and-Bit Allocation with Adaptive Cell Selection for OFDM Systems. **IEEE Transactions on Communications**, v. 3, n. 5, p. 1566–1575, Sept. 2004. DOI: 10.1109/TWC.2004.833501.

76 SIERKSMA, G. **Linear and Integer Programming: Theory and Practice, Second Edition**. [S.l.]: Taylor & Francis, 2001.

77 3GPP. **Study on 3D channel model for LTE**. [S.l.], Dec. 2016. Available from: <http://www.3gpp.org/DynaReport/36873.htm>. Visited on: 12 Apr. 2017.

78 JAECKEL, S. et al. QuaDRiGa: A 3-D Multi-Cell Channel Model With Time Evolution for Enabling Virtual Field Trials. **IEEE Transactions on Antennas and Propagation**, v. 62, n. 6, p. 3242–3256, June 2014. DOI: 10.1109/TAP.2014.2310220.

79 PETER, M. et al. **Measurement Campaigns and Initial Channel Models for Preferred Suitable Frequency Ranges**. [S.l.], Mar. 2016. Available from: <https://bscw.5g-mmmagic.eu/pub/bscw.cgi/d94832/mmMAGIC_D2-1.pdf>. Visited on: 20 Apr. 2017.

80 RAPPAPORT, T. S. et al. Wideband Millimeter-Wave Propagation Measurements and Channel Models for Future Wireless Communication System Design. **IEEE Transactions on Communications**, v. 63, n. 9, p. 3029–3056, Sept. 2015. DOI: 10.1109/TCOMM.2015.2434384.

81 3GPP. **Evolved Universal Terrestrial Radio Access (E-UTRA); Physical channels and modulation**. [S.l.], Sept. 2018. Available from: <http://www.3gpp.org/ftp/Specs/html-info/36211.htm>. Visited on: 15 Oct. 2018.

82 ________. **Evolved Universal Terrestrial Radio Access (E-UTRA); Base Station (BS) radio transmission and reception**. [S.l.], Oct. 2018. Available from: <http://www.3gpp.org/ftp/Specs/html-info/36104.htm>. Visited on: 15 Oct. 2018.

83 IBM. **IBM ILOG CPLEX Optimizer**. [S.l.: s.n.]. Available from: <http://www-01.ibm.com/software/integration/optimization/cplex-optimizer/>. Visited on: 19 Oct. 2018.

84 WANG, H.; ROSA, C.; PEDERSEN, K. I. Dual Connectivity for LTE-advanced Heterogeneous Networks. **Wireless Networks**, Springer, v. 22, n. 4, p. 1315–1328, 2016. DOI: 10.1007/s11276-015-1037-6.

85 ZAIDI, A. A. et al. Waveform and Numerology to Support 5G Services and Requirements. **IEEE Communications Magazine**, v. 54, n. 11, p. 90–98, Nov. 2016. DOI: `10.1109/MCOM.2016.1600336CM`.

86 MIAO, H. et al. **Joint Beam-Frequency Multiuser Scheduling for Millimeter-Wave Downlink Multiplexing**. In: PROCEEDINGS of the IEEE Vehicular Technology Conference (VTC). [S.l.: s.n.], May 2016. p. 1–5. DOI: `10.1109/VTCSpring.2016.7504304`.

A COMPUTATIONAL COMPLEXITY OF PROPOSED DISTRIBUTED FRAMEWORK

A.1 BS Selection

Each UE executes Alg. 5.1 for each RAT. In this analysis, we consider U_b as the number of UEs connected to BS b.

In l. 2, there is **1** comparison. In the worst case, the set $\hat{\mathcal{B}}$ is not empty, thus the algorithm continues to be executed.

The loop in ll. 5-8 has B_n steps, one per BS of RAT n. Considering that to find the minimum element among i elements we need to do $i-1$ comparisons, in l. 7, for each BS b there are $(U_b - 1)$ comparisons. Thus, in this loop there are $\sum_{b=1}^{B_n}(U_b - 1) = \mathbf{U_n} - \mathbf{B_n}$ comparisons.

Lines 9-10 sum B_n terms, thus we have $\mathbf{2}(\mathbf{B_n} - \mathbf{1})$ sums.

Loops between ll. 11-16 and ll. 12-14 have B_n and 2 steps, respectively. Thus, the division in l. 13 is repeated $\mathbf{2B_n}$ times and the multiplication in l. 15, $\mathbf{B_n}$ times.

Similar to l. 7, in l. 17 there are $\mathbf{B_n} - \mathbf{1}$ comparisons.

The comparison in l. 18 is done **once**. In the worst case, this test is false and the next line is not executed. Finally, in l. 21 there are $\mathbf{T}^* + \hat{\mathbf{T}} - \mathbf{1}$ comparisons.

Therefore, in the worst case, the number of operations in the BS selection procedure is

$$1 + U_n - B_n + 2(B_n - 1) + 2B_n + B_n + B_n - 1 + 1 + T^* + \hat{T} - 1 = U_n + 5B_n + T^* + \hat{T} - 2. \quad (A.1)$$

In the worst case $U_n = U$ and $B_n = B$, thus the complexity of the BS selection procedure is $O(U + B)$.

A.2 Resource Assignment

Each BS executes Alg. 5.2 independently. In this analysis, we will consider a BS b of RAT n with U_b UEs connected to it.

Alg. 5.2 has 3 loops, ll. 4-8, 9-17 and 20-26. As explained in Section 5.5.2, in the first loop, we check if the UEs are already satisfied. In the second one, we allocate RBs until all RBs have been assigned or all the UEs have achieved their throughput requirement, or even both events have happened. Finally, on the third one, we allocate the remaining RBs.

We will analyze the possible cases for loop 2.

A.2.1 All RBs are Assigned in Loop 2

Thus, loop 2 is repeated K_n times and loop 3 does not happen. The worst case is when none UE gets satisfied, neither in loop 1 nor in loop 2.

Concerning loop 1, it is repeated U_b times, one per connected UE. In l. 5, we have 1 comparison which will be repeated U_b times, so this line has $\mathbf{U_b}$ comparisons. The operation in l. 6 is not executed, since none UE is satisfied.

In l. 9, we have 2 comparisons which will be repeated $K_n + 1$ times, so l. 9 has $\mathbf{2(K_n + 1)}$ comparisons.

In l. 10, the set $\mathcal{K}_n$ starts with K_n RBs and decreases in one at each iteration of loop 2. So, after assigning i RBs, $\mathcal{K}_n$ has $K_n - i$ RBs. Similarly, each UE that gets satisfied is removed from $\mathcal{U}_b$, l. 15. In this case, we do less comparisons in l. 10, since we do not consider the elements $r_{u,k,b}$ of the satisfied UEs. In the worst case, no one gets satisfied and we need to do more operations. Considering that to find the maximum element among i elements we need to do $i-1$ comparisons, to find the maximum $r_{u,k,b}$ in l. 10, after i assignments, we need to do $[U_b(K_n - i) - 1]$ comparisons, in the worst case. Thus, we have $\sum_{i=0}^{K_n-1}[U_b(K_n - i) - 1] = \frac{1}{2}\left(\mathbf{U_b K_n^2 - 2K_n + U_b K_n}\right)$ comparisons in l. 10.

In order to update the UE throughput in l. 12, 3 operations are done: one multiplication, one sum and one division. Since this update is repeated K_n times, we have $\mathbf{3K_n}$ operations. The operation in l. 13 and the comparison in l. 14 are also repeated K_n times, so, in these lines, we have $\mathbf{K_n}$ subtractions and $\mathbf{K_n}$ comparisons, respectively. In the worst case, the operation in l. 15 is not computed, since no one gets satisfied.

Thus, the number of operations is

$$U_b + 2(K_n + 1) + \frac{1}{2}\left(U_b K_n^2 - 2K_n + U_b K_n\right) + 3K_n + K_n + K_n = \frac{1}{2}\left(U_b K_n^2 + U_b K_n + 12K_n + 2U_b + 4\right). \quad \text{(A.2)}$$

Therefore, the complexity of the first case is $O\left(U_b K_n^2\right)$.

A.2.2 All UEs Achieve Their Required Throughput in Loop 2

In this case, we consider that in loop 1, $U_b - L$ UEs were already satisfied, thus L UEs gets satisfied in loop 2. It is also considered that D RBs are allocated on the second loop, where $L \leq D < K_n$, so, on the third one, $K_n - D$ RBs are allocated. The case $D = K$ is included in previous case. That way, loop 2 is repeated D times and loop 3, $K_n - D$ times.

Similar to the first case, in l. 5, one comparison is repeated U_b times, resulting in $\mathbf{U_b}$ comparisons. Since $U_b - L$ UEs were already satisfied, the operation in l. 6 is repeated $\mathbf{U_b - L}$ times. In a similar analysis, l. 9 has $\mathbf{2(D + 1)}$ comparisons.

The worst case for l. 10 is when the L UEs are satisfied on the last L iterations, resulting in $\sum_{i=0}^{D-L-1}[L(K_n - i) - 1] + \sum_{i=D-L}^{D-1}[(D - i)(K_n - i) - 1]$ comparisons.

Analogous to the first case, the number of operations required to update the UE throughput in ll. 12 and 24 is $3D$ and $3(K_n - D)$, respectively, resulting in $\mathbf{3K_n}$ operations.

The subtraction in l. 13 and the comparison in l. 14 are repeated D times, so, in these lines, we have **D** subtractions and **D** comparisons, respectively. The operation in l. 15 is computed **L** times.

The comparison in l. 18 is computed **once**, while the comparison in l. 20 is repeated $\mathbf{K_n - D + 1}$ times. Ll. 21 and 22 correspond to $\mathbf{(K_n - D)(U_b - 1)}$ and $\mathbf{\frac{(K_n-D)(K_n-D+1)}{2}}$ comparisons, respectively. Finally, l. 25 corresponds to $\mathbf{K_n - D}$ subtractions.

The total amount of operations in case 2, i.e., sum of the described operations, is presented in (A.3).

$$\begin{aligned} U_b + (U_b - L) + 2(D+1) + \sum_{i=0}^{D-L-1} [L(K-i) - 1] + \sum_{i=D-L}^{D-1} [(D-i)(K_n - i) - 1] + 3K_n \\ +2D + L + 1 + (K_n - D + 1) + (K_n - D)(U_b - 1) + \frac{(K_n - D)(K_n - D + 1)}{2} \\ + (K_n - D) = \\ \frac{1}{2}\left[(L-1)D^2 + D(-2U_b + 4LK_n + 3)\right] + \frac{1}{2}\left(LK_n - 2L^2K_n + K_n^2 + 9K_n + 2U_bK_n\right) \\ + \frac{1}{6}\left(-L^3 - 6L^2 + L\right) + 2U_b + 4. \end{aligned} \tag{A.3}$$

Since $D \leq K_n$ and $L \leq \min(U_b, K_n)$, the complexity of this case is $O\left(U_b K_n^2\right)$.

Since the complexity of both cases is $O\left(U_b K_n^2\right)$ and, in the worst case, $U_b = U$ and $K_n = K$, thus, it is concluded that the resource assignment is $O\left(UK^2\right)$.

Finally, considering the complexity of the BS selection and resource assignment procedures, we conclude that the complexity of the proposed framework is $O\left(UK^2\right)$.